Supramolecular coordination chemistry of the ligand 5,6-bis(2-pyridyl)pyrazine-2,3-dicarboxylic acid:

From the monomer to the polymer

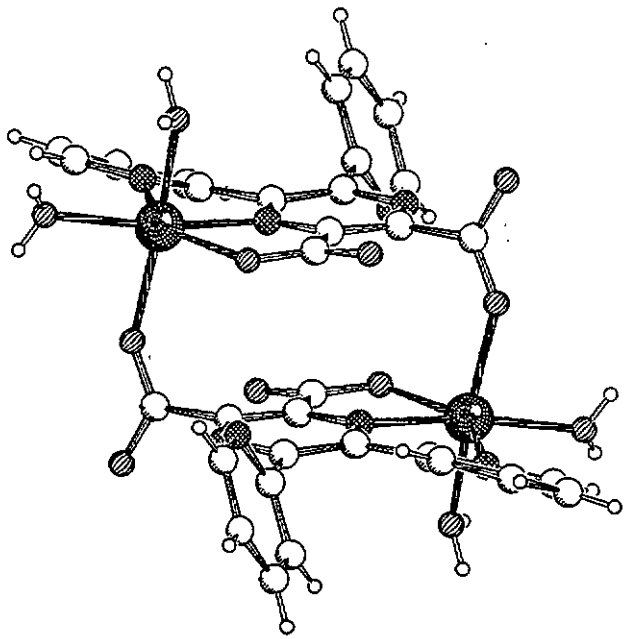

Montserrat Alfonso

Neuchâtel 1999

UNIVERSITÉ DE NEUCHÂTEL

FACULTÉ DES SCIENCES

INSTITUT DE CHIMIE

Supramolecular coordination chemistry of the ligand 5,6-bis(2-pyridyl)pyrazine-2,3-dicarboxylic acid:

From the monomer to the polymer

Thèse Présentée à la Faculté des Sciences de l'Université de Neuchâtel par

Montserrat Alfonso

Chimiste diplômée de l'Université de Barcelona/Espagne pour

l'obtention du grade de docteur ès sciences

Institut de Chimie

Université de Neuchâtel

Juin 1999

IMPRIMATUR POUR LA THÈSE

Chimie supramoléculaire du ligand acide 5,6-bis(2-pyridyl)pyrazine-2,3-dicarboxylique: du monomère au polymère

de Mme Montserrat Alfonso

UNIVERSITÉ DE NEUCHÂTEL

FACULTÉ DES SCIENCES

La Faculté des sciences de l'Université de Neuchâtel sur le rapport des membres du jury,

Mme H. Stoeckli-Evans (directrice de thèse) et
MM. K. Bernauer et S. Decurtins (Berne)

autorise l'impression de la présente thèse.

Neuchâtel, le 23 juin 1999

Le doyen:

F. Stoeckli

To my parents

Acknowledgements

This work has been carried out from October 1995 to June 1999 in the Laboratory of Chemical Crystallography at the University of Neuchâtel under the supervision of Professor Helen Stoeckli-Evans.

I would like to express my deepest gratitude to Professor Helen Stoeckli-Evans for offering me the possibility to work in her research group and introducing me in the fascinating field of the chemical crystallography. I sincerely thank the time she generously devoted to me, her enthusiasm and valuable advises.

I would like to thank the members of the jury, Professor Klaus Bernauer and Professor Silvio Decurtins (Universität Bern), for accepting to review this work.

I am especially indebted to Prof. Juan Rihas (Department of Inorganic Chemistry, University of Barcelona, Spain) for recording the EPR spectra, his keen interest and the constructive discussions on the molecular magnetism.

I wish to warmly thank all my colleagues in Chimie-Physique II: Dr. Antonia Neels who has recorded some of the crystallographic data, Mme. Ana Tesouro, Mr. Piotr Goetzen, Dr. Maciek Posel, Mr. Tokoure Assoumatine and Dr. Yi Wang, for creating a nice atmosphere that allowed me to achieve this work. I will always keep an excellent souvenir of the years we have spent together.

I am grateful to all those who have contributed their time to this work: Dr. Christiane Bobilier (NMR), Mr. Heinz Bursian (NMR), Mrs. Christine Poliart (MS) and the members of the group of Prof. Silvio Decurtins (Magnetic measurements).

As assistant I would like to thank the students in first year chemistry and biology for the personal enrichment they provided me. I extend as well my thanks to my colleagues-assistants in the laboratory of 1st year Inorganic Chemistry.

I acknowledge to all these people who contributed somehow to this project.

This work would not have been possible without the generous financial support from the Swiss National Science Foundation and the "Etat de Neuchâtel".

ABBREVIATIONS

bppz	2,3- or 2,5-bis(2-pyridyl)pyrazine
1D, 2D, 3D	one-, two- and three-dimensional
DCI, EI	desorption chemical ionization, electronic impact (mass spectrometry)
EPR	electron paramagnetic resonance
Et	ethyl
i-Pr	isopropyl
IR	infrared
H_2pyzdc	pyrazine-2,3-dicarboxylic acid
H_4pyztc	pyrazine-2,3,5,6-tetracarboxylic acid
L	ligand
M	metal
Me	methyl
m.p.	melting point
MS	mass spectrometry
NMR	nuclear magnetic resonance
py	pyridine
pyz	pyrazine
s, d, m	singlet, doublet and multiplet (NMR spectroscopy)
s, m, w, vw	strong, medium, weak, very weak (IR spectroscopy)
T	temperature
tamp	2,3,5,6-tetrakis(aminomethyl)pyrazine
tppz	2,3,5,6-tetra(2-pyridyl)pyrazine
UV	ultraviolet

Vis	visible
X	halogen
χ	magnetic susceptibility
δ	chemical shift
ε	extinction coefficient
λ	wavelength
μ	magnetic moment
τ	index of trigonality
υ	stretching vibration (IR spectroscopy)
SP	square pyramidal
TBP	trigonal bipyramidal

CONTENTS

INTRODUCTION

Ligand-bridged multinuclear complexes have grown into an active research area in chemistry. This increased importance appears to be largely due to two reasons:

Firstly, it has been observed that with simple bridging ligands, structurally sophisticated compounds can be formed despite the simplicity of the component parts. The subtle interactions that control the assembly of such complexes may be rationalised after the event but can rarely be predicted in advance. For this reason the preparation and structural characterization of these metal complexes will help our eventual understanding of the factors whicb control the formation of their sometimes unusual structures.

Secondly, polynuclear complexes in general are of great interest because of their potential physical properties, such as electrical conductivity, magnetism and photochemical behaviour.

Much attention has been given to one-, two- and three-dimensional coordination polymers, where the structure is assembled by the coordination of suitable ligands about a metal ion.

The research described here deals with the study of the supramolecular coordination chemistry of the ligand, 5,6-bis(2-pyridyl)-pyrazine-2,3-dicarboxylic acid (H_2L). It concerns the synthesis, characterization and X-ray structure determination of metal complexes containing this ligand. The measurement and interpretation of the temperature dependent magnetic susceptibility data is also considered.

1 PYRAZINE AND DERIVATIVES AS BRIDGING LIGANDS: A SURVEY

The ability of pyrazine (pyz) and substituted pyrazines to act as bridging ligands, thus giving rise to the formation of oligomeric and polymeric complexes, is well established[1,2]. The first such compounds were prepared already in the 1890's, but at that time it was impossible to establish their polymeric nature[3].

Coordination polymers result from the binary combination of a transition metal ion with a suitable polydentate ligand. A search in the Cambridge Crystallographic Data Base revealed that coordination polymers bridged by pyrazine and substituted pyrazines includes examples of one- (1D), two- (2D) and three-dimensional (3D) arrays. The geometry of the metal ions and the dimensionality of the polymeric structure seem to be influenced by the substituents on pyrazine. Several bonding modes have been described for pyrazine bridging ligands, the most common are:

- **Bis-monodeotate pyrazines**

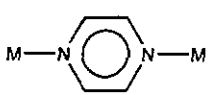

Examples:

pyrazine (pyz)[4-11]

2,3-, 2,5- and 2,6- dimethylpyrazine (Me_2pyz)[12-14]

Tetramethylpyrazine (Me_4pyz)[6]

2-chloropyrazine (Cl-pyz)[14]

- **Mooodeotate-bideotate chelating pyrazines**

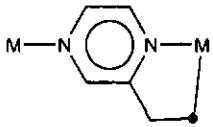

Example:

pyrazine-2-carboxylic acid[15-19]

- **Bis-bideotate chelatiog pyrazines**

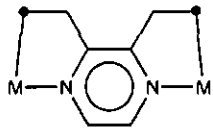

Examples:

2,3-bis(2-pyridyl)pyrazine (2,3-bppz) [20]

pyrazine-2,3-dicarboxylic acid (2,3-pyzdc)[21-23]

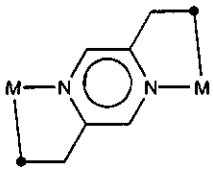

Examples:

2,5-bis(2-pyridyl)pyrazine (2,5-bppz) [24]

- **Bis-tridentate chelatiog pyrazioes**

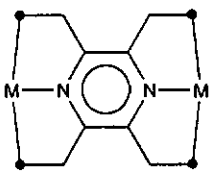

Examples:

2,3,5,6-tetra(2-pyridyl)-pyrazine (tppz) [25]

pyrazine-2,3,5,6-tetracarboxylic acid (pztc)[26,27]

3,6-bis(2-pyridyl)pyrazine-2,5-dicarboxylic acid[28]

2,3,5,6-tetrakis(aminomethyl)pyrazine (tamp)[29]

The ligand plays an important role in determining the structure. Accordingly, the difference in the substituents on the pyrazine ring offers the possibility to form coordination polymers of variable architectures.

1.1 One-dimensional coordination polymers

Numerous one-dimensional coordination polymers with pyrazine bridging ligands have been structurally charcterized. Different structural motifs can be constructed:

1.1.1 Linear chain structures

Such structural feature has been observed in compound $[Co(2,3\text{-pyzdc})(H_2O)_2]_n$[22], for example, which has extended chains of cobalt ions linked by bis-chelating $pyzdc^{2-}$ groups.

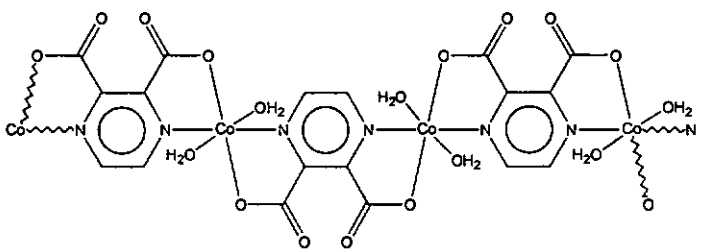

Figure 1. Linear-chain structure found in $[Co(2,3\text{-pyzdc})(H_2O)_2]_n$.

1.1.2 Zig-zag chain structures

A zig-zag polymeric chain structure has been described for compound $\{[Mn(H_2pztc)(H_2O)_2]\cdot 2\ H_2O\}_n$[27].

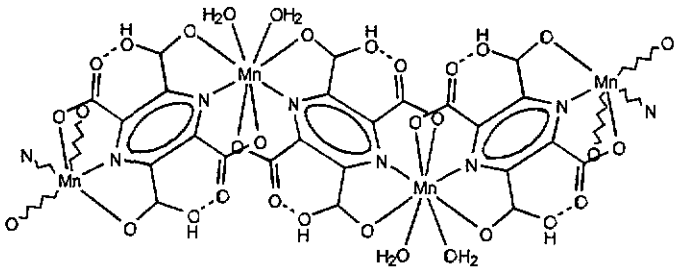

Figure 2. Zig-zag chain structure found in $\{[Mn(H_2pztc)(H_2O)_2]\cdot 2\ H_2O\}_n$.

In $\{[Mn(H_2pztc)(H_2O)_2]\cdot 2\ H_2O\}_n$ the ligand molecule coordinates in a bis-tridentate manner with four short and four long Mn-O and Mn-N bonds, building up a zig-zag polymer chain. The ligand is only partially deprotonated with strong intramolecular hydrogen bonds between adjacent carboxylate groups.

1.1.3 Ladder chain structures

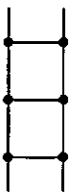

$\{[Cu_2(tamp)Cl_2]Cl_2\}_n$ belongs to this fascinating class of compounds[29], whose structure can be described as binuclear $[Cu_2(tamp)Cl_2]$ complexes linked by two parallel Cu···Cl···Cu bridges to form a ladder-type polymer.

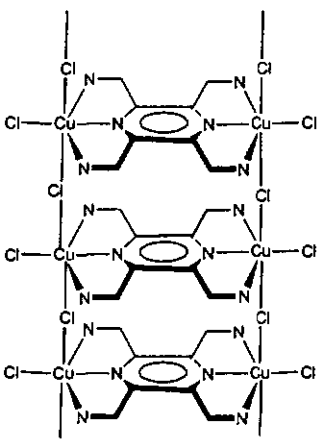

Figure 3. Ladder-like chain structure of $\{[Cu_2(tamp)Cl_2]Cl_2\}_n$.

$\{[Mn(2,3\text{-pyzdc})(H_2O)_2]\cdot 2H_2O\}_n$ is another example of a coordination polymer exhibiting this topology[23].

1.1.4 Helical chain structures

To our knoweledge only two examples of helical chain complexes have been prepared by using pyrazine-bridging ligands[28]. Pressumably, this is due to the fact that to form an extended helix a determined number and disposition of binding sites within the ligand is required.

Wang[28] reported the synthesis and structure of the helical complex, $\{[Cu(HL)(H_2O)](NO_3)\}_n$ (H_2L = 3,6-bis(2-pyridyl)pyrazine-2,5-dicarboxylic acid). Here the flexible ligand molecule binds to two metal ions in an assymmetric manner so forming a helix that twists around the chain direction.

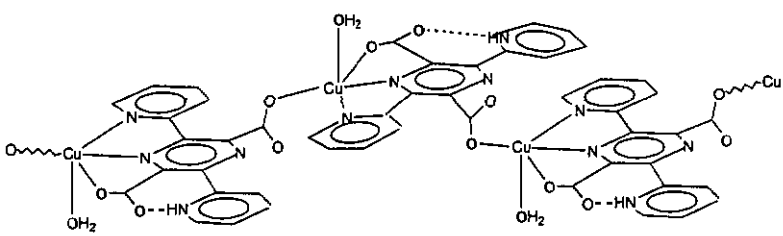

Figure 4. Schematic helical structure of complex $\{[Cu(HL)(H_2O)](NO_3)\}_n$, wbere the NO_3^- counterions have been omitted for clarity.

1.2 Two dimensional coordination polymers

The structure types commonly observed for the 2D coordination polymers formed by pyrazine or substituted pyrazine bridging ligands are:

1.2.1 Square grids

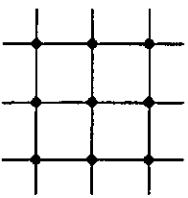

This structural motif has been found, for example, in $Fe(NCS)_2(pyz)_2$[5], $[Ag(pyz)_2][Ag_2(pyz)_3](PF_6)_3$[8], $Co(NCS)_2(pyz)_2$[30], $Ni(pzdc)(pyz)$[31] and $CdX_2(pyz)$[32].

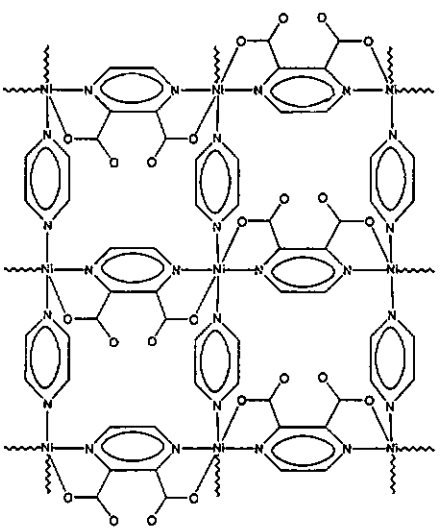

Figure 5. Schematic structure for $\{[Ni(pzdc)(pyz)]\cdot 2H_2O\}_n$.

1.2.2 Honeycomb grids

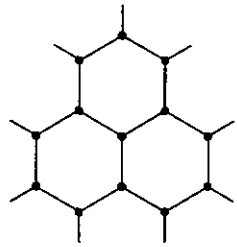

Some examples of six-membered layer structures, based on Cu^+ and Ag^+ centers and 1,4-diazines, have been reported in recent times[6,7,9,13,14,33].

The structure of complex $[Ag_2(pyz)_3](BF4)_2$[9] is made up of cationic two-dimensional layers, consisting of $Ag(pyz)_3^+$ units forming hexagons. An unusual structural feature of this 2D polymer is the folding in chair conformation of the six-membered $Ag_6(pyz)_6$ rings.

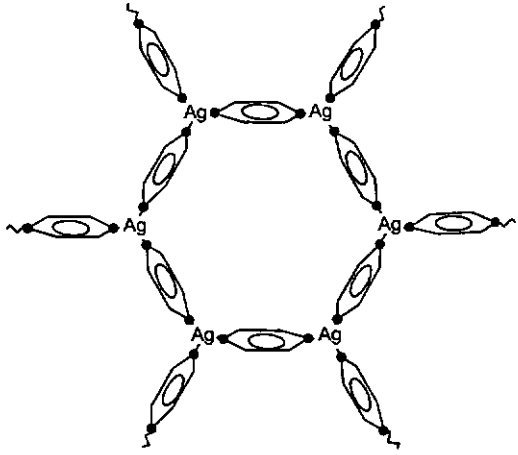

Figure 6. $Ag_6(pyz)_6$ hexagonal motifs that build up the 2D structure of $[Ag_2(pyz)_3](BF4)_2$

Other 2D coordination polymers with bridging pyrazine ligands exhibit structures that can not he described as square or honeycomb grids. For example, $\{[Cu_2L(H_2O)_2](NO_3)_2\}_n$[28] with a herring-hone hexagonal grid pattern.

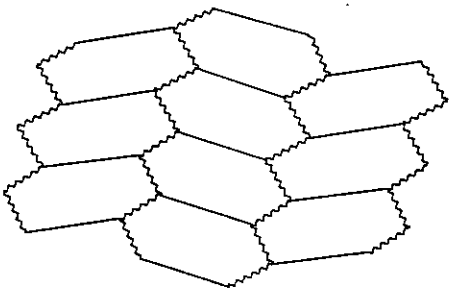

Figure 7. Schematic view of the 2D herring-bone hexagonal grid pattern in compound $\{[Cu_2L(H_2O)_2](NO_3)_2\}_n$[28].

1.3 Three dimensional coordination polymers

There are only a few examples in the literature of 3D coordination polymers with pyrazine bridging ligands. Recently, Hoskins and Robson[34] have proposed a strategy to prepare such 3D phases, described as «scaffolding-like materials», which has been fruitfull in the case of Cu(I)-pyrazine polymeric systems, leading to a diamondoid framework in the case of complex $[Cu(2,5\text{-}Me_2pyz)_2]PF_6$[13].

Our interest in using substituted pyrazines to build up coordination polymers arises from the structural variety found in such compounds. Some of the ligands previously investigated are illustrated in figure 8.

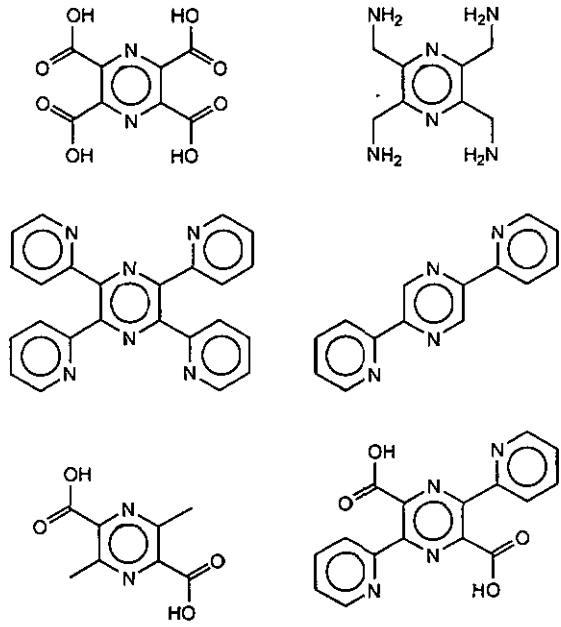

Figure 8. Some substituted pyrazines used as bridging ligands.

The coordination chemistry of such ligands bas proved to be extremely rich. By reacting these ligands with first-row transition metal ions a number of complexes with a considerable structural diversity have been obtained. The steric demands of the ligand seem to be an important factor in determinig the local metal environment and, consequently, the overall structure.

Some unexpected results have been found. For example, early reports on the ligand 2,3,5,6-tetra(2-pyridyl)-pyrazine (TPPZ) suggested that TPPZ was unlikely to behave as a bis-tridentate ligand owing to the steric repulsions between the adjacent pyridine rings[35,36]. However, the bridging bis-tridentate mode is now well established. To date several complexes containing the ligand TPPZ acting in a bis-tridentate manner have been reported[25, 37-39]. In a paper by Graf et al.[38] a fascinating macrocyclic structure has been described for $[Zn_2(\mu\text{-TPPZ})(H_2O)Cl(\mu\text{-}ZnCl_4)(\mu\text{-}ZnCl_2)(\mu\text{-}ZnCl_3H_2O)]_2$.

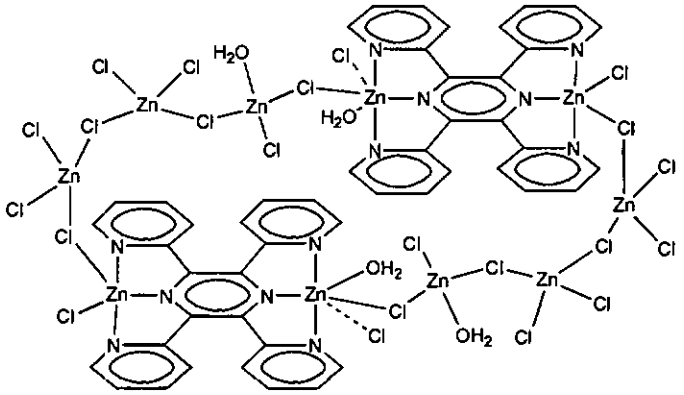

Figure 9. Schematic representation of the macrocycle $[Zn_2(\mu\text{-TPPZ})(H_2O)Cl(\mu\text{-}ZnCl_4)(\mu\text{-}ZnCl_2)(\mu\text{-}ZnCl_3H_2O)]_2$ structure.

The macrocyclic structure of $[Zn_2(\mu\text{-TPPZ})(H_2O)Cl(\mu\text{-}ZnCl_4)(\mu\text{-}ZnCl_2)(\mu\text{-}ZnCl_3H_2O)]_2$ is composed of two highly twisted binuclear Zn(II) complexes of TPPZ linked end to end by three Cl...Zn...Cl bridges.

2 MOLECULAR MAGNETISM

When a substance is placed in an homogeneous magnetic field it acquires a magnetization, M. The field within the sample, the magnetic induction B, is given as

$$B = H_0 + 4\pi M$$

where H_0 is the applied magnetic field and M the magnetization.

The volume magnetic susceptibility, χ, is related to M by

$$\chi = \frac{\partial M}{\partial H}$$

χ is the algebraic sum of two contributions associated with diferent phenomena

$$\chi = \chi^D + \chi^P$$

where χ^D and χ^P represent the diamagnetic and paramagnetic susceptibilities, respectively. The former is negative and the latter positive. When χ^D dominates, the sample is said to be diamagnetic; it is repelled by the magnetic field. When χ^P is the major contribution, the sample is said to be paramagnetic; it is attracted by the applied field.

Diamagnetism is due to the interaction of the magnetic field with the motion of the electrons in their orbits.

Paramagnetism arises from the spin and orbital angular moments of the unpaired electrons interacting with the field. The paramagnetic effect is one or two orders of magnitude greater than the diamagnetic effect. Thus, paramagnetism is dominant in all substances containing unpaired electrons.

There are more complex forms of magnetic behaviour which appear when the behaviour of adjacent magnetic centres is not independent. The more common are ferromagnetism, antiferromagnetism and ferrimagnetism.

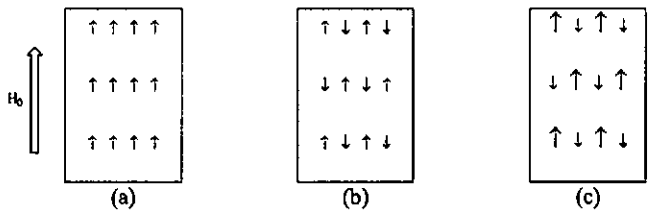

Figure 10. Alignment of the magnetic vectors in a compound (a) ferromagnetic, (b) antiferromagnetic and (c) ferrimagnetic.

Ferromagnetism is observed when the magnetic vectors of adjacent centres tend to allign parallel to each other.

Antiferromagnetism arises if the magnetic vectors of neighbouring centres tend to couple antiparallelly.

Ferrimagnetism is a special case of antiferromagnetism in which the magnetic vectors of adjacent centres are of different magnitude.

2.1 Magnetism of polynuclear transition metal complexes

The interpretation of the magnetic susceptibilities of polynuclear transition metal complexes involves two complementary approaches:

2.1.1 Molecular orbital theory

The molecular orbital theory takes into account the mechanism of the interaction and bonding in a complex. It is generally accepted that the mechanisms of the exchange interaction involves the mutual pairing or alignment of electronic spins via some form of orbital overlap. Two types of mechanisms are usually used to account for the spin-spin coupling.

Direct interaction. This mechanism operates between unpaired electrons on ions or molecules that are close enough to have significant overlap of their wave functions, leading to mutual pairing in the ground state.

Superexchange. This mechanism involves the interaction between unpaired electrons over a relatively large distance by acting through a intermediary. The interaction may occur in two ways: either via σ-bonding or π-bonding.

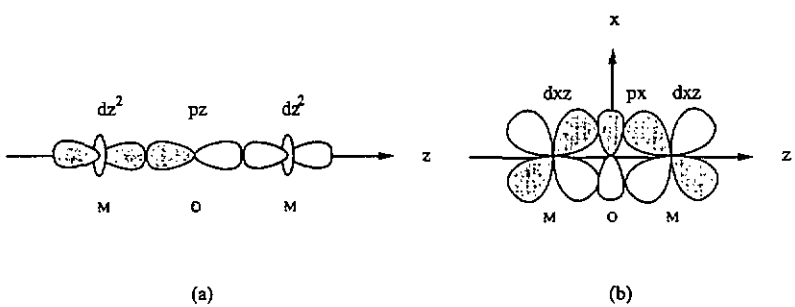

Figure 11. Superexchange interaction in a linear M-O-M system via (a) σ-bonding and (b) π-bonding.

2.1.2 The dipolar coupling approach

The dipolar coupling approach assumes the presence of an exchange interaction without reference to the mechanism and calculates the variation of the magnetic susceptibility with the temperature. The magnetic exchange between nearest neighbours may be represented by the Heisenberg-Dirac-Van Vleck Hamiltonian[40]

$$\hat{H} = - \sum_{\text{neighbours}} J_{ij} \hat{S}_i \hat{S}_j$$

where J_{ij} is an exchange integral between centres i and j. J_{ij} is negative for an antiferromagnetic interaction and positive for a ferromagnetic interaction.

The coupling constant, J, can be expressed as the sum of an antiferromagnetic (J_{AF}) and a ferromagnetic (J_F) contribution.

$$J = J_{AF} + J_F$$

J_{AF} depends on the degree of overlap of the (delocalized) orbitals which contain the unpaired electrons. If there is a finite overlap, then according to the Pauli Principal, the spins must be aligned antiparallel, that is, be paired, and the effect is antiferromagnetic. When the overlap between two orbitals is forbidden, because they are orthogonal, then the coupling can be ferromagnetic and the spins are coupled in a parallel manner.

If the orbitals which contain the unpaired electrons are mixed with the orbitals of a common bridging atom (or group of atoms), the nature of the exchange is determined by the degree of mixing of the metal orbitals with the orbitals of the bridge.

Calculations indicate that $|J_{AF}| >> |J_F|$ and, consequently when both, J_{AF} and J_F, are possible, the J_{AF} contribution usually dominates.

2.2 Magnetic behaviour of pyrazine bridged complexes

The ability of pyrazine and its derivatives to propagate magnetic exchange interactions in poly- or oligo-metallic complexes has been investigated by several groups. Such studies revealed that pyrazine bridging ligands are not strong mediators of spin-spin coupling. With the exception of the ferromagnetic polynuclear complex $[Cu(Hpzdc)Cl]_n$[21] all pyrazine bridged complexes reported so far exhibit weak antiferromagnetic or no significant exchange coupling.

A direct overlap of the magnetic orbitals can not be expected in pyrazine bridged complexes because of the large separation between the paramagnetic centers; therefore, a magnetic superexchange mechanism through the bridging ligand should be taken in consideration. Until recently, the available experimental data did not permit an unambiguous assignment of the superexchange pathway, whether σ or π. Several arguments concerning the superexchange mechanism through pyrazine ligands have been made:

- Hatfield and co-workers[41-44] studied a variety of Cu(II) bridging pyrazine complexes and proposed a π-pathway based on spectroscopic evidence. In the Hatfield model the orientation of the pyrazine ring related to the copper coordination plane is important in determining the magnitude of the magnetic exchange.

The exchange coupling only occurs if the heterocyclic ring is slightly tilted with respect to the copper coordination plane, thus leading to a significant overlap between the orbitals of both interacting paramagnetic centers and the bridging ligand.

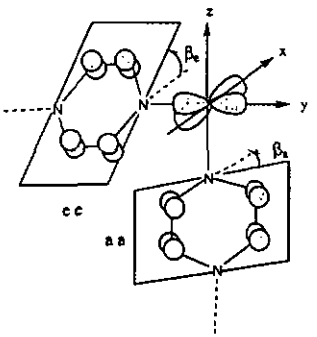

Figure 12. Superexchange mechanism showing the tilt of the pyz ring and the orbital overlap.

- At the same time Hoffman et al.[45] used the extended Hückel molecular orbital approach to predict that pyrazine would be a very effective ligand to transmit exchange interactions through the σ-pathway. The discrepancy with the small values of the coupling constant, J, determined experimentally was attributed to the fact that these calculations over emphasize the intermolecular overlap.

- Later Oshio et al.[46] have suggested that even through the σ-pathway the magnetic exchange should be weak due to the large metal-metal distance.

- Recently, Wang et al.[28] have established a relationship between the structure and the magnetic properties for a series of pyrazine bridging Cu(II) complexes. The results provide solid proof to support the σ-pathway.

RESULTS

1 THE LIGAND 5,6-BIS(2-PYRIDYL)-PYRAZINE-2,3-DICARBOXYLIC ACID

1.1 Choice of the ligand

The present work constitutes part of our continuing study of coordination compounds of transition metal ions with substituted pyrazine ligands, which show an interesting and in some cases unpredictable structural variety.

In this context, we embarked on the investigation of the coordination chemistry of the ligand 5,6-(2-pyridyl)-pyrazine-2,3-dicarboxylic acid (H_2L), with the principal aim to isolate and structurally characterize novel coordination polymers. This ligand was originally synthesized by Wang[28] who reported on the capacity of the ligand to form 1D coordination polymers, but its coordination chemistry remained practically unexplored.

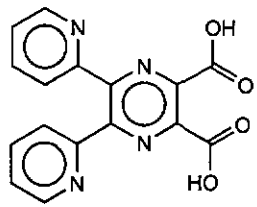

Figure 13. Scheme of the ligand 5,6-(2-pyridyl)-pyrazine-2,3-dicarboxylic acid.

Several considerations prompted us to re-examine this attractive ligand:

- The ligand combines the coordinating properties of the pyridine and carboxylate groups plus the fact that the pyrazine moiety may act as a bridge and, thus, enhance the formation of coordination polymers.
- By virtue of its polydentate character and flexibilty, the ligand can bind to metal ions in a variety of bonding modes. Each coordination mode being adopted by rotation of the substituents about the bonds connecting them to the central pyrazine ring.
- The use of complementary hydrogen-bond interactions has proved an effective tool in the formation of supramolecular aggregates[47]. The hydrogen bonding increases the dimensionality of the system and provides structural varieties in the crystal structure. The hydrogen-bonding mode and distances play an important role in the final structure of the hydrogen-bonded polymers (figure 14).

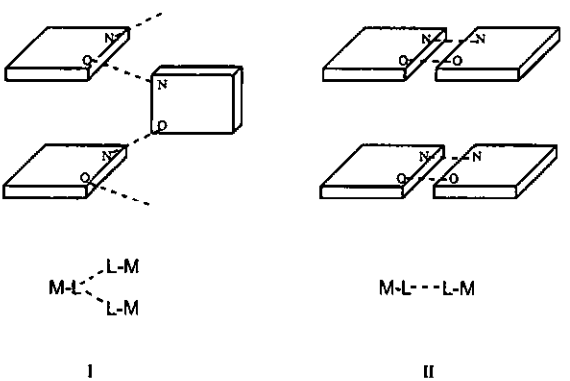

Figure 14. Schematic representation of two types of hydrogen-bonds in hydrogen-bonded supramolecules.

H_2L is a good candidate for constructing hydrogen-bonded metal-complex supramolecules as it has both coordination and hydrogen-bonding groups.

- Pyrazine, having a system of π delocalized electrons, can support spin-spin interactions between paramagnetic metal ions. In general, the magnitude of the exchange through this ligand is weak. By adding coordinating substituents to the pyrazine ring, one may investigate whether there is a steric restriction on the effectiveness of the bridge as a magnetic exchange pathway.

1.2 Synthesis

5,6-bis(2-pyridyl)-pyrazine-2,3-dicarboxylic acid (H_2L) was first synthesized by Wang[28] according to figure 15.

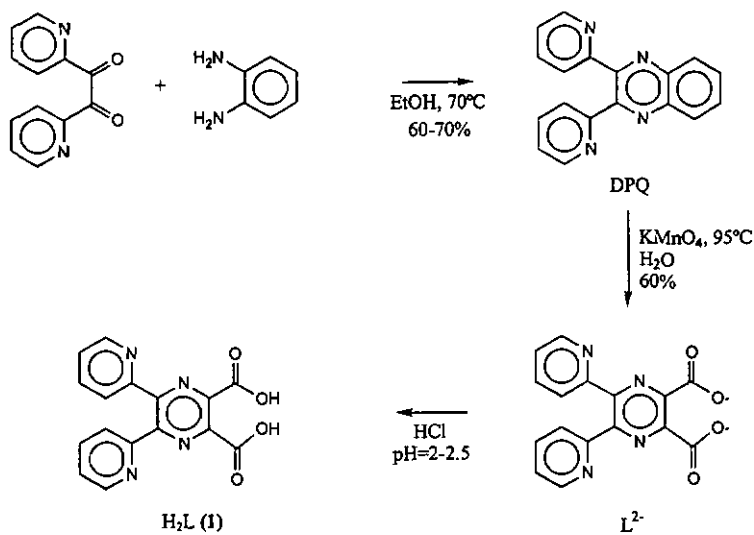

Figure 15. Synthesis of 5,6-bis(2-pyridyl)-pyrazine-2,3-dicarboxylic acid **(1)**.

The condensation of α,β-dicarbonyl compounds with α,β-diamino compounds has been much used in the synthesis of arylpyrazines. This reaction was used to prepare 2,3-bis(2-pyridyl)-quinoxaline (DPQ) by condensation of 2,2'-pyridyl and o-phenylenediamine in ethanol according to the procedure described by Goodwin and Lions[35]. This step was followed by permanganate oxidation of 2,3-bis(2-pyridyl)-quinoxaline (DPQ) to yield 5,6-bis(2-pyridyl)-pyrazine-2,3-dicarboxylate (L^{2-}); the oxidation of quinoxalines being the usual procedure to prepare pyrazine-carboxylic acids[48]. 5,6-bis(2-pyridyl)-pyrazine-2,3-dicarboxylic acid (H_2L) was isolated as a crystalline pale yellow solid upon acidification with HCl 6N until a pH between 2 and 2.5.

Recrystallisation from HCl 1N lead to the formation of the triprotonated form $[H_3L]Cl{\cdot}2.25H_2O$ **(2)**. The reaction of H_2L either with $HClO_4$ (1N) or $AgPF_6$ revealed the formation of a second triprotonated form $[H_3L]X{\cdot}3H_2O$ (X= ClO_4^-, PF_6^-) **(3, 4)**.

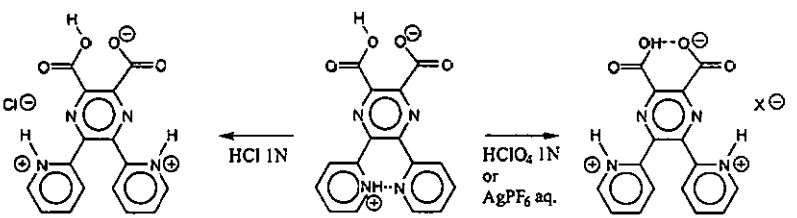

Figure 16. Protonation of the ligand 5,6-bis(2-pyridyl)-pyrazine-2,3-dicarboxylic acid.

1.3 Characterization

1.3.1 IR spectrum

The IR spectra of H_2L (1) exhibit strong bands at 1709, 1659 and 1340 cm^{-1}. Because it has been determined by X-ray analysis that H_2L (**1**) has a zwitterion structure, these bands are assigned to C=O stretching (1709 cm^{-1}), COO^- antisymmetric stretching (1659 cm^{-1}) and COO^- symmetric stretching vibrations (1340 cm^{-1}).

The IR spectra of the triprotonated forms **2-4** show strong bands at ca. 1720, 1620 and 1360 cm^{-1}, which can be assigned to C=O stretching, COO^- antisymmetric stretching and COO^- symmetric stretching vibrations, respectively. Therefore, these forms have both COOH and COO^- groups, indicating that protonation of the second pyridine ring has occurred.

Despite the complexity of the IR spectra of coropounds **1-4** an attempt has been made to assign the best defined absorptions[49] and their frequencies are compared in Table 1.

1

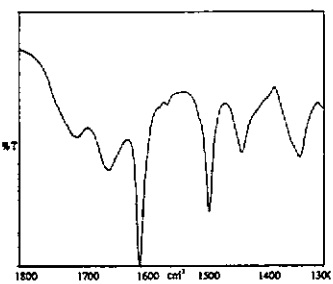

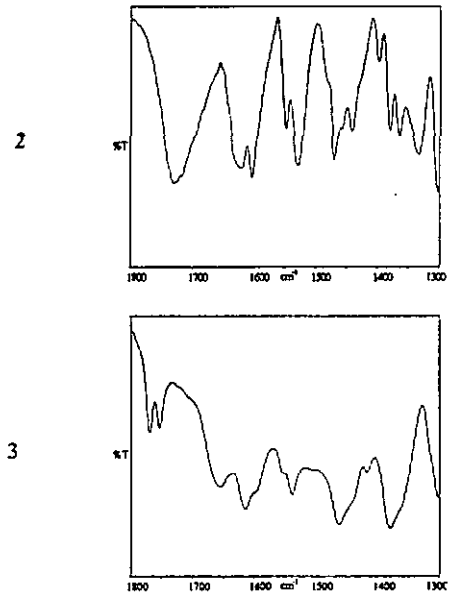

Figure 17. IR spectra of compounds 1-3.

Table 1. Assignment of IR absorptions (cm^{-1}) of compounds 1-4.

1	2	3	4	Assignment
3424 br. m, 2568 br. m	3543 w, 3289 br. s., 2839 br. s, 2200 br. m, 1891 br, m	3417 br. s, 3349 br. s, 2872 br. m, 2585 br. m, 2012 br. m	3387 br. s, 2590 br. m, 2107 br. m	Lattice H_2O and H-bonds
1709 m	1727 vs	1733 vs	1652 m	υ(C=O)
1659 s	1619 m	1620 m	1617 s	$\upsilon_{as}(COO^-)$
1602 s, 1557 w, 1488 s, 1435 m	1602 s, 1548 m, 1527 m, 1468 m, 1440 m	1607 s, 1529 m, 1460 m, 1436 w	1600 m, 1539 w, 1456 s, 1420 w	υ(C=N), υ(C=C)
1340 m	1379 m, 1364 m	1375 m, 1355 m	1378 vs	$\upsilon_s(COO^-)$, υ(C-O)

vs very strong, s strong, m medium, w weak, br broad

1.3.2 NMR spectra

The ^{1}H NMR spectra of H_2L (1) (figure 18) displays four sets of resonances in the aromatic region, and each is assigned to a given pair of equivalent nuclei on the basis of the expected splitting patterns.

Rotation of the substituents about the C-C bonds connecting them to the central pyrazine ring is supposed to occur easily in aqueous solution. This dynamic behaviour causes both pyridine rings to be equivalent, explaining the presence of four groups of signals instead of eight in the aromatic region. Moreover, the signals corresponding to the acid hydrogen, H2 and H3, do not appear due to a rapid exchange with the solvent.

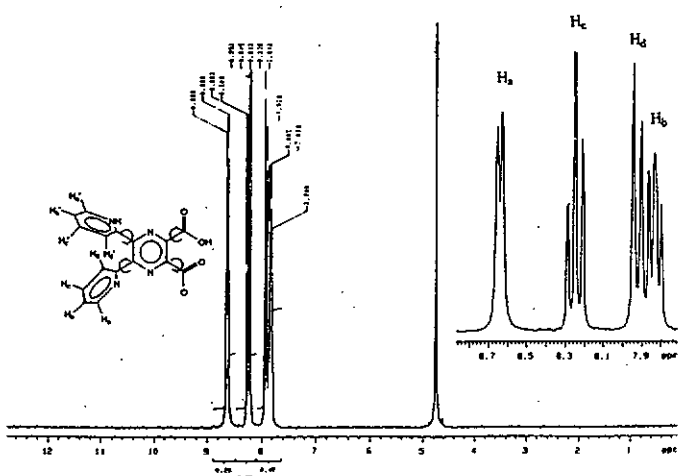

Figure 18. ^{1}H NMR spectra of compound **1** (D_2O, 400 MHz).

No significant differences have been observed in the ^1H NMR spectra of compounds 2-4 with respect to that of compound 1.

1.3.3 UV-VIS spectroscopy

The UV-Visible spectrum of the ligand in aqueous solution exhibits a broad band around 300 nm.

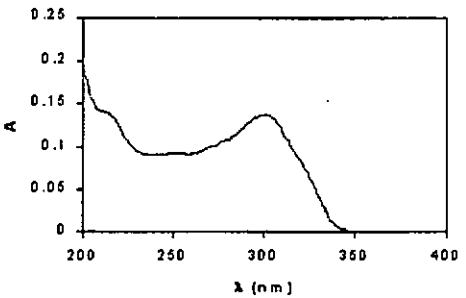

Figure 19. UV spectra of the ligand in aqueous solution.

Spectral results in aqueous solution are summarized in table 2.

Table 2. UV spectra of the ligand (c= 10^{-5}M, l=1cm)

λ_{max} (nm)		ε ($M^{-1}\cdot cm^{-1}$)
301		9971
212	(shoulder)	9524

1.3.4 Description of the structures

H_2L (1)

The X-ray structure analysis of H_2L (1) reported previously[28] revealed that this compound exists as an inner zwitterion salt. As a result of an intramolecular hydrogen-bond N^+-H...N between the N atoms of adjacent pyridine rings, which are only 2.530 Å appart, the pyridine rings are almost coplanar to the central pyrazine ring with dihedral angles HpyI^pyz= 4.4(1)° and pyII^pyz= 7.9(1)°. This rather short intramolecular hydrogen-bond (N3-H3= 1.234 Å and H3...N4= 1.313 Å) leads to a slight twist of the pyrazine ring ([C1-N1-C4]^[C2-N2-C3]= 3.5(4)°) as well as to two unusually large exocyclic angles, C3-C4-C5= 131.0(3)° and C4-C3-C10= 131.1(3)°. This type of hydrogen-bond has been reported previously for the substituted quinoxaline 2,3-bis(2-pyridyl)-6,7-dimethylquinoxaline tetrafluoroborate[50]. In addition, each molecule in the crystal is involved in two strong intermolecular hydrogen-bonds to two neighbouring molecules to form a double stranded molecular ribbon.

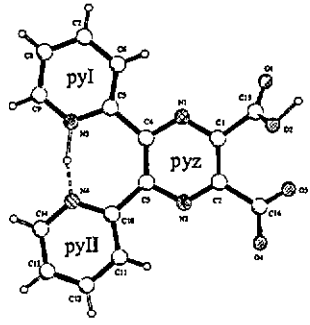

Figure 20. Molecular structure of compound H_2L (1).

$[H_3L]Cl{\cdot}2.25H_2O$ (2)

Recrystallization of H_2L (1) from HCl 1N yielded colourless single crystals of $[H_3L]Cl{\cdot}2.25H_2O$ (2), whose structure determination proved important changes. The largest difference concerns the orientation of the adjacent pyridine rings with respect to the pyrazine ring, which is very different from that observed in the diprotonated form 1. As a result of the protonation of both pyridine rings, they are rotated from their original positions (the dihedral angles being 49.2(1)° (pyl^pyz), 30.7(1)° (pyII^pyz) and 65.6(1)° (pyl^pyII)). This places the pyridine N-atoms slightly above and below the pyrazine plane. However, a deformation of the pyrazine ring is also observed in compound 2 (twist angle 4.9(2)°). As in the diprotonated form 1, the protonated carboxylate group is out of the plane of the pyrazine ring by 75.7(1)° (compared with 58.3(1) in 1) whereas the deprotonated carboxylate group is inclined to the pyrazine plane by only 15.5(4)° (compared with 38.0(1)° in 1).

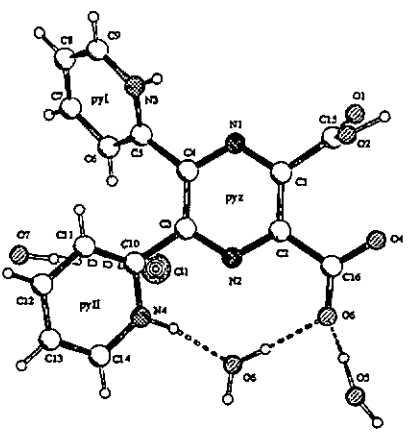

Figure 21. Molecular structure of compound $[H_3L]Cl{\cdot}2.25H_2O$ **(2)**.

The triprotonated form **2** also differs from **1** in the type of hydrogen bonding. There are no intramolecular hydrogen-bonds in the crystal structure of compound **2** and neighbouring molecules are linked by a 3D hydrogen-bonding network involving the N-atoms of both protonated pyridine rings, the O-atoms of the carboxylate groups, the lattice water molecules and the Cl^- anion.

$[H_3L]ClO_4 \cdot 3H_2O$ (3)

Colourless block-like crystals of a new triprotonated form $[H_3L]ClO_4 \cdot 3H_2O$ **(3)** have been obtained upon slow evaporation of a solution of H_2L **(1)** in $HClO_4$ 1N. The X-ray analysis showed that the structure of compound **3**, which possesses C_2 symmetry, differs significantly from that of compound **1**.

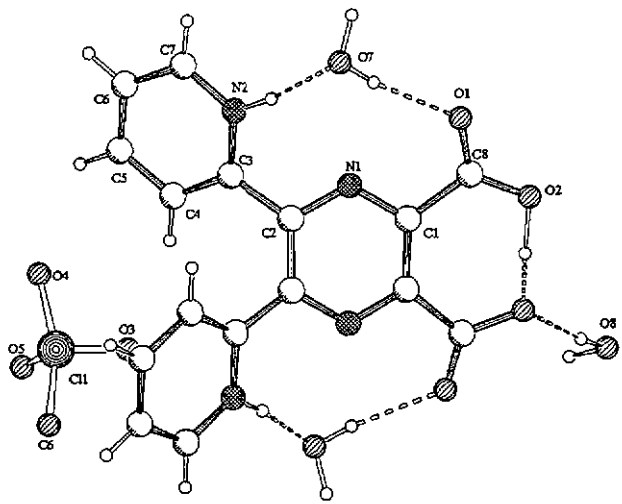

Figure 22. Molecular structure of compound $[H_3L]ClO_4 \cdot 3H_2O$ **(3)**.

Much of the difference results from the protonation of the second pyridine ring. As a consequence of the steric repulsion between the protons attached to N2 and $N2^{i}$ (symmetry operation i= -x, y, -z+1/2), the pyridine rings are twisted out of the pyrazine plane by 34.8(1)° and in opposite directions. Thus, the orientation of the pyridine rings is similar to that found in compound **2**. On the other hand, the protonated carboxylic group bas moved into the plane of the pyrazine ring (the carboxylate groups being inclined to the pyrazine plane by 19.6(4)° and to one another by 5.1(5)°). This results in a strong and symmetric intramolecular hydrogen-bond between adjacent carboxylate groups (O2-H2= H2...$O2^{i}$= 1.201(1) Å, O2...$O2^{i}$= 2.394(1) Å and O2-H2...$O2^{i}$= 171.14(8)°; symmetry operation i= -x, y, -z+1/2). This type of hydrogen bond has been described before for the ligands 2,3-pyrazine-dicarboxylic acid[51,52] and 2,3,5,6-pyrazine-tetracarboxylic acid[27]. It is interesting to note that the deviation from planarity of the pyrazine ring is larger than in compounds **1** and **2**, with a twisting angle of 9.5(6)°.

In the crystal structure of compound **3**, the $[H_3L]^+$ cations and the lattice water molecules participate in an extensive 2D hydrogen-bonding network.

$[H_3L]PF_6 \cdot 3H_2O$ (4)

In the reaction of H_2L with $AgPF_6$ in water no complex was formed but slow evaporation of the solution gave crystals of $[H_3L]PF_6 \cdot 3H_2O$ (**4**), whose structure analysis showed them to be isomorpbus with $[H_3L]ClO_4 \cdot 3H_2O$ (**3**).

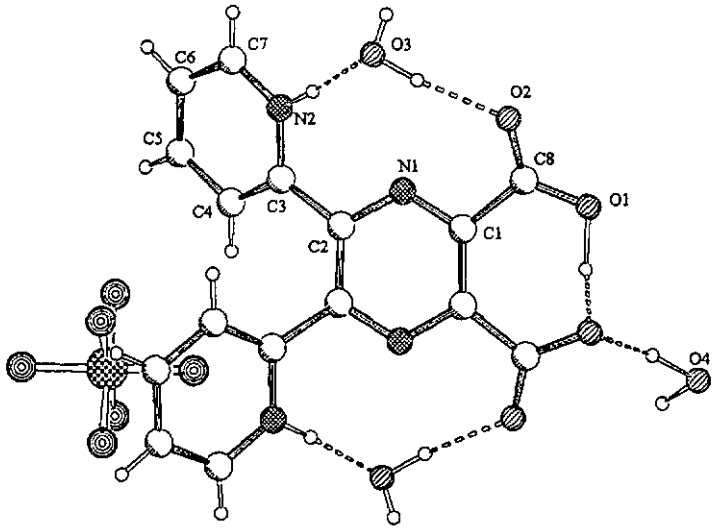

Figure 23. Molecular structure of compound $[H_3L]PF_6 \cdot 3H_2O$ (4)

1.3.5 Comparison of the structures 1-4

The diprotonated form H_2L (1) exhibits a strong intramolecular hydrogen-bond between the N-atoms of the pyridine rings which forces them to be simultaneously coplanar to the pyrazine system.

Protonation of the second pyridine N-atom in 2-4, hinders the planar conformation. The steric repulsion between protons attached to the N-atoms of the pyridine rings is minimized by rotation of the pyridine rings out of the pyrazine plane. Similar dihedral angles between the pyrazine ring and the groups attached to it are compared for

compounds **1-4** in Table 3. As seen from the twist angle, varying from 3.5° to 9.5°, the pyrazine ring is slightly twisted in all four compounds. The twist of the pyrazine ring seems to be imposed to minimise steric repulsions between the substituents. A similar distortion has been observed for the different forms of the ligand TPPZ[53-55]. In all four compounds the crystal cohesion is ensured by intermolecular hydrogen bonding but no significant π-π interactions between pyrazine or pyridine rings is observed.

Table 3. A comparison of various dihedral angles (°) in compounds 1-4.

Angles	1	2	3	4
pyz twist	3.5(4)	4.9(2)	9.5(6)	9.8(4)
pyz^pyI	4.4(1)	49.2(1)	34.8(1)	35.7(1)
pyz^pyII	7.9(1)	30.7(1)	34.8(1)	35.7(1)
pyI^pyII	3.8(1)	65.6(1)	62.2(1)	64.6(1)
COOH^pyz	58.3(1)	75.7(1)	19.6(4)	20.1(3)
COO^pyz	38.0(1)	15.5(4)	19.6(4)	20.1(3)
COOH^COO	59.7(4)	89.4(3)	5.1(5)	5.7(4)

2 TRANSITION METAL COMPLEXES WITH THE LIGAND 5,6-BIS(2-PYRIDYL)-PYRAZINE-2,3-DICARBOXYLIC ACID

The main objective of this work was to learn how the ligand 5,6-bis(2-pyridyl)-pyrazine-2,3-dicarboxylic acid (hereafter H_2L) reacts with transition metal ions particularly from the point of view of structure and exchange coupling. Consequently, we have concentrated on the isolation of crystalline products amenable to X-ray structural characterization.

The combination of H_2L with transition metal ions was anticipated to yield interesting results. The ligand H_2L as well as the single HL^- and double deprotonated L^{2-} forms have eight possible coordination sites and, therefore, were expected to bind to metal ions in a variety of ways.

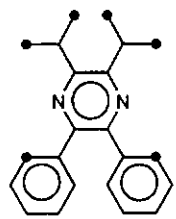

So far eight different coordination modes, shown in figure 24, have been observed for this extremely versatile ligand. The non-bridging modes (a)-(c) involve a bis-chelate tridentate interaction to one metal ion, leaving the rest of the donor atoms uncoordinated. Consequently, complexes exhibiting these bonding modes could be used as ligands towards other metals. In the binucleating bridging modes (d) and (e), besides the tridentate interaction, bonding to a second metal atom through a single carboxylate oxygen is also observed. In (f) two metal ions are linked by a ligand molecule acting in a bis-tridentate manner. The extraordinary diversity of the ligand is proved once more in the unusual tri- and tetranucleating modes (g) and (h), respectively.

non-bridging modes

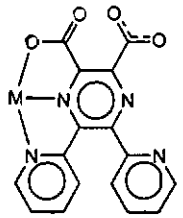

(a)

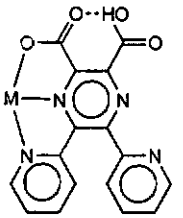

(b)

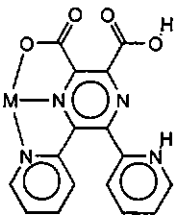

(c)

bridging modes

binucleating modes

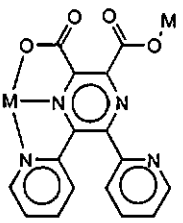

(d)

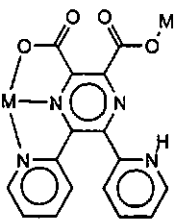

(e)

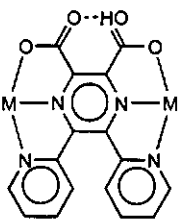

(f)

tri- and tetranucleating modes

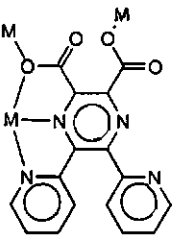

(g)

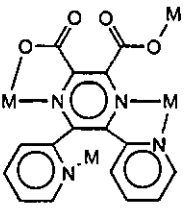

(h)

Figure 24. The main types of coordination modes of ligand H_2L and its deprotonated forms HL^- and L^{2-}.

2.1 Maoganes(II) complex

A dinuclear complex of manganes(II), $[Mn_2L_2(H_2O)_4]\cdot 4H_2O$ **(5)**, was obtained by adding H_2L to an aqueous solution of $MnCl_2\cdot 4H_2O$. On leaving the resulting solution to stand for several days, yellow crystals of complex **5** were obtained.

$$MnCl_2 \cdot 4H_2O + H_2L \xrightarrow[54\%]{H_2O,\ rt} [Mn_2L_2(H_2O)_4] \cdot 4H_2O\ (5)$$

The IR spectrum of complex **5** shows just one broad band in the υ(C=O) region, at 1636 cm^{-1}, indicating the presence of deprotonated carboxylate groups only. Tbe shift to lower frequency of the $\upsilon_{as}(COO^-)$ absorption band compared to the free ligand (see Table 4) indicates coordination of both carboxylate groups.

Table 4. Comparison of the IR absorptions (cm^{-1}) of compound **5** with those of the free ligand H_2L **(1)**.

	H_2L **(1)**	$[Mn_2L_2(H_2O)_4]\cdot 4H_2O$ **(5)**
$\upsilon(C=O)/\ \upsilon_{as}(COO^-)$	1727 vs, 1659 s	1636 s
υ(C=N), υ(C=C)	1602 s, 1557 w, 1488 s, 1435 m	1598 vs, 1545 w, 1475 m, 1440 m, 1410 w
$\upsilon_s(COO^-)$	1340 m	1366s, 1348 s

vs very strong, s strong, m medium, w weak

The bands at 1366 and 1348 cm^{-1}, which are assigned to the symmetric stretching mode, $\upsilon_s(COO^-)$, suggest two different carboxylate coordination modes. The carboxylate groups may coordinate to metal ions in one of the bonding modes depicted in figure 25. The separation (Δ) between $\upsilon_{as}(COO^-)$ and $\upsilon_s(COO^-)$ depends on the carboxylate coordination mode[56]. In complexes containing N,O-pyrazine ligands it is difficult to determine the coordination mode of the carboxylate group from the IR spectra due to the large number of bands in the region of study. The bands associated with the υ(C=N) and υ(C=C) stretching vibrations of the heterocyclic rings occur between 1400 and 1600 cm^{-1}.

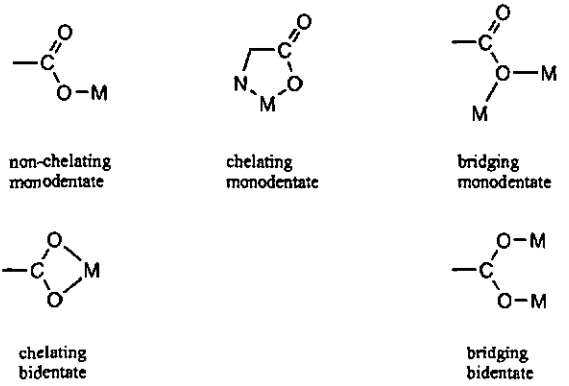

Figure 25. Carboxylate coordination modes in pyrazine-carboxylate complexes.

$[Mn_2L_2(H_2O)_4]\cdot 4H_2O$ (5)

Single-crystal X-ray analysis established that compound **5** exhibits a dinuclear structure, $[Mn_2L_2(H_2O)_4]\cdot 4H_2O$, where each ligand molecule coordinates in an asymmetric manner; while one side of the ligand is coordinated in a bis-chelate

tridentate fashion the opposite side coordinates in a monodentate way linking two MnL units related by a center of symmetry. This gives rise to a "box-like" dimer. On one side of the ligand the N-atoms of the pyrazine and pyridine moieties remain uncoordinated. The pyridine ring is considerably twisted out of the plane of the pyrazine ring; the dihedral angle pyz^pyII being 65.4(1)°. Although the tridentate domain of the ligand is almost coplanar to the pyrazine system (with dihedral angles pyz^pyI= 18.6(2)° and pyz^$COO_{chelat.}$= 7.8(6)°), the monodentate carboxylate is almost perpendicular to the pyrazine plane (pyz^$COO_{mono.}$= 82.9(2)°).

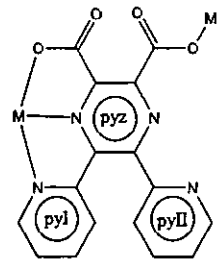

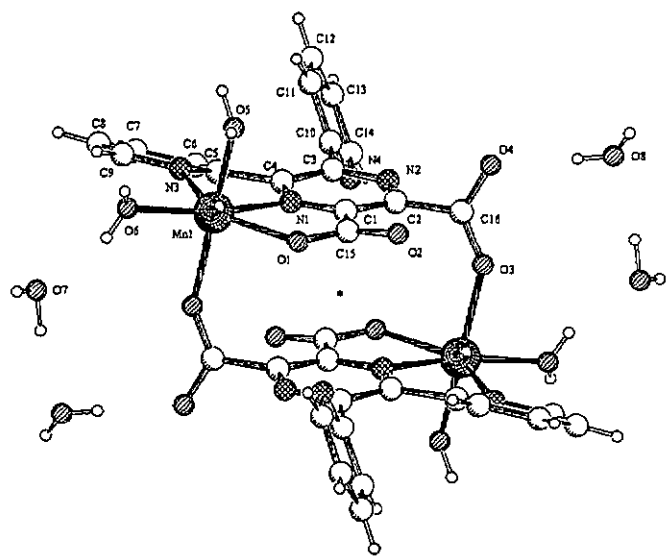

Figure 26. View of the dinuclear complex $[Mn_2L_2(H_2O)_4]\cdot 4H_2O$ **(5)** emphasising the box-like structure.

Each metal is further coordinated by two water molecules, the overall geometry about the Mn(II) ions being distorted octahedral. All the Mn-N and Mn-O distances are normal for octahedral high-spin Mn(II) ions, including the Mn1-N3 distance of 2.311(3)Å which is longer than any other. In Table 5 the bond distances and angles involving the Mn(II) atoms are compared for compound 5 and the Mn(II)-pyrazine complexes reported in the Cambridge Crystallographic Data Base (CSD). It can be seen that except in the case of $\{[Mn(H_2pztc)(H_2O)_2]\cdot 2H_2O\}_n$[27] the geometries about the Mn(II) ions are very similar.

Table 5. A comparison of metal bond distances and chelate angles in Mn(II) complexes containing substituted pyrazine ligands.

	Bond distances (Å)					*Bond angles (°)*	
Compound	$Mn\text{-}N_{pyz}$	$Mn\text{-}N_{py}$	$Mn\text{-}O_{chelate}$	$Mn\text{-}O_{bridge}$	$Mn\text{-}O_{w}$	$N_{pyz}\text{-}Mn\text{-}N_{py}$	$N_{pyz}\text{-}Mn\text{-}O$
$[Mn_2L_2(H_2O)_4]\ 4H_2O$ (5)	2.239(1)	2.311(3)	2.226(1)	2.139(1)	2.144(1)	70.03(1)	71.90(1)
					2.147(1)		
$\{(H_3O)_2[Mn(pzdc)_2]\}_n$[23]	2.308(1)		2.149(1)	2.136(1)			73.58(4)
$\{[Mn(pzdc)(H_2O)_2]\cdot 2H_2O\}_n$[22]	2.294(2)		2.160(2)	2.167(2)	2.115(2)		73.62(8)
				2.226(2)	2.151(2)		
$\{[Mn(H_2pztc)(H_2O)_2]\cdot 2H_2O\}_n$[27]	2.463(1)		2.233(1)		2.203(1)		67.05(3)
			2.411(1)				63.91(3)
$\{K_2[Mn(pztc)(H_2O)]\cdot 2.25H_2O\}_n$[27]	2.198(4)		2.238(4)	2.157(4)	2.135(4)		72.0(1)
			2.257(4)	2.178(4)			71.5(1)
$[Mn_2(NO_3)_4(bppz)(H_2O)_2]$[57]	2.274(4)	2.242(5)			2.151(5)	72.44(1)	

Hydrogen-bonding plays an important role in the packing scheme of this compound. Hydrogen-bonding interactions involving the carboxylate O-atoms and coordinated and crystallisation water molecules link neighbouring dinuclear units, resulting in a one-dimensional hydrogen-bonded polymer whicb runs parallel to the [011] direction (figure 27).

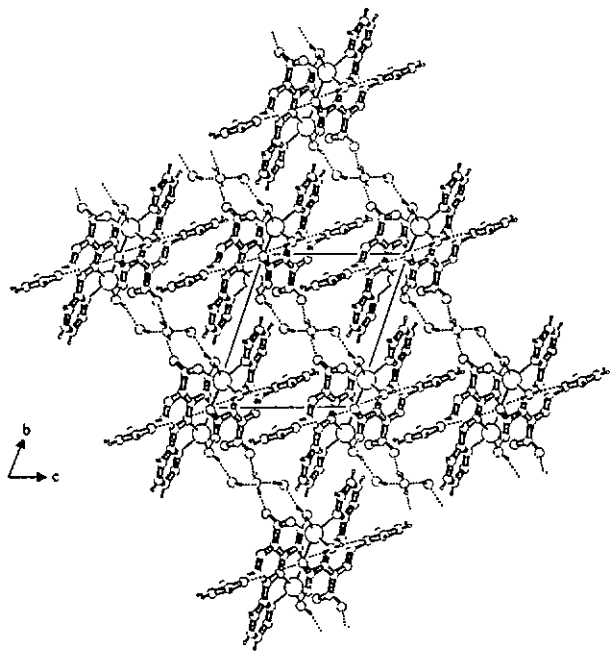

Figure 27. Packing diagram for complex **5** down the a-axis showing the hydrogen-bonding.

The possibility of magnetic exchange interactions mediated by the bridging ligand L^{2-} in **5** was investigated by examining the magnetic susceptibility of a powdered sample in the T range 300-2 K. The μ_{eff}/Mn in compound **5** is 5.90 M.B. at 300K, which is close to the value for a high-spin S=5/2 ion with g_i= 2.0 (5.92 M.B.), and remains almost constant with decreasing temperature until 17K (5.68 M.B.), whereupon it falls sharply to 4.53 M.B. at 2.5K.

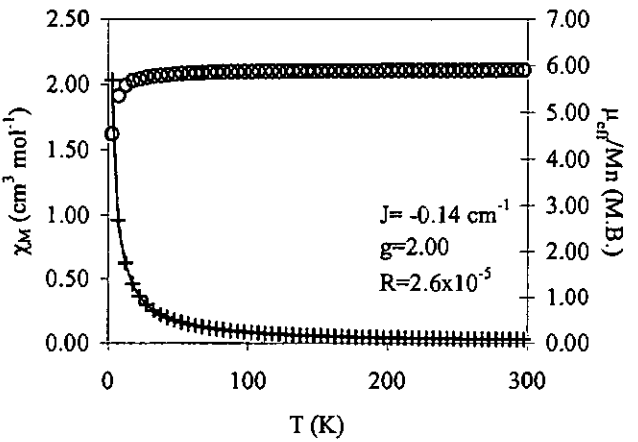

Figure 28. Experimental and theoretical (—) temperature dependence of χ_M(+) and μ_{eff}(o) for complex **5**.

In view of the known dinuclear structure of compound **(5)**, the experimental data was fitted to the theoretical expression derived from the isotropic Heisenberg model $\hat{H} = -2JS_1S_2$ for a $S_1 = S_2 = 5/2$ situation[58].

$$\chi_M = \frac{Ng^2\beta^2}{kT}\frac{2e^x + 10e^{3x} + 28e^{6x} + 60e^{10x} + 110e^{15x}}{1 + 3e^x + 5e^{3x} + 7e^{6x} + 9e^{10x} + 11e^{15x}}$$

The best fit to the experimental data was found for J= -0.14 cm^{-1} and g= 2.00, which agrees with the presence of Mn(II) ions which do not exhibit second-order spin-orbit coupling. The magnitude of J is small and shows that the antiferromagnetic exchange in compound **5** is very weak. The CO_2^- group engaged in the non-chelate bonding mode is almost perpendicular to the heterocyclic plane, sucb a situation does not favour magnetic exchange interactions.

The ESR spectra of a powdered sample of complex **5** was recorded at room temperature. The room-temperature X-band powder spectra of complex **5** is typical of a high spin Mn(II), suggesting the two Mn(II) ions in the dinuclear complex to be magnetically equivalent. The expected six-line hyperfine structure for ^{55}Mn (I=5/2) is isotropic and centred at g= 2.00 with an average byperfine coupling constant $|A| = 98 \pm 1G$ (figure 29). The temperature dependence of the lineshape has been studied. The six-line resonance pattern looses intensity upon cooling which is consistent with the presence of some Mn(II) nearest neighbour interactions leading to the broadness of the EPR absorption.

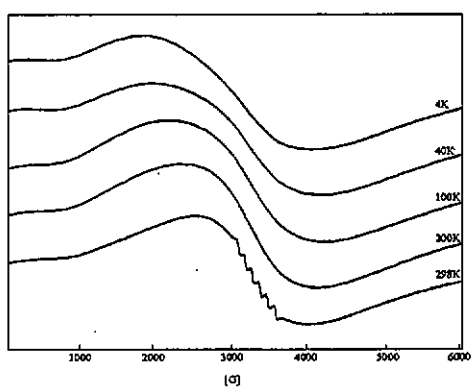

Figure 29. X-band ESR spectra of a polycrystalline sample of compound $[Mn_2L_2(H_2O)_4]\cdot 4H_2O$ **(5)**.

2.2 Iron(II) complex

When $FeCl_2 \cdot 4H_2O$ was added to a degassed aqueous solution of H_2L a deep purple solution was obtained. Purplish black crystals of compound **6** formed, after slow evaporation, within a period of several weeks.

$$FeCl_2 \cdot 4H_2O + H_2L \xrightarrow[H_2O,\ 70°C]{} [Fe_2L_2(H_2O)_4] \cdot 4H_2O\ (\mathbf{6})$$

46%

The IR spectrum lends to support the fact that complex **6** may be isomorphus with **5** (consistent with the elemental analysis).

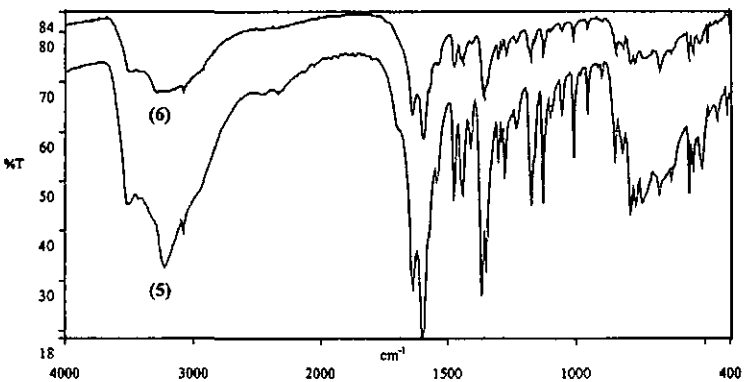

Figure 30. Comparison of the IR spectra of complexes $[Mn_2L_2(H_2O)_4] \cdot 4H_2O$ **(5)** and $[Fe_2L_2(H_2O)_4] \cdot 4H_2O$ **(6)**

Table 6. Comparison of the IR absorptions (cm^{-1}) of compounds **5** and **6**.

	$[Mn_2L_2(H_2O)_4]\cdot 4H_2O$ **(5)**	$[Fe_2L_2(H_2O)_4]\cdot 4H_2O$ **(6)**
$\upsilon(C=O)/\ \upsilon_{as}(COO^-)$	1636 s	1640 s
$\upsilon(C=N)$, $\upsilon(C=C)$	1598 vs, 1545 w, 1475 m, 1440 m, 1410 w	1593 vs, 1545 w, 1475 m, 1440 m, 1405 w
$\upsilon_s(COO^-)$	1366s, 1348 s	1359 s

vs very strong, s strong, m medium, w weak

$[Fe_2L_2(H_2O)_4]\cdot 4H_2O$ (6)

A preliminary study of the cell parameters of complex *6* confirmed it to be isomorphus with the Mn(II) complex **5**, described above. In the dinuclear $[Fe_2L_2(H_2O)_4]$ core, each metal center is coordinated to two symmetry related L^{2-} molecules; to a tridentate bis-chelating domain of one molecule and to a monodentate non-chelating carboxylate of the second molecule. As a result, a rectangular cavity is formed with a M...M separation of 6.501(1)Å.

The bond distances and angles involving the Fe(II) atom in complex 6 are comparable with those of Fe(II)-pyrazine complexes found in the Cambridge Crystallographic Data Base (CSD) (see table 7). The analysis of the metal-ligand bond distances suggests a high-spin Fe^{2+} situation.

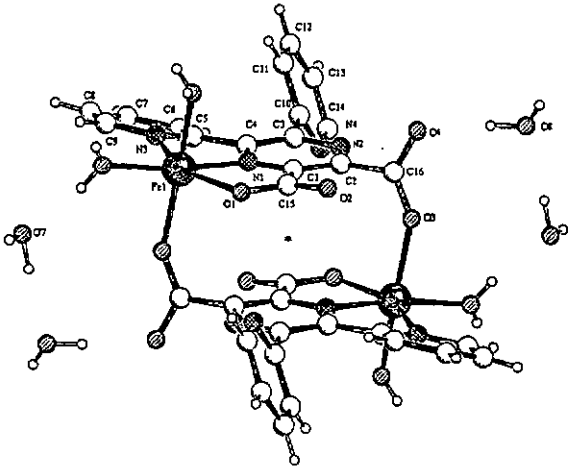

Figure 31. Molecular structure of compound $[Fe_2L_2(H_2O)_4]\cdot 4H_2O$ **(6)** showing the rectangular cavity.

Table 7. Metal bond distances in Fe(II) complexes with pyrazine ligands.

Compound	*Bond distances (Å)*				
	$Fe\text{-}N_{pyz}$	$Fe\text{-}N_{py}$	$Fe\text{-}O_{chelat.}$	$Fe\text{-}O_{mono.}$	$Fe\text{-}O_{w}$
$[Fe_2L_2(H_2O)_4]\ 4H_2O$ **(6)**	2.126(2)	2.205(3)	2.132(2)	2.105(2)	2.067(2)
					2.115(2)
$[Fe(L)_2(H_2O)_2]$ with HL= pyrazinecarboxylic acid[59]	2.12(1)		2.11(1)		2.14(1)
$\{[Fe(H_2pztc)(H_2O)_2]\cdot 2H_2O\}_n$[60]	2.219(8)		2.075(6)		2.133(6)
$[Fe_2(SO_4)_2(bppz)(H_2O)_6]\cdot 2H_2O$[57]	2.18(1)	2.18(2)			2.06(1)-
					2.16(2)
$[Fe^{II}(TPPZ)][(dipic)_2Fe^{III}]_2$	1.87(1)	1.94(1)			
$dipicH_2$= dipicolinic acid[61]	1.89(1)	1.96(1)			

The magnetic properties of complex **6** are depicted in figure 32 in the form of both χ_M and μ_{eff} versus T plots. The magnetic moment per iron of 5.35 M.B. at 300K indicates that the Fe(II) ions are high-spin at room temperature. The μ_{eff}/Fe decreases slowly down to 20K (4.90 M.B.) and then more rapidly from 20K to 1.8K (3.25 M.B.), indicating a very weak antiferromagnetic coupling of the S=2 systems of the two ferrous ions of each dinuclear unit and/or possibly single-ion zero-field splitting (ZFS). We have analyzed the temperature variation of the magnetic susceptibility of complex **6** by using the expression derived from the isotropic spin-exchange Hamiltonian $\hat{H} = -2JS_1S_2$ $(S_1 = S_2 = 2)$ [62]. The least-squares refinement of the experimental data to the theoretical magnetic susceptibility calculated from this model afforded the parameters J= -0.30 cm^{-1} and g= 2.11 (residual $1.28 \cdot 10^{-3}$).

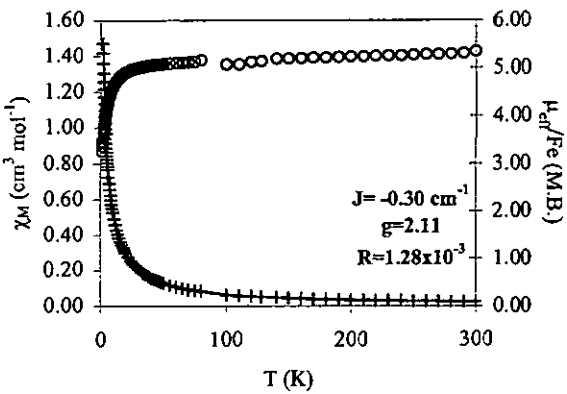

Figure 32. Magnetic susceptibility (+) and magnetic moment (o) of complex **6** plotted against temperature.

2.3 Cobalt(II) complexes

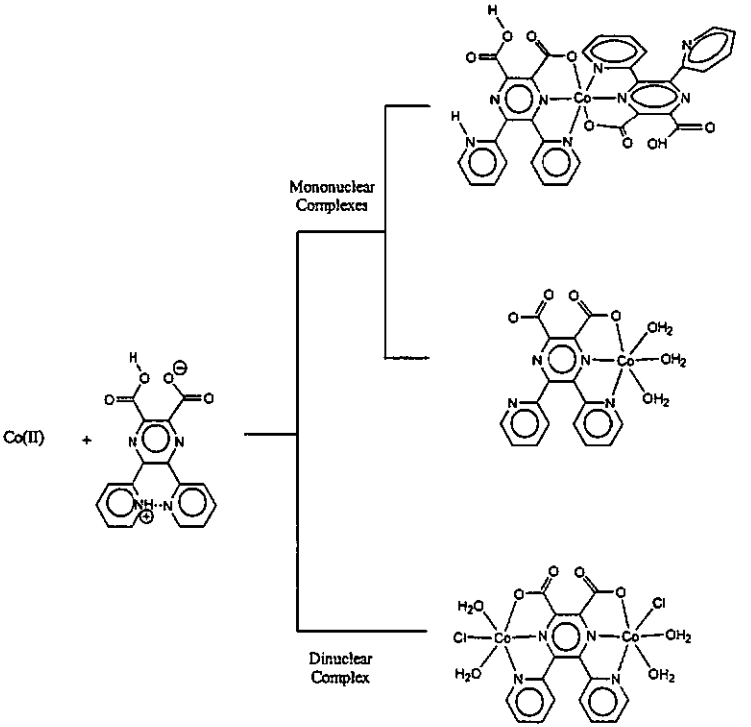

Three complexes of formula $[Co(HL)(H_2L)]ClO_4 \cdot 2H_2O$ (7), $[CoL(H_2O)_3] \cdot 3H_2O$ (8) and $[Co_2(HL)Cl_2(H_2O)_4]Cl \cdot 4H_2O$ (9) were obtained by reacting the ligand H_2L with cobalt(II) salts in different solvents.

$$Co(ClO)_4 \cdot 6H_2O + H_2L \xrightarrow[H_2O/MeOH,\ rt]{} [Co(HL)(H_2L)]ClO_4 \cdot 2H_2O \ (7)$$

$$Co(NO_3)_2 \cdot 6H_2O + H_2L \xrightarrow[H_2O,\ rt]{} [CoL(H_2O)_3] \cdot 3H_2O \ (8)$$

$$CoCl_2 \cdot 6H_2O + H_2L \xrightarrow[MeOH,\ rt]{} [Co_2(HL)Cl_2(H_2O)_4]Cl \cdot 4H_2O \ (9)$$

The IR spectra of complexes 7-9 show the bands characteristic of the ligand. Evidence for the ligand coordination is provided by the shift of the stretching frequencies υ(C=O), $\upsilon_{as}(COO^-)$, $\upsilon_s(COO^-)$ and υ(C=N) compared to the free ligand. Despite the complexity of the IR spectra in the region of study, it is possible to distinguish the different coordination modes of the ligand (see table 8).

Table 8. Comparison of the IR absorptions (cm^{-1}) for compounds 7-9.

	7	8	9
υ(C=O)/ $\upsilon_{as}(COO^-)$	1740 m, 1725 s, 1657 vs, 1632 s	1635 s,1619 s	1701 m, 1628 s
υ(C=N), υ(C=C)	1602 s, 1541 m, 1525 m, 1473 m, 1447 m, 1402 w	1598 vs, 1470 m, 1450 m, 1426 w, 1403 m	1600 vs, 1544 m, 1472 m, 1454 m
$\upsilon_s(COO^-)$	1354 s	1366 s, 1340 s	1372 vs

vs very strong, s strong, m medium, w weak

[Co(HL)(H$_2$L)]ClO$_4$·2H$_2$O (7)

[Co(HL)(H$_2$L)]ClO$_4$·2H$_2$O (7) *is a mononuclear complex in which two ligand* molecules, corresponding to a monoanion (HL^-) and a neutral molecule (H_2L), define a distorted octahedron around the Co(II) ion. Each ligand molecule acts in a mono-tridentate bis-chelating manner (see figure 24 (b)-(c)). The narrow chelate angles N1-Co1-N3 (76.3(2)°), N1-Co1-O1 (76.5(2)°), N5-Co1-N7 (75.1(2)°) and N5-Co1-O5 (77.4(2)°), imposed by the tridentate coordination of both HL^- and H_2L molecules, give rise to a significant distortion from the regular octahedral geometry about the

Co(II) ion. The Co-N and Co-O distances are within the usual range observed for high-spin Co(II) octahedral complexes[63]. The pyrazine rings are canted by 3.0(3)° (HL') and 79.9(2)° (H_2L) relative to the equatorial plane (defined by O1, N1, N3 and N5). The lower basicity of the H_2L molecule (perpendicular to the basal plane) is defined by the larger M-Npy bond distance (Co1-N7= 2.139(5)Å compared to Co1-N3= 2.097(5)Å) and the M-O bond distance (Co1-O5= 2.136(5)Å compared to Co1-O1= 2.086(5)Å).

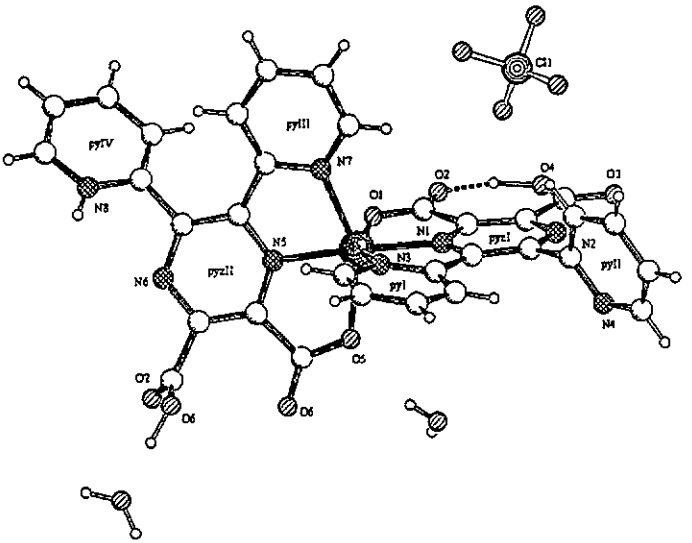

Figure 33. Molecular structure of 7, showing the distorted octahedral geometry around the Co(II) ion.

Finally, a network of hydrogen bonds connects the $[Co(HL)(H_2L)]^+$ units and lattice water molecules, the shortest Co...Co^i (i= -x+1/2, y+1/2, -z+3/2) distance being 10.018(2) Å. The electroneutrality is ensured by the presence of the counterion ClO_4^- which occupies the cavities in the hydrogen-bonding network.

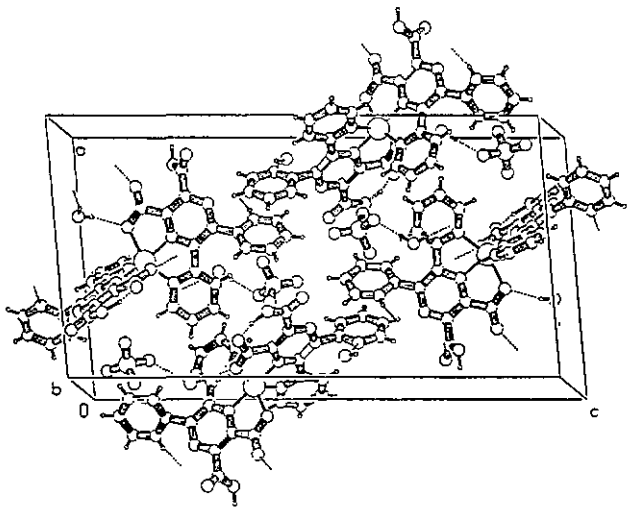

Figure 34. Crystal packing in complex 7 showing the hydrogen-bonding.

Magnetic measurements of complex 7 were undertaken from room temperature down to 1.8K. Magnetic susceptibility data reveal Curie-Weiss law behaviour over a wide temperature range (linear regression yields C=2.88, θ= -5.02K) with a magnetic moment of 4.78 M.B. per cobalt atom at room temperature. This value is typical for high-spin Co(II) complexes[64].

$$\chi = \frac{C}{T-\theta} \quad \text{where} \quad C = \frac{Ng^2\beta^2S(S+1)}{3k}$$

The slight decrease of the μ_{eff} at low temperatures is indeed expected, due to an important orbital contribution as well as to single-ion anisotropy. The g-value of 2.48, being far from 2.00, shows a strong orbital contribution.

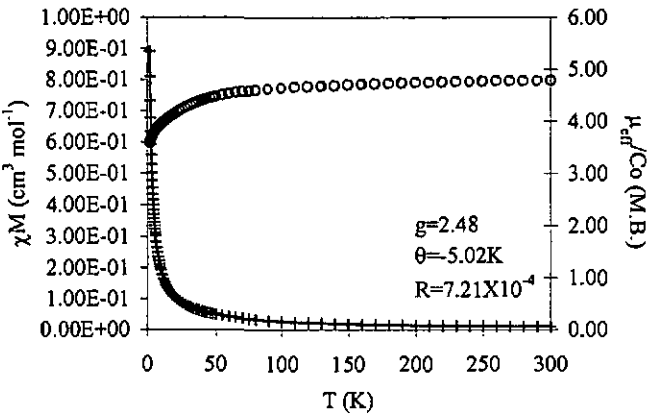

Figure 35. The temperature dependence of the magnetic susceptibility, χ_M (+), and the effective magnetic moment μ_{eff} (o) of $[Co(HL)(H_2L)]ClO_4 \cdot 2H_2O$ (7).

The EPR spectra of complex 7 was recorded for a polycristalline sample at 4K and displays a typical distorted axial pattern for high-spin Co(II) with two resonances. The effective g-values are $g_\perp = 5.87$ and $g_\parallel = 3.93$. In the EPR spectra there is no evidence of resolved hyperfine structure from the ^{59}Co nuclear spin momentum (I=7/2). This spectrum is consistent with that expected for S=3/2 molecules, with a

strong and anisotropic orbital contribution where only the Kramer's doublet ($m_s=\pm1/2$), identified from the effective g-values, is resonant.

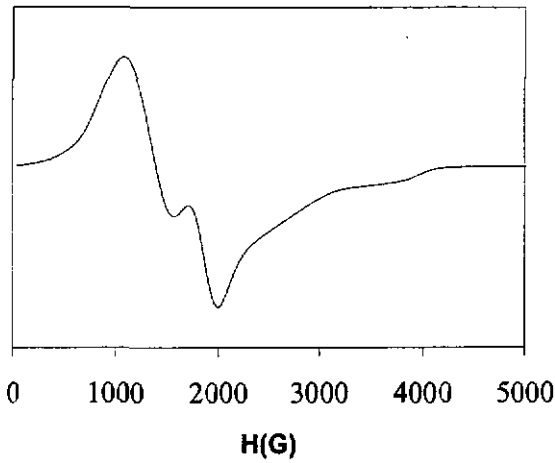

Figure 36. X-band powder EPR spectra of $[Co(HL)(H_2L)]ClO_4 \cdot 2H_2O$ (**7**) at 4K.

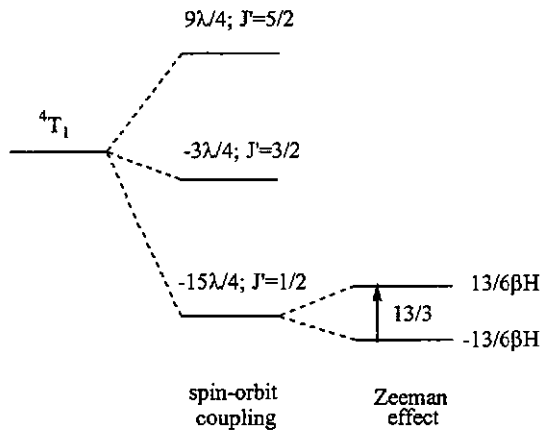

Figure 37. Illustration of the transition between Zeeman states observed in the EPR spectra at 4K. Different g-values are found for an anisotropic compound.

$[CoL(H_2O)_3]\cdot 3H_2O$ (8)

Treatement of the ligand H_2L with an equivalent of $Co(NO_3)_2\cdot 6H_2O$ yielded an orange solution, from which very small single crystals of complex 8 were isolated after slow evaporation. The structure of complex 8 was established by X-ray analysis and consists of discrete $[CoL(H_2O)_3]\cdot 3H_2O$ monomeric units with two independent molecules per asymmetric unit, which differ only slightly in bond lengths and angles.

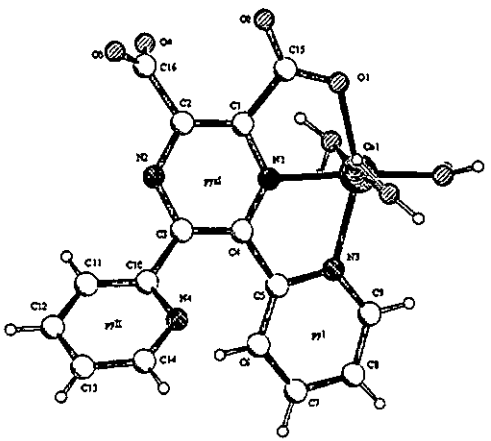

Figure 38. Molecular structure of complex $[CoL(H_2O)_3]\cdot 3H_2O$ (8). Only molecule 1 is represented for simplicity.

The Co(II) ion is in a slightly distorted octahedral environment provided by a monotridentate anion L^{2-} (see figure 38) and three water molecules. The donor atoms of the organic ligand together with a water molecule occupy the equatorial positions of the octahedron while the apical positions are filled by two water molecules.

The mono-tridentate behaviour of the ligand results in the formation of two nearly coplanar five-membered chelate rings which have in common the Co-Npyz bond. Despite the planarity of the tridentate domain, the equatorial plane is not coplanar to the pyrazine system (14.2(5)° in molecule 1 and 14.5(5)° in molecule 2). Moreover, the ligand is considerably twisted with the non-coordinated pyridine ring and carboxylate group rotated out of the plane of the pyrazine ring (with dihedral angles pyzI^pyII= 44.4(3)° (molecule 1), pyzII^pyIV= 43.7(3)° (molecule 2), pyzI^COO_{free}= 63.2(6)° (molecule 1) and pyzII^COO_{free}= 63.2(6)° (molecule 2)).

The completely deprotonated ligand molecule uses only three of its coordination sites, the rest of them are not involved in coordination. This means that complex 8 itself should be able to serve as a ligand to other metals of higher acceptor capacity.

The crystal packing of 8 shows an extensive hydrogen-bonding network within the unitcell (see figure 39). Hydrogen-bonding linkages gives rise to a one-dimensional hydrogen-bonded chain which runs along the crystallographic c-axis. Neighbouring hydrogen bonded chains are linked by a second type of hydrogen-bonding interactions. Finally, hydrogen bonding contacts involving both coordinated and lattice water molecules complete the 2D network.

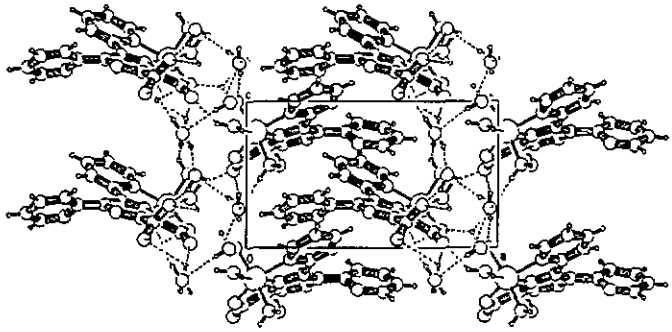

Figure 39. View of the crystal packing down the crystallographic b-axis in complex 8.

Measurements of the magnetic susceptibility were undertaken from 300K down to 2K in order to determine whether magnetic interactions are present. The magnetic susceptibility and effective magnetic moment are plotted as a function of temperature in figure 40. Magnetic susceptibility data revealed a Curie-Weiss law behaviour over a wide temperature range with a magnetic moment at room temperature of 4.82 M.B., this value being significantly higher than the spin-only value for a high-spin S=3/2 situation ($\mu_{eff} = g\beta\sqrt{S(S+1)} = 3.87$ M.B.). However, the observed value corresponds well to those generally reported for mononuclear octahedral high-spin Co(II) complexes, which typically have a magnetic moment between 4.7 and 5.2 M.B. due to an important orbital contribution to the effective magnetic moment[65].

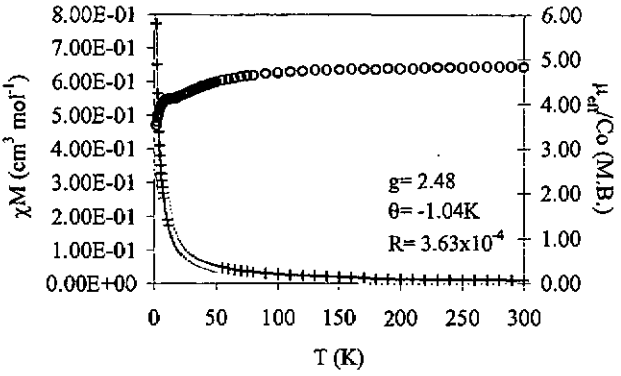

Figure 40. Temperature dependence of the magnetic susceptibility (+) and magnetic moment (o) for complex **8**. The solid line represents the calculated curve.

A simple Curie-Weiss model for S=3/2 situation was used to fit the experimental data:

$$\chi_M = \frac{Ng^2\beta^2S(S+1)}{3k(T-\theta)}$$

The best fit to the experimental data was obtained for a g-value of 2.48 and a Curie-Weiss constant θ of –1.04K. The quality of the regression was measured by the discrepancy factor R, defined as $R = \sum(\chi_{calc} - \chi_{obs})^2 / \sum\chi^2_{obs}$, which was found to be $3.63\text{-}10^{-4}$. Taking into account that hydrogen bonding should be required to propagate magnetic exchange, we believe the slight decrease in magnitude of the effective magnetic moment as T approaches 0K is occuring in the absence of significant magnetic exchange and is due to single ion anisotropy.

$[Co_2(HL)Cl_2(H_2O)_4]Cl{\cdot}4H_2O$ (9)

In the reaction of a methanolic solution of $CoCl_2{\cdot}6H_2O$ with H_2L in a 10:1 molar ratio the immediate precipitation of an orange solid was always observed. However on leaving the above solution to evaporate slowly a few orange crystals of complex **9** were also obtained and the crystal structure elucidated by X-ray diffraction.

Complex **9** is a binuclear complex, $[Co_2(HL)Cl_2(H_2O)_4]Cl{\cdot}4H_2O$, where two cobalt centers are bridged by a mono-deprotonated ligand molecule, HL-, acting in a bis-tridentate manner, resulting in a Co...Co distance of 6.879(1)Å.

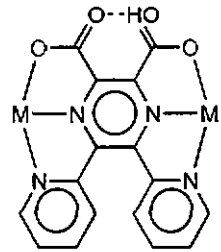

The octahedral geometry about each metal ion is completed by a Cl- ion and two water molecules. The distortion from regular octahedral geometry about the cobalt centers is primarly due to the small bite angles N1-Co1-O1 (75.4(1)°), N1-Co1-N3 (75.0(1)°), N2-Co2-O3 (74.7(1)°) and N2-Co2-N4 (74.7(1)°) required at the metal centers by the bis-tridentate chelating ligand. It is interesting to note that the coordination sphere of Co1 differs from that of Co2. The Cl^- ion occupies an equatorial position in the Co1 coordination sphere and an apical position in the Co2 coordination sphere; the Co2-Cl2 axial distance of 2.414(1)Å being longer than the Co1-Cl1 equatorial distance of 2.331(1)Å.

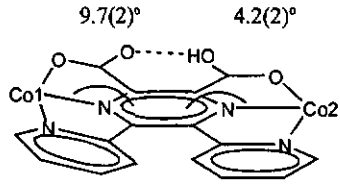

The dihedral angles between the plane of the pyrazine ring and the mean equatorial planes around Co1 (defined by atoms O1, N1, N3 and Cl1) and Co2 (defined by atoms O3, N2, N4 and O8) are 9.7(2)° and 4.2(2)°, respectively.

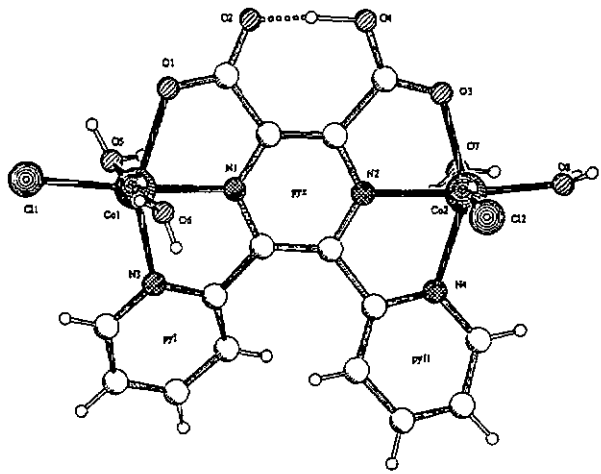

Figure 41. Molecular structure of complex $[Co_2(HL)Cl_2(H_2O)_4]Cl{\cdot}4H_2O$ (9).

In complex 9 the bis-tridenate ligand is slightly distorted from planarity. The nature of this distortion is mainly a bending along the line N1...N2 (the pyrazine ring being twisted by 5(1)°). Furthermore, the pyridine rings are inclined to one another by 40.4(2)°, and by 24.4(2)° and 24.0(2)° relative to the central pyrazine ring. The acid

hydrogen atom, H4, bound to O4 participates in a very strong intramolecular hydrogen bond with atom O2. Due to this interaction the two adjacent carboxylate groups and the central pyrazine ring are almost coplanar (the dihedral angles being COOH^pyz= 7.5(8)°, COO^-^pyz= 5.5(5)° and COOH^COO^-= 2.5(9)°). A similar trend has been reported previously in a series of transition metal complexes of ligands 2,3-pyrazine-dicarboxylic acid[21,23,66] and 2,3,5,6-pyrazine-tetracarboxylic acid[27].

Intermolecular hydrogen bonding interactions link the cations, the Cl- counterions and both the coordinated and the lattice water molecules to form a 3D hydrogen-bonded network.

The magnetic exchange through the ligand in complex **9** bas not been investigated since only a small amount of pure compound has been isolated.

Comparison of the structures 7-9

In complexes **7** and **8** the ligand acts in a non-bridging mono-tridentate manner forming Co(HL)(H_2L) and CoL monomeric units, respectively. However, in complex **9** the ligand behaves in a bis-tridentate manner giving a Co_2(HL) binuclear complex (9). It is important to iodicate that in the preparation of complex **9** a large excess of the Co(II) salt was used.

In Table 9 a comparison of important bond lenghts and bond angles for complexes **7-9** is presented. In all three complexes the Co-N and Co-O distances are comparable to standard values[63].

Table 9. A comparison of selected bond distances (Å) in complexes 7-9.

	Standard values	7	8		9
			Mol. 1	Mol. 2	
Co...Co					6.879(1)
Co-Npyz	2.095-2.210	2.049(5)	2.08(1)		2.101(3)
		2.048(5)	2.09(1)		2.117(4)
Co-Npy	2.059-2.121	2.097(5)	2.157(9)	2.167(9)	2.121(4),
		2.139(5)			2.140(4)
Co-O	2.037-2.094	2.086(5)	2.135(9)	2.133(9)	2.154(3),
		2.136(5)			2.117(4)
Co-Ow			2.006(8)	2.113(9)	2.094(4),
					2.157(4)
			2.146(9)	1.979(8)	2.015(4),
					2.145(4)
			2.093(9)	2.141(9)	
Npyz-Co-Npy		76.3(2)	74.1(3)	74.7(4)	75.0(1),
		75.1(2)			74.7(1)
Npyz-Co-O		76.5(2)	76.4(4)	76.2(4)	75.4(1),
		77.4(2)			74.7(1)

It is interesting to note that the bis-tridentate mode (9) shows the longest Co-Npyz bond length.

The ligand is twisted in all three complexes as can be appreciated by noting the dihedral angles between the pyrazine moiety and the susbstituents attached to it (see Table 10).

Table 10. A comparison of various dihedral angles (°) in compounds 7-9.

Angles	7	8	9
pyz twist	3(1)	7(1)	5(1)
	6.2(5)	7(1)	
pyI^pyz	9.3(3)	12.2(6)	24.4(2)
pyIII^pyz	16.9(2)	12.3(6)	
pyII^pyz	74.2(2)	44.4(3)	24.0(2)
pyIV^pyz	48.6(2)	43.7(3)	
pyI^pyII	68.6(2)	56.6(3)	40.4(2)
	63.6(2)	56.0(3)	
$COO_{chel.}$^pyz	3.5(8)	15(1)	7.5(8) (COOH)
	7.9(8)	16(1)	5.5(5) (COO^-)
COO_{free}^pyz	3(1)	63.2(6)	
	71.8(2)	61.2(6)	
COO_{chel}^COO_{free}	6(1) H-bonded	77(1)	2.5(9) H-bonded
	79.6(7)	76(1)	

The dihedral angles of the coordinated pyridine rings relative to the central pyrazine are larger in the bis-tridentate coordination mode, while the dihedral angle between adjacent pyridine rings is smaller.

2.4 Nickel(II) complex

In the reaction of nickel(II) salts with H_2L in aqueous conditions the precipitation of $Ni(OH)_2$ was always observed. However, when the protonated form **2** of the ligand was used a pale green solution was obtained and single crystals of complex **10** were deposited after several weeks.

$$NiSO_4 \cdot 7H_2O + [H_3L]Cl \xrightarrow[H_2O,\ rt]{} [NiL(H_2O)_3] \cdot 3H_2O\ (\mathbf{10})$$

The IR spectra of complex **10** appeared to be almost identical to that of compound **8**. Consequently, complex **10** was expected to exhibit a similar structure.

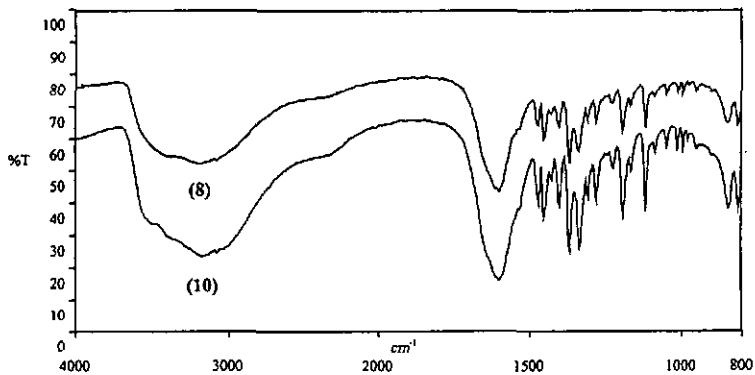

Figure 42. Comparison of the IR spectra of complexes $[CoL(H_2O)_3]\cdot 3H_2O$ (**8**) and $[NiL(H_2O)_3]\cdot 3H_2O$ (**10**)

[NiL(H$_2$O)$_3$]·3H$_2$O (10)

The structural characterization of complex **10** has shown that the structure consists of discrete monomeric units where nickel achieves an octahedral coordination by means of a mono-tridentate ligand molecule, L^{2-}, and three water molecules. The equatorial plane comprises two N-atoms and one O-atom of the ligand anion, L^{2-}, and a water molecule. The apical positions are occupied by two water molecules. As can be seen from figure 43 complex **10** was found to be isostructural with the cobalt(II) complex **8** (Figure 38).

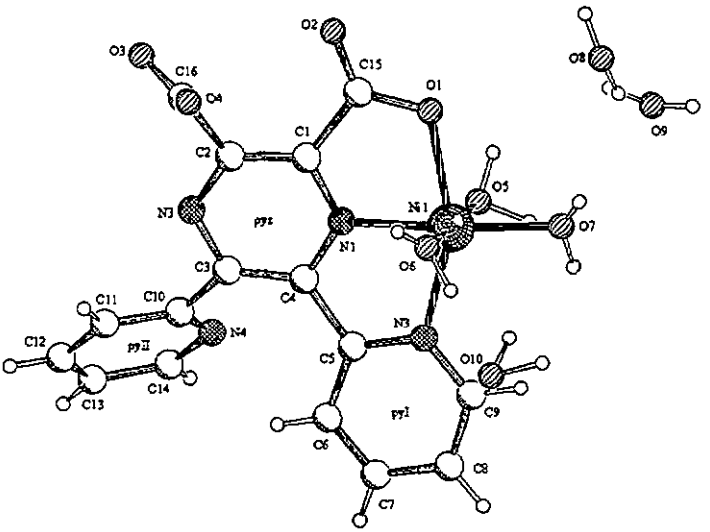

Figure 43. Molecular structure of compound [NiL(H$_2$O)$_3$]·3H$_2$O **(10)**

Table 11. A comparison of Ni-N,O distances in Ni(II) pyrazine complexes.

Distances	Ni-Npyz	Ni-Npy	Ni-Ochel.	Ni-Ow
$[NiL(H_2O)_3]\cdot 3H_2O$	1.980(6)	2.126(8)	2.129(7)	2.028(6)-
				2.081(7)
$\{[Ni(pzdc)(pyz)]\cdot 2H_2O\}n$[31]	2.066(7)		2.035(5)	
	2.120(6)			
$[Ni_2(TPPZ)(H_2O)_6](NO_3)_4\cdot 2.5H_2O$[39]	2.026(5)	2.087(5)		2.005(6)-
	2.005(5)	2.094(6)		2.104(6)
		2.079(6)		
		2.059(6)		
$[Ni_2(TPPZ)(H_2O)_6](squarate)_2\cdot 5H_2O$[39]	2.009(2)	2.0089(2)		1.985(2)-
				2.092(2)

It is interesting to note that the distance Ni-N_{pyz} is consistently shorter and the Ni-N_{py} distance longer in complex **10** compared to the values found in other Ni(II)-pyrazine compounds[31,39].

The crystal packing of complex **10** show an extensive hydrogen-bonded network which is illustrated in figure 44. Two types of hydrogen bonds can be distinguisbed. The coordinated water molecules O5 and O7 are hydrogen bonded to the non-coordinated carboxylate groups O3 and O4 (O5-H51...O3 and O7-H71...O4) giving rise to a one-dimensional hydrogen bonded chain along the crystallographic b-axis. O7-H72...O2 bydrogen bonding interaction links neighbouring hydrogen bonded chains related by a glide plane. Hydrogen bonding contacts involving both coordinated and lattice water molecules complete the 2D network.

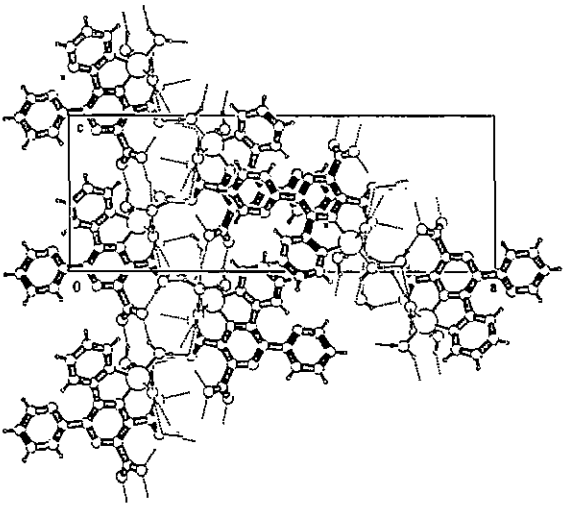

Figure 44. Crystal packing of $[NiL(H_2O)_3]\cdot 3H_2O$ **(10)** down the b-axis, showing the hydrogen bonding

Variable temperature (300-2K) magnetic susceptibility data were collected for a microcrystalline sample of compound $[NiL(H_2O)_3]\cdot 3H_2O$ **(10)**. The effective magnetic moment appears to be invariant as a function of temperature over a wide temperature range indicative of a classical paramagnet following the Curie-Weiss law (see Figure 45). The effective magnetic moment per nickel atom is 3.27 M.B. at 300K in agreemcnt with the values found in the literature for octahedral Ni(II) compounds which lie between 2.83 (spin-only value) and 3.35 M.B.[67]. The μ_{eff} decreases slowly from 3.27 M.B. at 300K to 3.04 M.B. at 12.01K. Below this temperature, μ_{eff} drops rapidly to 2.36 M.B. at 2K.

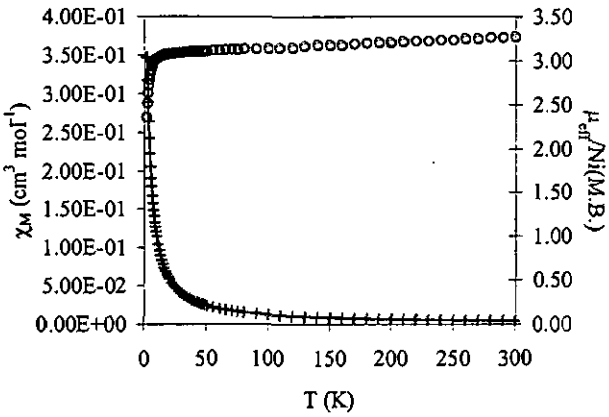

Figure 45. Temperature dependence of the magnetic susceptibility (+) and magnetic moment (o) for complex **10**. The solid line represents the best fit curve.

Fitting the experimental data indicates a deviation from Curie-Weiss behaviour at low temperatures. The fitted parameters are listed in Table 12. Taking into account that the deviation from the Curie-Weiss law may have other origins than intermolecular interactions we believe the decrease of μ_{eff} at very low temperatures may result from zero-field splitting of the S=1 spin-multiplet. Hence, the experimental data can be fitted using a model which includes a zero-field splitting term. The magnetic susceptibility is expressed as follows[65]

$$\chi_M = \frac{2Ng^2\beta^2}{3k(T-\theta)} \cdot \frac{2/x - 2\exp(-x)/x + \exp(-x)}{1+2\exp(-x)} \quad \text{with} \quad x = D/kT$$

A least-squares fitting of the experimental data was carried out, allowing D, θ and g to vary. A set of the best fitting parameters are listed in Table 12. The positive value of the parameter D means that the m_s=0 spin state, which lies below the m_s=±1 state, is the ground state.

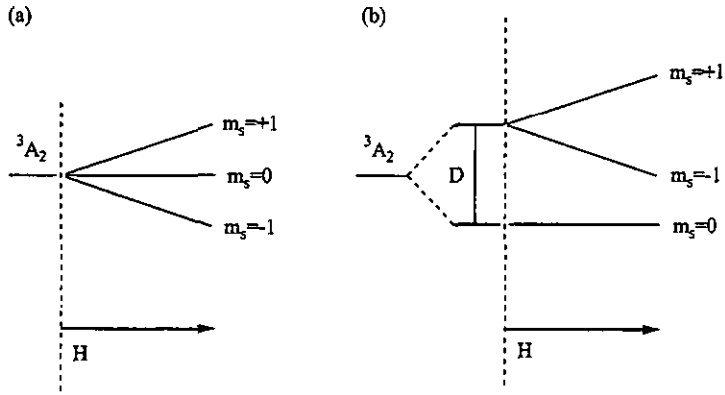

Figure 46. Zero-field splitting (ZFS) of a molecule with S=1. (a) No ZFS effect (D=0) and (b) positive ZFS effect (D>0).

Table 12. Magnetic parameters for $[NiL(H_2O)_3]\cdot 3H_2O$ **(10).**

Model	g	θ (K)	D (cm^{-1})	R
S=1 Curie-Weiss	2.33	-1.77		$7.54\cdot10^{-4}$
S=1 Zero-field splitting	2.23	-0.84	2.79	$3.54\cdot10^{-4}$

The quality of the fitting was measured by the discrepancy factor $R = \sum(\chi_{calc} - \chi_{obs})^2 / \sum\chi_{obs}^2$.

2.5 Copper(II) complexes

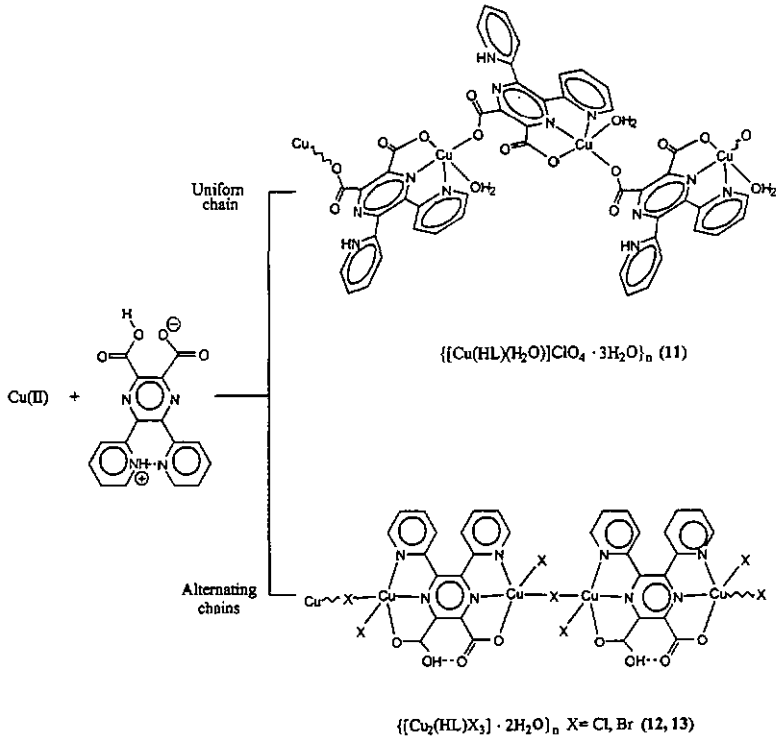

The reaction of Cu(II) salts with H_2L led to the formation of three new complexes:

$$Cu(ClO)_4 \cdot 6H_2O + H_2L \xrightarrow[\text{squaric acid}]{H_2O/MeOH,\ 50°C} \{[Cu(HL)(H_2O)]ClO_4 \cdot 3H_2O\}_n \ (11)$$

$$CuCl_2 \cdot 2H_2O + H_2L \xrightarrow[H_2O,\ rt]{} \{[Cu_2(HL)Cl_3] \cdot (H_2O)\} \ (12)$$

$$CuBr_2 + H_2L \xrightarrow[H_2O,\ rt]{} \{[Cu_2(HL)Br_3] \cdot (H_2O)\} \ (13)$$

The IR spectra of complex **11** shows two intense bands (see table 13) consistent with $\upsilon_{as}(COO^-)$ in coordinated carboxylate groups. Evidence for pyridine protonation is provided by the frequency of the $\upsilon(C=N)$ absorption, which is comparable to that of the free ligand (1602 cm^{-1}). Complexes **12** and **13** show IR spectra almost identical, which suggests very similar structures for these compounds. The intense bands around 1690 and 1660 cm^{-1} are characteristic of coordinated protonated and deprotonated carboxylate groups, respectively.

Table 13. Comparison of the IR absorptions (cm^{-1}) for compounds **11-13**.

	11	**12**	**13**
$\upsilon(C=O)/\upsilon_{as}(COO^-)$	1682 vs, 1620 s	1694 vs,1665 s	1691 vs,1663 s
$\upsilon(C=N), \upsilon(C=C)$	1605 s, 1570 m, 1541 m, 1477 m, 1453 m	1599 s, 1570 sh, 1547 m, 1469 m, 1422 m	1598 s, 1570 m, 1552 m, 1470 s, 1422 m
$\upsilon_s(COO^-)$	1374 s	1374 m	1368 s

vs very strong, s strong, m medium, w weak, sh sboulder

{[Cu(HL)(H$_2$O)]ClO$_4$·3H$_2$O}$_n$ (11)

The single-crystal X-ray analysis revealed that the structure of complex **11** is very similar to that of the previously studied complex $\{[Cu(L)(H_2O)]\cdot 5H_2O\}_n$[28]. Complex **11** can be described as extended helical chains of Cu(II) ions linked by mono-deprotonated HL- ligand molecules coordinated to two metal centers as depicted in Figure 47. The repeated structural moiety consists of $[Cu(HL)(H_2O)]^+$ units related to one another by a two-fold screw axis to give the helical chain, which runs parallel to

the crystallographic b-axis, with an intramolecular Cu(1)... $Cu(1)^{i}$ (Symmetry operation: i= -x, y-1/2, -z+2) distance of 7.747(1)Å.

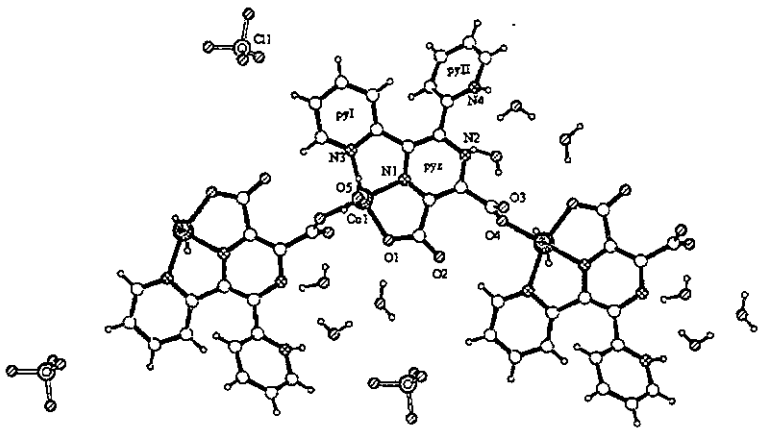

Figure 47. Polymeric structure of complex $\{[Cu(HL)(H_2O)]ClO_4 \cdot 3H_2O\}_n$ **(11)**.

The Cu(II) ion has a well-established tendency to be engaged in a pentacoordinated environment with a conformation between the trigonal-bypiramidal (TBP) and the square-pyramidal (SP). The distortion of the pentacoordinate complex from the TBP or SP can be well expressed by using the index τ introduced by Addison et al.[68], which is defined as

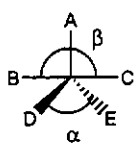

$$\tau = \frac{(\beta - \alpha)}{60}$$

For a perfectly square-pyramidal geometry the index τ is zero while it becomes unity for a perfectly trigonal-bipyramidal geometry. The calculated τ value for complex **11** is 0.24, indicating that the coordination polyhedron aroud the Cu(II) ion could be well described as a square-based pyramid with a trigonal-bipyramidal distortion. As usual the copper atom is displaced by 0.08(1)Å out of the basal plane, defined by atoms N1, N3, O1 and $O4^{i}$ (Symmetry operation: i= -x, y+1/2, -z+2), towards the O5 axial donor. The bond distances are similar to those reported previously for Cu(II) related compounds.

The present structure may be compared to that of $\{[Cu(L)(H_2O)]\cdot 5H_2O\}_n$ helical polymer of the same ligand synthesized by Wang[28]. In complex **11** the uncoordinated pyridine is protonated and the orientation of this ring is different from that found in $\{[Cu(L)(H_2O)]\cdot 5H_2O\}_n$.

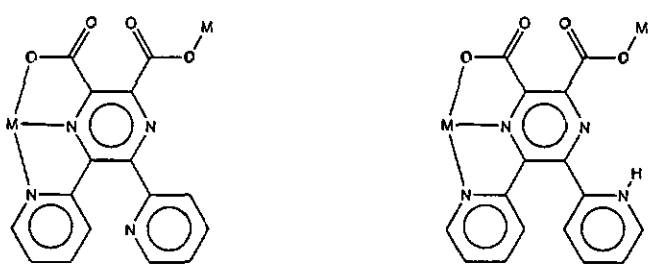

Figure 48. Orientation of the uncoordinated pyridine ring in complexes $\{[Cu(L)(H_2O)]\cdot 5H_2O\}_n$ and $\{[Cu(HL)(H_2O)]ClO_4\cdot 3H_2O\}_n$ **(11)**.

Table 14. A comparison of selected bond distances (Å) and angles (°) in complexes $\{[Cu(L)(H_2O)]\cdot 5H_2O\}_n$[28] and $\{[Cu(HL)(H_2O)]ClO_4\cdot 3H_2O\}_n$ **(11)**

	$\{[Cu(L)(H_2O)]\cdot 5H_2O\}_n$	$\{[Cu(HL)(H_2O)]ClO_4\cdot 3H_2O\}_n$ **(11)**
Distances		
Cu-Npyz	1.932(4)	1.917(5)
Cu-Npy	2.028(5)	2.051(5)
Cu-Ochel.	2.013(4)	1.987(5)
Cu-Omono.	1.923(4)	1.942(5)
Cu-Ow	2.326(7)	2.227(6)
Cu...Cu	7.755(5)	7.747(1)
Angles		
Npyz-Cu-Npy	79.2(2)	79.5(2)
Npyz-Cu-Ocbelat.	80.5(2)	81.5(2)
Npyz-Cu-Omono.	176.7(3)	174.4(2)
Npyz-Cu-Ow	91.6(2)	96.1(3)
Npy-Cu-Ochelat.	157.1(2)	160.1(2)
Npy-Cu-Omono.	101.4(2)	99.6(2)
Npy-Cu-Ow	93.6(3)	95.7(3)
Ochel.-Cu-Omono.	99.4(2)	98.8(2)
Ochel.-Cu-Ow	97.6(2)	92.2(3)
Omono.-Cu-Ow	85.1(2)	89.4(3)

In complex **11** the ligand molecule is considerably distorted with a dihedral angle of 51.1(2)° between pyridine rings. The central pyrazine is also slightly twisted by 3.1(2)°. The monodentate carboxylate group is almost perpendicular to the central

pyrazine (pyz^$COO_{mono.}$= 87.2(3)°). Such an arrangement has already been observed in complexes **5** and **6**. In Table 15 the dihedral angles between the pyrazine ring and the pyridine and carboxylate groups in complex **11** are compared with those of complex $\{[Cu(L)(H_2O)]\cdot 5H_2O\}_n$[28].

Table 15. A comparison of various dihedral angles (°) in compounds.

Angles	$\{[Cu(L)(H_2O)]\cdot 5H_2O\}_n$[28]	$\{[Cu(HL)(H_2O)]ClO_4\cdot 3H_2O\}_n$ **(11)**
Pyz twist	5.2(7)	3.1(2)
PyI^pyz	21.4(3)	17.9(2)
PyII^pyz	39.8(2)	42.9(2)
pyI^pyII	54.9(2)	51.1(2)
$COO_{chel.}$^pyz	12.6(4)	8.4(4)
$COO_{mono.}$^pyz	84.6(4)	87.2(3)
$COO_{chel.}$^ $COO_{mono.}$		80.5(9)

In the crystal, the helical chains are linked by bydrogen bonds involving the carboxylate O-atoms and the coordinated and crystallisation water molecules leading to a loosely connected 3D network.

Magnetic susceptibility measurements in the temperature range 4-300K were performed to investigate the magnetic exchange in compound **11**. Down to 4K, no maximum was observed in the χ versus T curve, indicating a paramagnetic, or a very weakly antiferromagnetic coupled compound. The experimental data, fitted for an isotropic linear-chain compound with $S=\frac{1}{2}$ and $\hat{H}=-2J\sum S_iS_j$, gave the best-fit parameters J= -0.24cm^{-1} and g= 2.24[69].

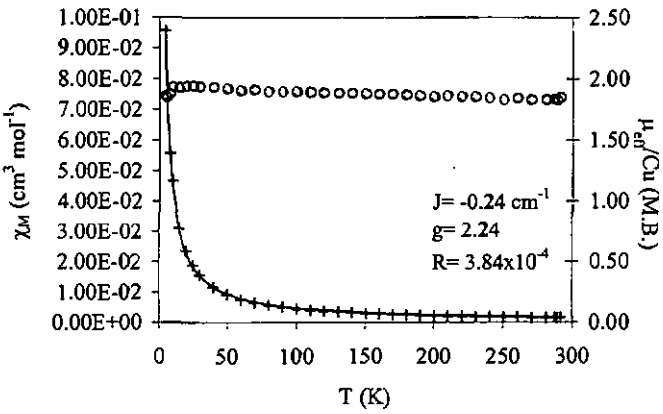

Figure 49. Temperature dependence of the magnetic susceptibility (+) and magnetic moment (o) for complex **11**. The solid line represents the best fit curve.

{[Cu$_2$(HL)Cl$_3$]·2H$_2$O}$_n$ (12)

Complex **12** was obtained by treating an aqueous solution of $CuCl_2 \cdot H_2O$ with H_2L in a 10:1 molar ratio. Within a few minutes a green solid precipitated, which was filtered off and discarded. Platelets of complex **12** were obtained by slow evaporation of the clear green solution. Unfortunately, twining of the crystals prevented an accurate structure solution. For this reason, detailed structural information is not given bere, and we just describe the overall structure of complex **12**.

Complex **12** consists of polymeric $\{[Cu_2(HL)Cl_3]\cdot 2H_2O\}_n$ zig-zag chains in which $[Cu_2(HL)Cl_2]^+$ units are linked by single Cu-Cl-Cu bridges; the chain runs parallel to the crystallogarphic b-axis.

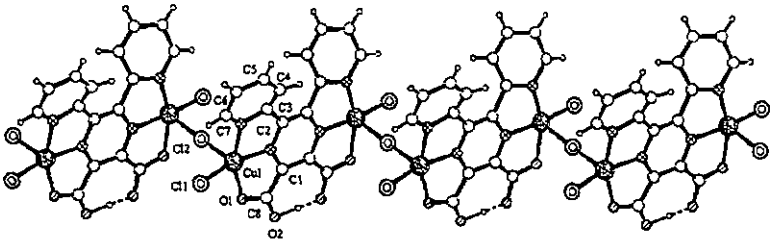

Figure 50. View of the structure of the zig-zag polymer $\{[Cu_2(HL)Cl_3]\cdot 2H_2O\}_n$ **(12).**

The molar susceptibillity of a powdered sample of complex **12** has been measured in the temperature range 4-298K. The χ versus T curve shows a maximum at 19.9K (χ= $2.18\cdot10^{-2}$ $cm^3\cdot mol^{-1}$) indicating a moderate antiferromagnetic interaction between Cu(II) ions. The value of the magnetic moment at room temperature is 2.79 M.B., which is in agreement with the values found for Cu(II) dimers having antiferromagnetic coupling. There are two possible exchange pathways; through the bridging chlorine atom and through the HL^- organic molecule. It could be assumed that the interaction through the HL^- is negligible. This assumption seems reasonable since the interaction in monochloro-bridged Cu(II) compounds is, in general, stronger than in pyrazine-bridged Cu(II) complexes. Moreover, the Cu-Cu distance is considerably shorter in the Cu-Cl-Cu bridge. Thus, the experimental data bave been fitted to the expression for the magnetic susceptibility based on the isotropic spin Hamiltonian $\hat{H} = -2JS_1S_2$ with $S_1 = S_2 = 1/2$[58].

$$\chi_M = \frac{Ng^2\beta^2}{kT}\left[\frac{2}{3+\exp\left(\frac{-2J}{kT}\right)}\right] + TIP$$

Numerical values for the exchange parameter J, the g factor and a paramagnetic impurity of –24.33 cm^{-1}, 2.25 and 3.35-10^{-3} $cm^3 \cdot mol^{-1}$, respectively, have been obtained by a non-linear least-squares fitting procedure in which the R factor defined as $R = \sum(\chi_{calc} - \chi_{obs})^2 / \sum \chi_{obs}^2$ was minimized.

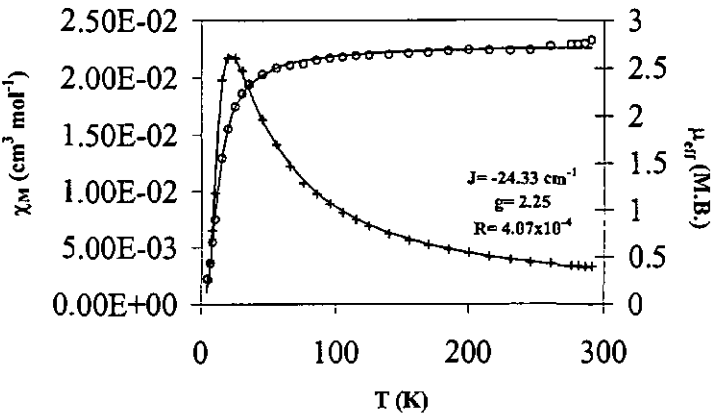

Figure 51. Temperature dependence of the magnetic susceptibility (+) and magnetic moment (o) for complex **12**. The solid line represents the best fit curve.

The conclusion drawn from the magnetic susceptibility data is that in spite of the polymeric structure of complex **12**, it can be treated as a dinuclear 1/2-1/2 system since no significant exchange is occuring through the HL- bridge.

{[Cu_2(HL)Br_3]·2H_2O}$_n$ (13)

Uofortunately, it was impossible to find untwinned crystals of 13. Eventually, a small crystal was found in which the separatioo of the reflectioos belonging to the two individuals was sufficiently wide to allow the indexing and the collection of the intensities belonging to one of the two individuals.

Single-crystal X-ray analysis confirmed that complex 13 is isomorphus with complex 12, the primary differences being those expected as a result of the larger size of the bromine atoms.

Complex 13 is a zig-zag polymer which runs parallel to b–axis. The HL^- molecule straddles a C_2 axis. The HL^- of consecutive units have the same orientation and are parallel to each other.

The Cu(II) atom is pentacoordinated and the dispositioo of donor atoms around it can be well-described as a square pyramid with a τ value of 0.02. The basal plane is defined by atoms N1, N2, O1 and Br1 whereas the apical position is occupied by the bridging halide Br2. The terminal Cu-Br1 distance of 2.359(2)Å is sborter than the bridging Cu-Br2 distance of 2.521(4)Å. Figure 52 shows the extended structure of complex 13.

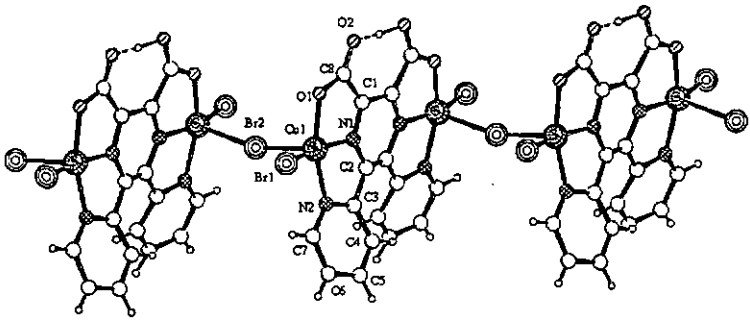

Figure 52. Zig-zag structure of the alternating polymer $\{[Cu_2(HL)Br_3]\cdot 2H_2O\}_n$ **(13)**.

The coordination of the monodeprotonated HL^- ligand may be compared to that found in complex **9**. The ligand HL^- is not planar, the pyridine rings are inclined to one another by approximately 40°, and by 21° relative to the pyrazine ring. The -OH function of the protonated carboxylate group is involved in a strong intramolecular hydrogen bond with the adjacent carboxylate group, which makes them almost coplanar. The metal-metal distance separation through the HL- ligand is 6.525(1)Å. The Cu-N and Cu-O distances are comparable to the distances found in Cu(II) related compounds[26-28,37,39]. The Cu...Cu distance through the bromine atom is 4.984(1)Å and the Cu-Br-Cu angle is 162.74(3)°. Though a certain number of mono-(μ-chloro)-bridged copper chain complexes are known[70-74], the mono-(μ-bromo)-bridged chain structures are very rare[72-74].

It would be interesting to investigate the magnetic exchange in compound **13** and compare it with that found in **12**. The small amount of compound **13** that was obtained did not allow an accurate measurement of the magnetic susceptibility temperature dependence.

3 COMPLEXES OF THE LIGAND 5,6-BIS(2-PYRIDYL)PYRAZINE-2,3-DICARBOXYLIC ACID WITH d^{10} METAL IONS

Using Ag(I), Zn(II), Cd(II) and Hg(II) as representative examples, we have studied the coordination chemistry of 5,6-bis(2-pyridyl)pyrazine-2,3-dicarboxylic acid with d^{10} metal ions.

3.1 Silver(I) complex

The preparation of silver complexes containing the ligand H_2L under aqueous conditions resulted in the precipitation almost immediately of a white solid upon combination of the reactants. However, the reaction of Ag(I) salts with H_2L under ammonical conditions gave a crystalline product with an elemental analysis (C, H, N) indicative of an unusual stoichiometry, consistent with the presence of coordinated NH_3.

$$AgNO_3 + H_2L \xrightarrow[rt]{NH_3\ 10\%} \{[Ag_4L_2(NH_3)_2] \cdot H_2O\}_n \quad (14)$$

Amine coordination should result in the appearance of a strong band in the 3200-3000 cm^{-1} region due to υ(N-H) vibrations, but in this region there is considerable interference due to the presence of υ(O-H) absorptions associated with the lattice water molecules.

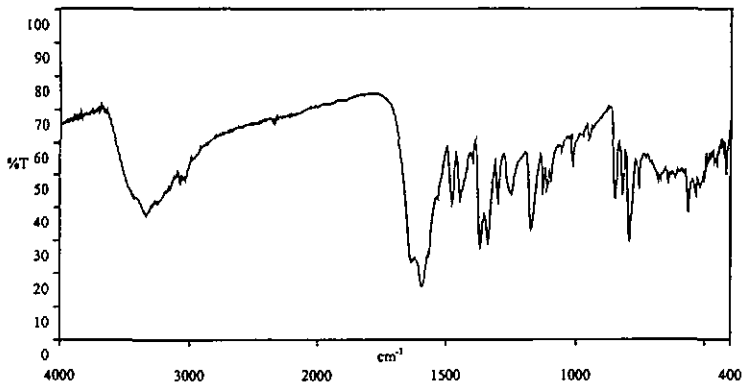

Figure 53. IR spectrum of complex $\{[Ag_4L_2(NH_3)_2]\cdot H_2O\}_n$ **(14)**

$\{[Ag_4L_2(NH_3)_2]\cdot H_2O\}_n$ (14)

Slow evaporation of the solution obtained upon mixing $AgNO_3$ and H_2L ammonical solutions gave yellow flattened square rod-like crystals. Only partial structure determination was possible due to the poor quality of the crystals. Therefore, the details of the stuctural determination are not reported, and we just describe the overall structure of $\{[Ag_4L_2(NH_3)_2]\cdot H_2O\}_n$ **(14).**

The single crystal X-ray analysis bas shown that complex **14** is a two-dimensional polymer where the basic molecular unit $[Ag_4L_2(NH_3)_2]$ contains four silver centers; two very distorted tetrahedral AgN_2O_2 and two distorted trigonal planar AgN_3 centers.

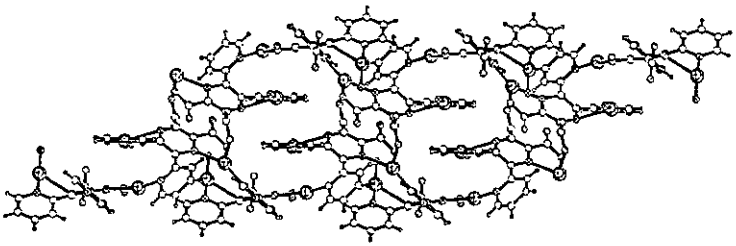

Figure 54. A view of the polymeric structure of complex $\{[Ag_4L_2(NH_3)_2]\cdot H_2O\}_n$ **(14)**

The polymeric structure of complex **14** is unusual in several respects:

- The ligand acts as a tetranucleating bridge.

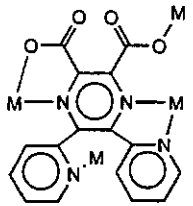

Each ligand molecule is highly distorted. The pyrazine moiety is significantly twisted. The pyridine rings are rotated in opposite directions with respect to the pyrazine plane. On the other hand, the chelating carboxylate group is almost coplanar to the pyrazine ring while the monodentate non-chelating carboxylate group is almost perpendicular.

- Coordination of the NH_3 group acting in a space-filling capacity. The formation of mixed pyrazine-amine coordination complexes with Ag(I) has a precedent in the chemical literature for the ligand pyrazine-2,3-dicarboxylate[75].
- Another notable feature of the molecular disposition is the significant π-π interaction between pyridine rings related by a center of symmetry, with the close contact N4...C14^{i} [3.445(1)Å; i= -x,-y,-z].

3.2 Zinc(II) complexes

We expected that the coordinative flexibility of zinc would allow a variable structural chemistry of its complexes with H_2L. Five zinc(II) salts were chosen for the reactions with H_2L: $ZnCl_2$, $Zn(NO_3)_2$ and $Zn(AcO)_2$ as species with coordinating anions, and $ZnSO_4$ and $Zn(ClO_4)_2$ as species with non-coordinating anions. However, only two crystalline products were obtained. Preparation with a large excess of zinc did not alter the outcome.

$$ZnSO_4 \cdot 7H_2O + H_2L \xrightarrow[50°C]{H_2O} [ZnL(H_2O)_3] \cdot 3H_2O \quad \textbf{(15)}$$

$$ZnCl_2 + [H_3L]Cl \cdot 2.25H_2O \xrightarrow[rt]{H_2O} [ZnCl_2(H_2L)] \quad \textbf{(16)}$$

The IR spectra of complex **(15)** is almost identical with that of the nickel compound **(10)**.

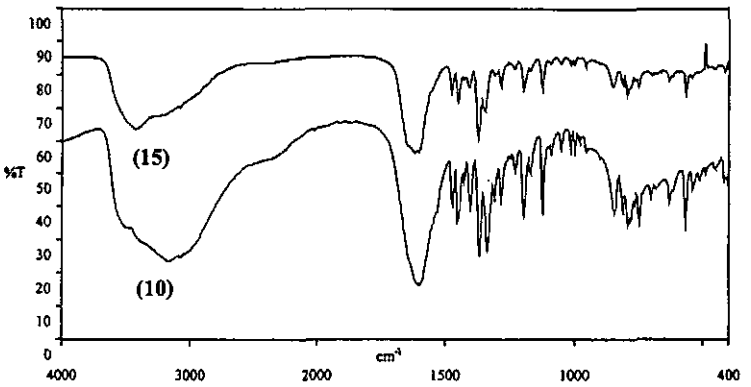

Figure 55. A comparison of the IR spectra of complexes $[NiL(H_2O)_3]\cdot 3H_2O$ **(10)** and $[ZnL(H_2O)_3]\cdot 3H_2O$ **(15).**

On the other band, the IR spectrum of complex **(16)** shows two bands at 1715 and 1632 cm^{-1} consistent with υ(C=O) in protonated and coordinated carboxylate groups, respectively.

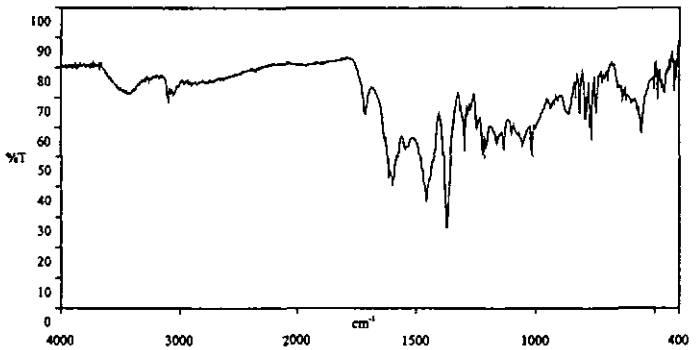

Figure 56. IR spectrum of complex $[ZnCl_2(H_2L)]$ **(16)**

$[ZnL(H_2O)_3]\cdot 3H_2O$ (15)

When H_2L was reacted with $ZnSO_4$ well shaped colourless single crystals were obtained and characterized as $[ZnL(H_2O)_3]\cdot 3H_2O$. X-ray single-crystal structure determination of complex **15** revealed that it is isomorphus with the nickel complex **10**.

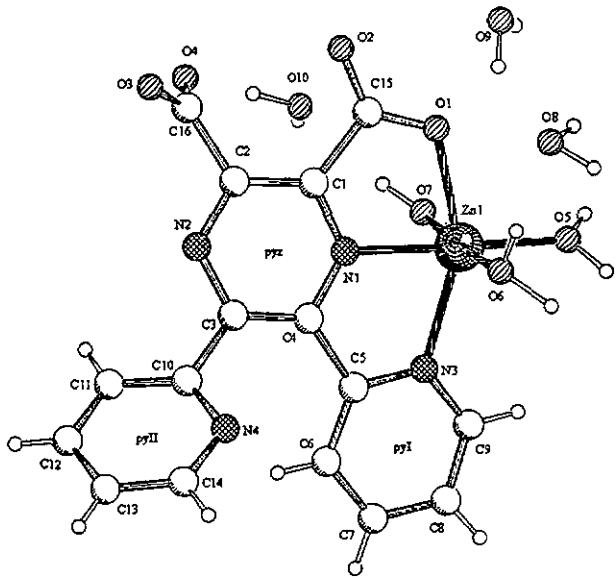

Figure 57. Molecular structure of complex $[ZnL(H_2O)_3]\cdot 3H_2O$ **(15)**.

Each zinc atom is approximately octahedrally coordinated by a mono-tridentate L^{2-} anion and three water molecules. All the metal-ligand bond lengths (see Table 16) are within the usual range observed for octahedral zinc complexes (2.05-2.25)[76].

[$ZnCl_2(H_2L)$] (16)

The crystal structure of complex **16** consists of mononuclear [$ZnCl_2(H_2L)$] molecules, where not only a neutral H_2L molecule but also two chloride ions are involved in the bonding to zinc. The organic base coordinates in a mono-tridentate manner and an intramolecular hydrogen bond between adjacent carboxylate groups is observed. The uncoordinated pyridine ring is protonated. Important bond lengths and angles are given in Table 16.

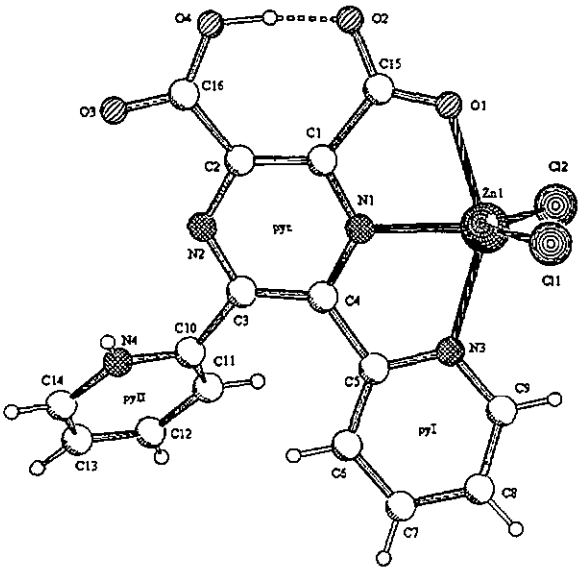

Figure 58. Mononuclear structure of complex [$ZnCl_2(H_2L)$] **(16)**.

In this complex the Zn atoms is pentacoordinated. In order to know whether the observed angles allow a description of the geometry about zinc as either a distorted trigonal bipyramid or a distorted square pyramid, an analysis of the shape-determining bond angles has been carried out using the approach of Addison et al.[68]. The value of 0.44 obtained for τ places the structure almost midway between the two ideal geometries.

As in other complexes the ligand is considerably distorted. The pyrazine ring has a twist conformation (with a twist angle of 6.5(2)°). The coordinated part of the ligand is almost planar. The dihedral angles pyz^pyl and pyz^COO are 14.6(1)° and 13.4(4)°, respectively. The uncoordinated pyridine ring is inclined to the central pyrazine ring by 47.4(1)°. The dihedral angle between adjacent pyridine rings is 60.8(1)°. The hydrogen bonded carboxylate groups are almost coplanar with a dihedral angle COOH^COO of 13.3(5)°.

Comparison of the structures

By reacting zinc(II) salts with H_2L only two different compounds were obtained, both of them exhibiting a monomeric structure with the ligand acting in a mono-tridentate mode. The solubility properties of the neutral complexes $[ZnL(H_2O)_3]\cdot 3H_2O$ **(15)** and $[ZnCl_2(H_2L)]$ **(16)** may be the reason for the precipitation of a mono- rather than a binuclear or polymeric complex. However, electronic grounds can not be excluded; coordination of one side of the ligand may withdraw electron density from the other side with the result that once the first metal is bound it is more difficult to bind the second. In terms of a recently proposed classification[77] this ligand is termed

bypodentate, indicating that not all the potential donor atoms are utilized in binding metal centers.

The general structural features of the metal-ligand combination in **15** and **16** can be compared with those of Zn(II) complexes with TPPZ and H_4pztc ligands. In contrast with complexes $[Zn_2(TPPZ)Cl_4]$ and $[Zn_2(TPPZ)(H_2O)_6](NO_3)_4 \cdot 1.5H_2O$[78], in compounds **15** and **16** the Zn-Npy distance is found to be longer than the central Zn-Npyz distance. The Zn-$O_{chelate}$ distances in complexes **15** and **16** are shorter than the same distance in the polymeric compound $\{K_2[Zn(pztc)(H_2O)] \cdot 2H_2O\}_n$[27].

Table 16. A comparison of metal bond distances (Å) and chelate angles (°) in Zn(II) complexes containing substituted pyrazine ligands.

Compound	*Bond distances (Å)*						*Bond angles (°)*	
	$Zn\text{-}N_{pyz}$	$Zn\text{-}N_{py}$	$Zn\text{-}O_{chelate}$	$Zn\text{-}O_{monod.}$	$Zn\text{-}O_{w}$	Zn-Cl	$N_{pyz}\text{-}Zn\text{-}N_{py}$	$N_{pyz}\text{-}Zn\text{-}O$
$[ZnL(H_2O)_3]\ 3H_2O$ **(15)**	2.08784)	2.172(5)	2.150(5)		2.003(4)-2.133(5)		74.0	76.7(2)
$[ZnCl_2(tl_2L)]$ **(16)**	2.144(2)	2.165(2)	2.165(2)			2.241(1) 2.265(1)	73.69(8)	73.54(8)
$[Zn(TPPZ)Cl_2]$[37]	2.156(2)	2.175(3) 2.204(3)				2.237(1) 2.276(1)	73.11(9) 73.31(9)	
$[Zn_2(TPPZ)Cl_4]$[78]	2.182(5) 2.210(5)	2.147(5) 2.134(6) 2.159(6) 2.153(6)				2.251(2) 2.276(2) 2.255(2) 2.259(2)	72.5(2) 73.1(2) 73.5(2) 73.7(2)	
$[Zn_2(TPPZ)(H_2O)_6](NO_3)_4\ 1.5H_2O$[78]	2.125(6) 2.127(6)	2.155(6) 2.149(6) 2.137(7) 2.171(7)			1.983(5)-2.209(6)		75.0(2) 75.3(2)	
$\{K_2[Zn(pztc)(H_2O)]\ 2H_2O\}_n$[27]	2.036(4)		2.181(3) 2.203(3)	2.100(3) 2.130(3)	2.024(4)		74.5(1) 75.7(1)	

3.3 Cadmium(II) complexes

The d^{10} configuration of cadmium(II) permits a wide variety of geometries and coordination numbers. We have prepared and structurally characterized two Cd(II) complexes with the ligand H_2L.

$$CdCl_2 \cdot H_2O + H_2L \xrightarrow[H_2O,\ rt]{} [CdL(H_2O)_2]_n \text{ (17)}$$

$$CdI_2 + H_2L \xrightarrow[H_2O,\ rt]{} [Cd_3(HL)_2I_4] \text{ (18)}$$

The IR spectra of complex 17 presents a broad band centered at 1630 cm^{-1} assigned to $\upsilon_{as}(COO)$, the shift to lower frequencies with respect to the free ligand (1659 cm^{-1}) is in agreement with coordination of both carboxylate groups.

The IR spectra of complex 18 exhibits intense bands at 1705 and 1633 cm^{-1} consistent with coordination of both protonated and deprotonated carboxylate groups, respectively.

Table 17. Main IR absorptions (cm^{-1}) in compounds $[CdL(H_2O)_2]_n$ (17) and $[Cd_3(HL)_2I_4]$ (18).

	17	18
υ(C=O)	1630 m	1705 m, 1633 m
υ(C=N), υ(C=C)	1598 vs, 1533 m, 1469 m, 1442 m, 1414 m	1596 s, 1547 w, 1520 m, 1448 m, 1433 m
υ(C-O)	1362 s	1370 vs

vs very strong, s strong, m medium, w weak

$[CdL(H_2O)_2]_n$ (17)

Complex **17** crystallizes as a two-dimensional polymer in which cadmium atoms are bridged by a trinucleating L^{2-} anion. The polymeric structure of complex **17** can be described as being made up of $[CdL(H_2O)_2]$ *units where* the metal center is coordinated to a tridentate domain of L^{2-}.

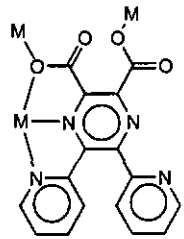

The carboxylate O-atom involved in the tridentate coordination is acting as a monoatomic bridge between two metal centers related by a center of symmetry with a Cd...Cd distance of 3.876(1)Å, this being shorter than the M...M distance in any other complex of this ligand. This rather uncommon monoatomic bridging mode of the carboxylate group is asymmetric since Cd-O bond distances with different lengths are involved.

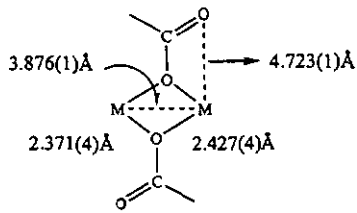

There is no apparent interaction of the dangling O-atom with any of the bridging metal ions.

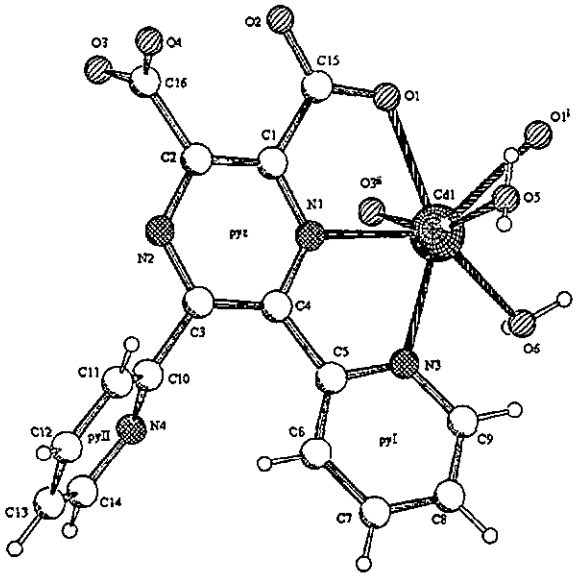

Figure 59. View of the coordination sphere of the cadmium(II) atom.

The cadmium atom is heptacoordinated; water molecules complete the coordination sphere about the cadmium ion. The Cd-N bond lengths are within the range of similar Cd-$N_{aromatic}$ bonding distances[63]. The Cd-O bond lengths are also within the range of typical values[63] (see Table 18).

Table 18. Selected bond distances (Å) and angles (°) for complex $[CdL(H_2O)_2]_n$ (17)

Distances			
Cd1-O5	2.293(5)	Cd1-N1	2.417(4)
Cd1-O6	2.318(3)	Cd1-O1^{ii}	2.426(4)
Cd1-O1	2.372(4)	Cd1-N3	2.430(4)
Cd1-O3^{i}	2.378(4)		

Angles

O5-Cd1-O6	104.6(2)	O1-Cd1-O3^{i}	80.4(1)
O5-Cd1-O1	80.3(2)	O1-Cd1-N1	68.0(1)
O5-Cd1-O3^{i}	157.5(2)	O1-Cd1-O1^{ii}	72.3(1)
O5-Cd1-N1	91.7(2)	O1-Cd1-N3	131.3(1)
O5-Cd1-O1^{ii}	76.6(2)	O3^{i}-Cd1-N1	91.8(1)
O5-Cd1-N3	87.8(2)	O3^{i}-Cd1-O1^{ii}	86.5(1)
O6-Cd1-O1	150.6(1)	O3^{i}-Cd1-N3	113.7(1)
O6-Cd1-O3^{i}	86.9(1)	N1-Cd1-O1^{ii}	139.9(1)
O6-Cd1-N1	139.3(1)	N1-Cd1-N3	65.4(1)
O6-Cd1-O1^{ii}	80.7(1)	O1^{ii}-Cd1-N3	149.4(1)
O6-Cd1-N3	78.0(1)		

Symmetry operation: i= x, -y+5/2, z-1/2; ii= -x+1, -y+2, -z+1.

The second carboxylate group of each ligand molecule links $[CdL(H_2O)_2]$ units related by a glide plane with a Cd...Cd distance of 8.674(1)Å. This results in the formation of a two-dimensional polymer.

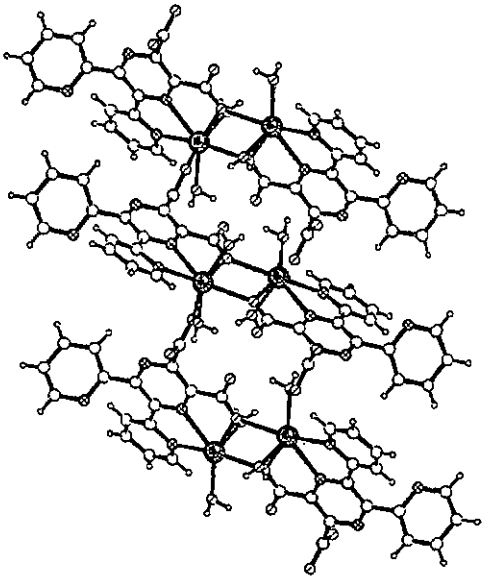

Figure 60. Polymeric structure of complex $[CdL(H_2O)_2]_n$ **(17)**.

$[Cd_3(HL)_2I_4]$ (18)

Single crystal X-ray diffraction studies reveal that although complex **18** has similar unit-cell dimensions and crystallizes in the same space group as compound **16**, the two compounds are neither isomorphus nor isostructural. Unexpectedly, complex **18** is a trinuclear species with two bridging HL^- molecules acting in a bis-tridentate manner. This contrasts structurally with the zinc complex **16**, which is monometallic.

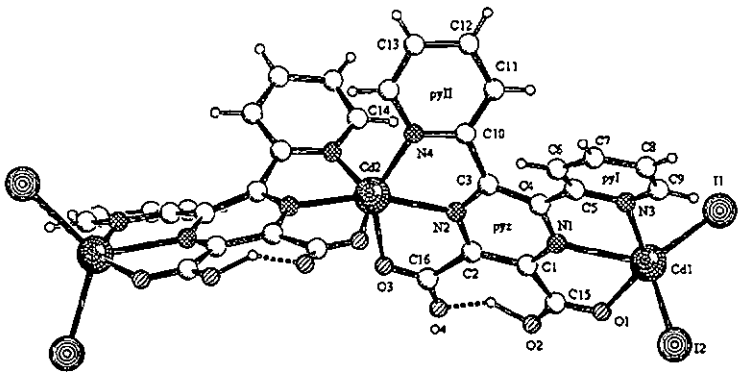

Figure 61. A view of the trinuclear structure of compound $[Cd_3(HL)_2I_4]$ **(18)**.

The trinuclear $[Cd_3(HL)_2I_4]$ molecule possesses a two-fold axis on which lies the atom Cd(2). The asymmetric unit contains two cadmium centers of non-identical geometries with a Cd1...Cd2 distance of 7.235(1)Å. Atom Cd(1) posseses a geometry intermediate between the SP and TBP. If we use the parameter τ to quantify the geometry, a value of 0.18 is obtained, indicating a distorted SP geometry. Atom Cd(2) displays a distorted octahedral geometry, the main contribution to the distortion from the ideal geometry being a consequence of the narrow chelate angles imposed by the tridentate coordination of the ligand.

The metal-ligand bond lengths are slightly longer for Cd1 compared to Cd2, but they are still comparable to Cd-N,O distances found in similar compounds[63]. The Cd-I bond lengths are within the range of values observed for CdI_2 complexes[63].

Table 19. Selected bond distances (Å) and angles (°) for complex $[Cd_3(HL)_2I_4]$ (18)

Distances			
Cd1-O1	2.366(1)	Cd2-N2	2.207(1)
Cd1-N1	2.373(1)	Cd2-N3	2.219(1)
Cd1-N3	2.377(1)	Cd2-O3	2.364(1)
Cd1-I1	2.699(1)		
Cd1-I2	2.728(1)		
Angles			
N1-Cd1-N3	68.77(1)	N2-Cd2-N4	74.9(7)
N1-Cd1-O1	67.35(1)	N2-Cd2-O3	69.2(7)
N3-Cd1-O1	136.05(1)	N2-Cd2-O3^{i}	99.5(7)
N1-Cd1-I1	124.74(1)	N2-Cd2-N4^{i}	116.6(7)
N1-Cd1-I2	112.82(1)	N2-Cd2-N2^{i}	162.3(9)
N3-Cd1-I1	105.43(1)	N4-Cd2-O3	143.7(8)
N3-Cd1-I2	94.99(1)	N4-Cd2-O3^{i}	86.7(9)
O1-Cd1-I1	101.19(1)	N4-Cd2-N4^{i}	105(1)
O1-Cd1-I2	99.45(1)	O3-Cd2-O3^{i}	104(1)
I1-Cd1-I2	122.43(1)		

Symmetry operation: i= -x-1/2, y, -z.

3.4 Mercury(II) complex

Hg(II) derivatives are among the most toxic pollutants, reacting with thiol groups of enzymes[79] and DNA constituents[80]. Hg(II) poisoning is treated by converting the metal ion to a soluble chelate complex using a proper chelate agent. Thus finding possible new and more effective agents for the elimination of heavy metals from the human organism or from contamined waste water has become an important goal.

The Hg^{2+} has indeed a strong tendency to complex formation, the most stable complexes being those with C, N, P and S as ligand donor atoms. There appears to be considerable covalent character in the mercury-ligand bonds.

We studied the interaction of the H_2L ligand with Hg^{2+} salts and found that chelate coordination of the ligand to the metal ion takes place. The addition of H_2L to an aqueous solution of $HgCl_2 \cdot H_2O$ led always to a monomeric compound of formula $[HgCl_2(H_2L)]$ even though several metal to ligand molar ratios have been engaged.

$$HgCl_2 \cdot H_2O + H_2L \xrightarrow[H_2O,\ rt]{} [HgCl_2(H_2L)] \quad (19)$$

[$HgCl_2(H_2L)$] (19)

The structural characterisation of complex **19** indictated that it is isomorphus with the zinc complex **16**.

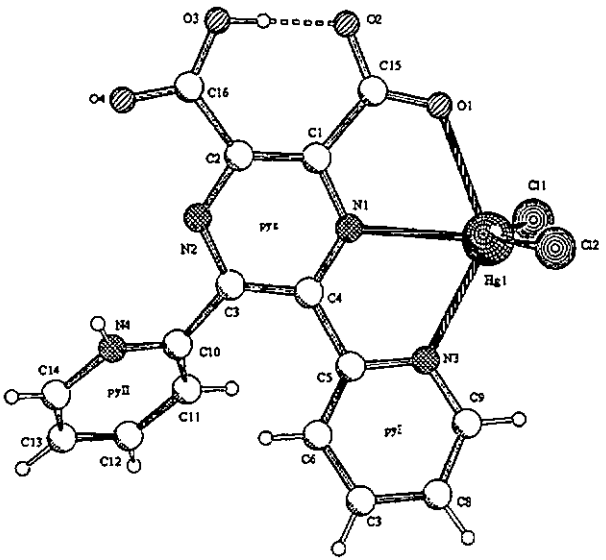

Figure 62. Molecular structure of the mononuclear compound [$HgCl_2(H_2L)$] **(19)**.

Complex **19** is a monomeric compound where the mercury atom is coordinated to a tridentate domain of a neutral H_2L molecule and two chloride atoms. The mercury atom displays five-coordination with a value of 0.01 for the trigonality index, τ. Thus, the geometry about mercury(II) can be described as a SP where the basal plane consists of the atoms O1, N1, N3 and Cl2 with Cl1 occupying the apical site; the Hg1 lies 0.70Å out of the equatorial plane towards Cl1.

Table 20. Selected bond distances (Å) and angles (°) for complex $[HgCl_2(H_2L)]$ (19)

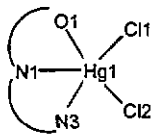

		Hg1-Cl2	2.367(3)
		Hg1-N3	2.374(7)
		Hg1-Cl1	2.415(3)
		Hg1-N1	2.494(6)
		Hg1-O1	2.495(7)
Cl2-Hg1-N3	107.4(2)	N3-Hg1-N1	66.5(2)
Cl2-Hg1-Cl1	130.8(1)	N3-Hg1-O1	130.7(2)
Cl2-Hg1-N1	116.5(2)	Cl1-Hg1-N1	111.9(2)
Cl2-Hg1-O1	97.6(2)	Cl1-Hg1-O1	95.6(2)
N3-Hg1-Cl1	98.7(2)	N1-Hg1-O1	64.3(2)

As in the other complexes the ligand is considerably distorted in **19**. The pyrazine ring is bent, with a dihedral angle [C1-N1-C4]^[C2-N2-C3]= 3.6(9)°). The tridentate domain of the ligand deviates slightly from planarity, with dihedral angles pyz^pyl= 20.0(4)° and pyz^COO= 11(2)°. The uncoordinated pyridine ring is inclined to the central pyrazine ring by 46.5(3)°. The dihedral angle between adjacent pyridine rings is 60.3(3)°. Due to an intramolecular bydrogen bond the adjacent carboxylate groups are almost coplanar with a dihedral angle COOH^COO of 12(1)°.

4 THE ESTER DERIVATIVES OF THE 5,6-BIS(2-PYRIDYL)PYRAZINE-2,3-DICARBOXYLIC ACID

4.1 Synthesis

The compounds methyl-, ethyl- and isopropyl-5,6-bis(2-pyridyl)pyrazine-2,3-dicarboxylate were obtained by the usual esterification procedure in acidic medium from 5,6-bis(2-pyridyl)pyrazine-2,3-dicarboxylic acid and an excess of the corresponding alcohol[81].

$$H_2L + ROH \xrightarrow[24h]{H^+,\ reflux} R_2L + H_2O$$

R= Me- **(20)**, Et- **(21)**, ^{i}Pr- **(22)**

4.2 Characterisation

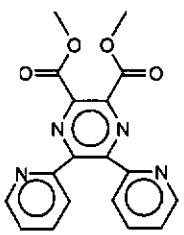

Me_2L **(20)**

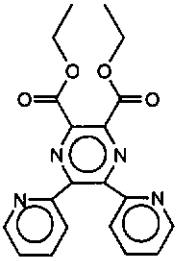

Et_2L **(21)**

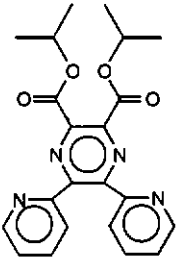

i-Pr_2L **(22)**

4.2.1 IR Spectra

The IR spectra of the ester derivatives **20-22** display significant absorptions in the 1400-1800cm^{-1} region, which are listed in Table 22. A comparison with the spectrum of the corresponding acid H_2L (**1**) show an increase in the υ(C=O) frequency to ca. 1740 and 1720 cm^{-1} (1709 cm^{-1} for H_2L), as expected for the ester derivatives. The bands corresponding to the υ(C=N) and υ(C=N) occur in the region 1400-1600cm^{-1} and they are very close with respect to their positions and intensities for the three compounds. The spectra of compounds **20-22** are shown in figure 63.

Table 22. Comparison of the IR absorptions (cm^{-1}) for compounds **20-22**.

	20	**21**	**22**
υ(C=O)	1743 s, 1729 vs	1737 s, 1723 vs	1740 s, 1720 vs
υ(C=N), υ(C=C)	1587 m, 1572 m, 1540 w, 1479 m, 1450 m, 1437 m, 1401 m	1587 m, 1571 m, 1539 w, 1479 m, 1467 m, 1438 m, 1408 m	1589 w, 1570 m, 1538 m, 1468 m, 1414 w
υ(C-O)	1283 vs	1276 vs	1278 vs

vs very strong, s strong, m medium, w weak

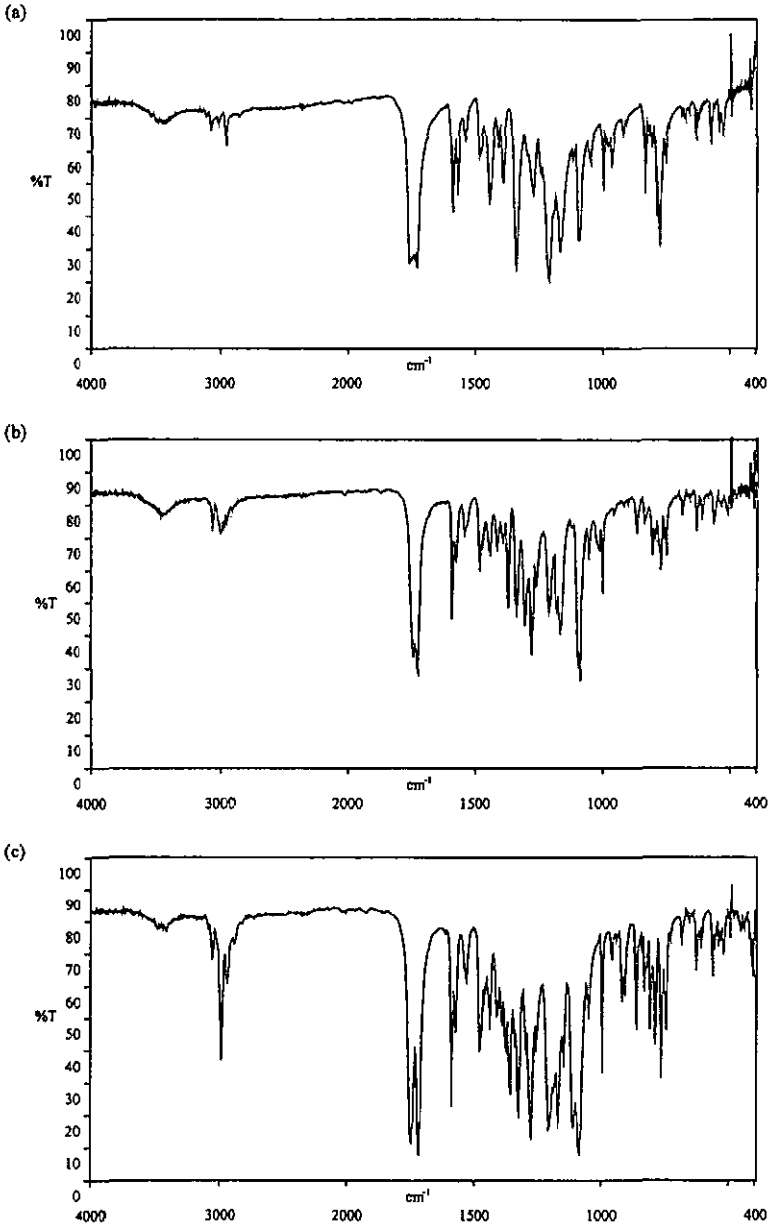

Figure 63. IR spectra of compounds (a) Me_2L **(20)**, (b) Et_2L **(21)** and (c) i-Pr_2L. **(22)**.

4.2.2 NMR Spectra

The ^{1}H NMR spectrum of compounds 20-22 in $CDCl_3$ exhibit a set of four resonances in the aromatic region for the 2-pyridyl rings which have similar positions each time. The resonances corresponding to the alkyl groups occur at the expected chemical shift (δ) and their intensities are those required.

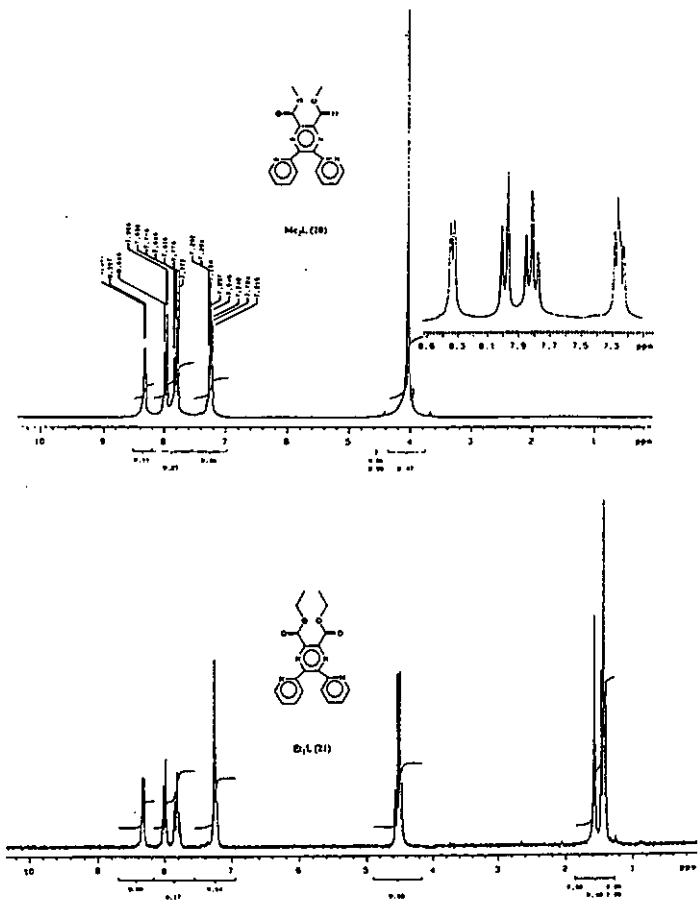

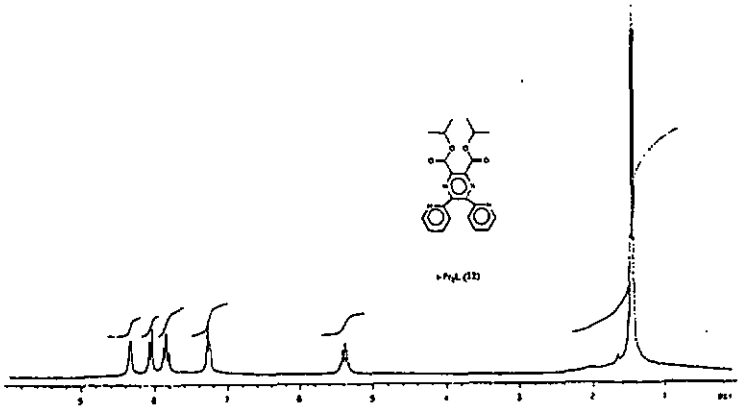

Figure 64. ^{1}H NMR of compounds (a) Me_2L (20), (b) Et_2L (21) and (c) i-Pr_2L. (22).

Me_2L (20)

Single crystals suitable for an X-ray analysis were obtained upon slow diffusion of MeOH into a solution of compound 20 in CH_2Cl_2.

In compound 20 the pyridine rings are inclined to the central pyrazine by 50.2(1)° (pyz^pyI) and 44.9(1)° (pyz^pyII). The ester moieties are twisted by 59.7(1)° and 50.4(1)° out of the pyrazine plane. The different twisting angles of the ester groups rend them inequivalent.

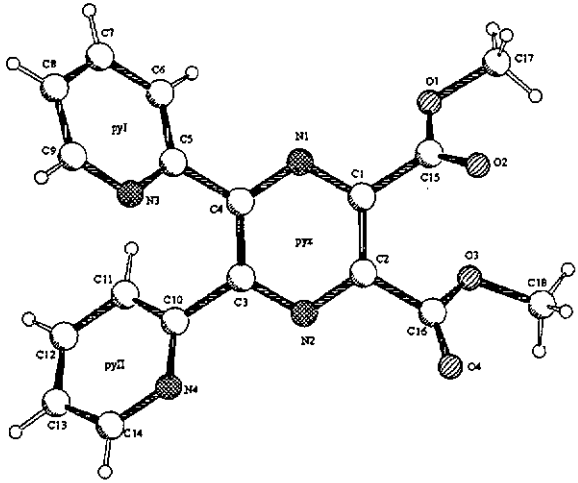

Figure 65. Molecular structure of Me_2L **(20)**.

The crystal cohesion is ensured by Van der Waals contacts, the shortest nonbonded distance being 2.714(1)Å between the H-atoms of the methyl groups and the N-atom of the pyridine rings.

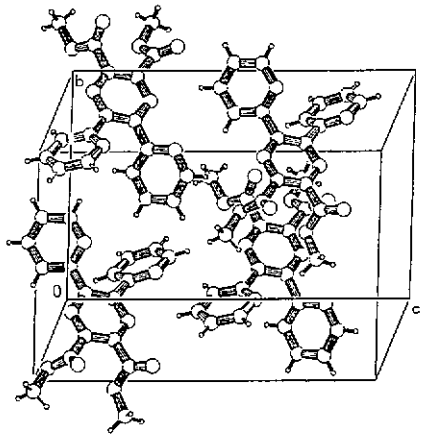

Figure 66. Crystal packing in compound Me_2L **(20)**.

Et_2L (21)

Slow evaporation of an ethanolic solution gave single crystals of a tetragonal form of compound Et_2L (21). The X-ray structure analysis showed that a crystallographic twofold axis bisects the Et_2L molecule, which is not planar; the pyridine rings and the ester groups are inclined toward the pyrazine system by 40.72(7)° and 39.4(1)°, respectively.

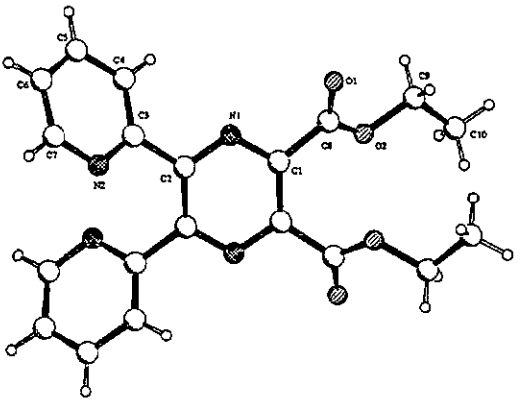

Figure 67. Molecular structure of compound Et_2L (21).

The molecules are hold together in the crystal by means of Van der Waals contacts.

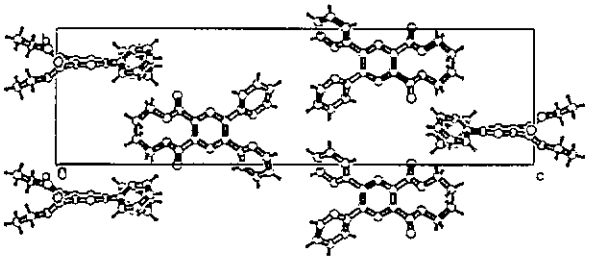

Figure 68. Crystal packingt in compound Et_2L (21).

Comparison of structures

The differences in the substituents of the pyrazine molecule cause different manners of packing and this influences the dihedral angles between the central pyrazine ring and the groups attached to it. The main differences concern the shortest intramolecular contacts. For example, in compound **20** the adjacent pyridine rings are twisted out of the pyrazine plane in the same direction with a N...N distance of 3.795(1)Å, while in compound **21** the pyrazine rings are twisted out of the pyrazine plane in opposite directions with a N...N distance of 3.242(1)Å.

Table 23. A comparison of various dihedral angles (°) and short intramolecular distances (Å) in Me_2L **(20)** and Et_2L **(21)**.

	Me_2L **(20)**	*Et_2L* **(21)**
Angles		
pyz twist	7.0(1)	4.0(1)
pyz^py	50.2(1), 44.9(1)	40.72(7)
pyz^COOR	59.7(1), 50.4(1)	39.4(1)
Distances		
$N_{py}...N_{py}$	3.795(1) (N3...N4)	3.042(1) (N2...N2^{i})
$N_{pyz}...C_{py}$	2.897(1) (N1...C11)	2.959(1) (N1...C4)
$N_{py}...C_{py}$	3.252(1) (N4...C6)	
$N_{pyz}...O_{COOR}$	2.902(1) (N1...O1)	2.795(1) (N1...O1)
	2.943(1) (N2...O4)	
$O_{COOR}...O_{COOR}$	2.961(1) (O2...O3)	2.839(1) (O2...O2^{i})

5 METAL CATALYZED HYDROLYSIS OF THE ESTER DERIVATIVES

Metal-catalysed hydrolysis of amino acid esters is a well-documented fact[82]. Stoeckli-Evans and co-workers have recently shown that the reaction of Cu(II) salts with the bis-methyl esters of pyrazine-2,3-dicarboxylic acid[83] and 2,5-dimethylpyrazine-3,6-dicarboxylic acid[84] resulted in the partial hydrolysis of the ligand and the formation of a two-dimensional coordination polymer and a mooonuclear complex, respectively.

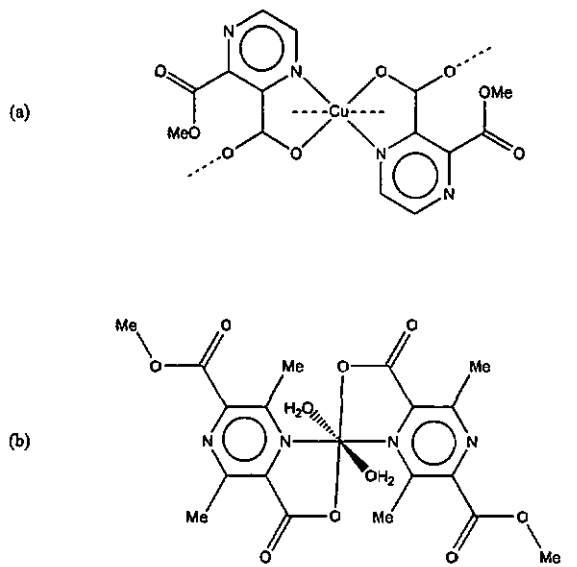

Figure 69. Schematic representation of (a) the centrosymmetric monomeric unit of the two-dimensional polymer $[Cu(C_7H_5N_2O_4)_2]_n$ and (b) the centrosymmetric mononuclear complex $[Cu(C_9H_9N_2O_4)_2(H_2O)_2]$.

Hence, the metal-ion-promoted ester hydrolysis leads to the formation of new ligands, becoming an extremely attractive manner to prepare new coordination compounds.

The metal-catalysed hydrolysis of esters can be represented by the following scheme

$$M^{2+} + Me_2L \xrightarrow[H_2O]{} [M(MeL)]^+ + MeOH$$

In this work we bave studied the effect of a variety of metal ions on the hydrolysis of the bis-methyl ester of 5,6-bis(2-pyridyl)pyrazine-2,3-dicarboxylic acid (hereafter Me_2L). We have found that in the reaction of Me_2L with $MnCl_2{\cdot}4H_2O$ and $CuCl_2{\cdot}H_2O$ partial hydrolysis of the bis-methyl ester takes place.

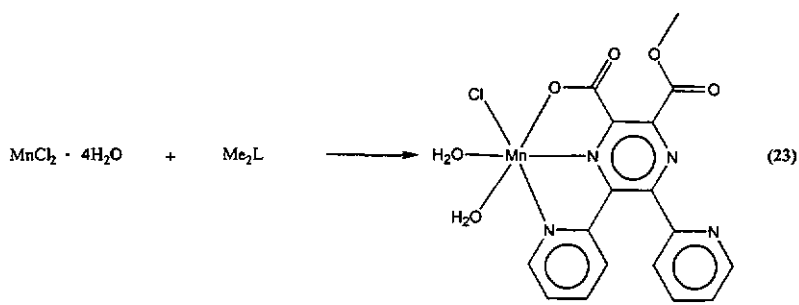

(23)

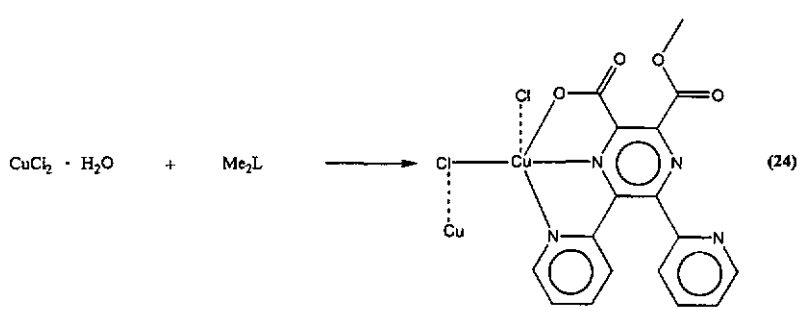

(24)

Two mechanisms can be proposed for the partial hydrolysis of this particular double ester[85]:

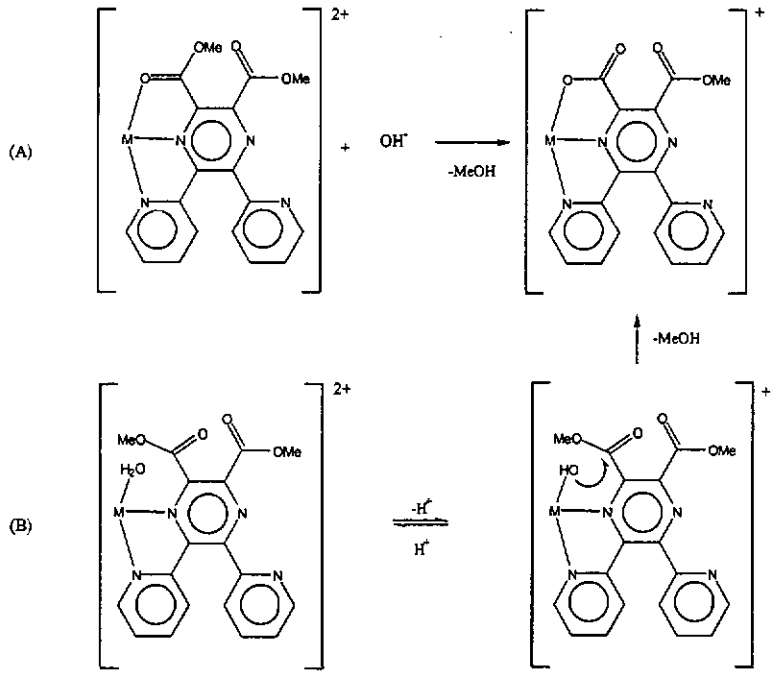

(A) involves attack by an hydroxide ion (or water molecule) on a complex in which the ester group is bound to the metal ion via the carbonyl oxygen atom. Mechanism (B) involves an acid-base pre-equilibrium with formation of a hydroxo-complex followed by intra-molecular bydroxide-ion attack.

When Fe(II), Co(II) and Ni(II) salts were added to a solution of Me_2L no reaction was observed. After slow evaporation of the reaction mixture, crystals of Me_2L together with the starting metal salt were deposited.

When d^{10} metal chlorides were reacted with Me_2L coordination of the ligand to the metal ion without hydrolysis of the ester groups occurred.

$ZnCl_2$ + Me_2L ⟶ 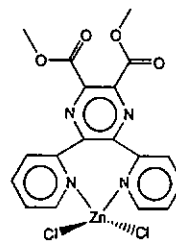 (25)

$CdCl_2 \cdot 2H_2O$ + Me_2L ⟶ 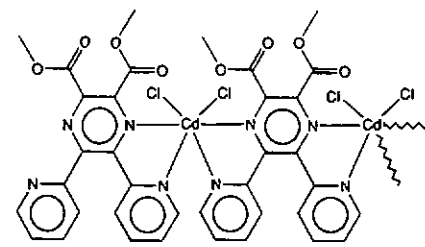 (26)

$HgCl_2 \cdot 2H_2O$ + Me_2L ⟶ 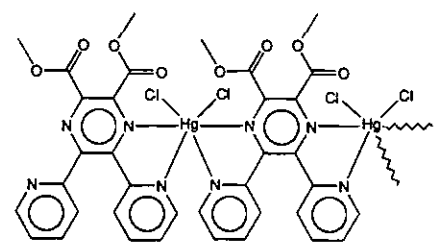 (27)

5.1 Manganese(II) complex

The addition reaction of Me_2L to $MnCl_2 \cdot 4H_2O$ leads to a compound of formula $[Mn(MeL)Cl(H_2O)_2]$ (23).

$$MnCl_2 \cdot 4H_2O + Me_2L \xrightarrow[MeOH,\ rt]{} [Mn(MeL)Cl(H_2O)_2] \text{ (23)}$$

In contrast to the free ligand the IR spectra of complex 23 shows two C=O absorption bands at ca. 1740 and 1680 cm^{-1}, indicating the presence of an uncoordinated –COOMe group and a coordinated $-COO^-$ group, respectivcly. The C=N and C=C stretching frequencies for the heterocyclic rings are found in the region between 1400 and 1600cm^{-1} and are not significantly displaced compared with the free ligand.

Table 24 . A comparison of the IR main absorptions of $[Mn(MeL)Cl(H_2O)]$ (23) with those corresponding to Me_2L (20).

	20	23
υ(C=O)	1743 s, 1729 vs	1738 s, 1682 br. vs
υ(C=N), υ(C=C)	1587 m, 1572 m, 1540 w, 1479 m, 1450 m, 1437 m, 1401 m	1600 s, 1569 m, 1531 m, 1488m, 1463 m, 1442 m, 1401 m
υ(C-O)	1283 vs	1294 s

vs very strong, s strong, m medium, w weak

[Mn(MeL)Cl(H$_2$O)$_2$] (23)

The structural characterisation has shown that complex **23** consists of discrete monomeric units in which a partially hydrolysed ligand is coordinated, in a mono-tridentate fashion, to the Mn atom.

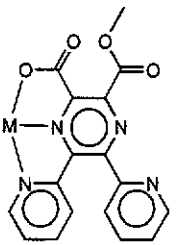

The coordination sphere of the Mn atom is completed by a terminal chloride and two water molecules. Long range Mn...O interactions involving the coordinated carboxylate O-atom of two molecules related by a centre of symmetry, gives rise to a dinuclear association. Thus, Mn atoms achieve an effective coordination number of seven. Although the Mn1-O1^{i} (symmetry code i= -x+1, -y, -z) distance of 2.763(1)Å is long, it does lie within the sum of van der Waals' radii (2.15Å for Mn and 1.52Å for O). Thus, complex **23** could be described as a weakly bonded dimer with a Mn...Mn distance of 4.329(6)Å.

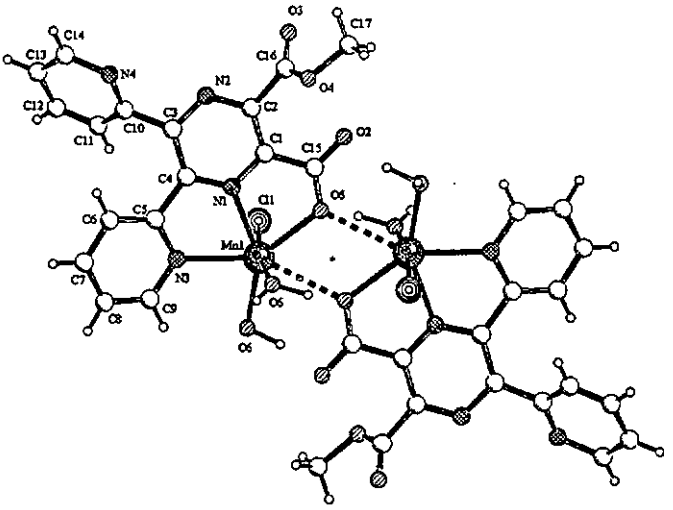

Figure 70. Asymmetric bridging of two $[Mn(MeL)Cl(H_2O)_2]$ monomeric units in complex **23**. The secondary Mn...O interactions are represented by dashed lines.

The formation of the dimer by the interaction of two monomers proceeds by means of highly unsymmetrical Mn_2O_2 bridges. The bridging Mn_2O_2 unit is strictly planar (the dihedral angle between planes [O1-Mn1-O1^i] and [O1^i-Mn1^i-O1] being ca. 1°), there being a crystallographic inversion centre in the middle of the dimer.

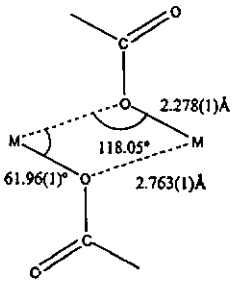

5.2 Copper(II) complex

The reaction of $CuCl_2 \cdot 2H_2O$ with Me_2L resulted in the formation of a complex of formula $[Cu(MeL)Cl]_n$. The low solubility of complex **24** in all common solvents suggested a polymeric structure.

$$CuCl_2 \cdot 2\,H_2O + Me_2L \xrightarrow[MeOH,\ rt]{} [Cu(MeL)Cl]_n \textbf{ (24)}$$

The IR spectra of complex **24** shows two bands in the ν(C=O) region, assigned to an uncoordinated –COOMe group ($1738cm^{-1}$) and to a coordinated $-COO^-$ group ($1640cm^{-1}$), indicating the partial hydrolysis of the Me_2L.

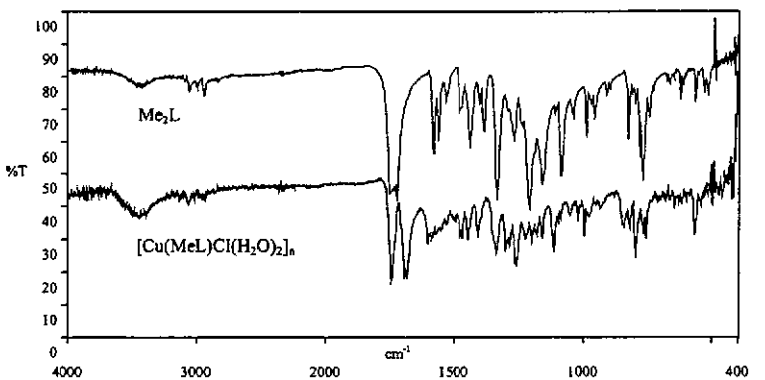

Figure 71. A comparison of the IR spectra of complex $[Cu(MeL)Cl]_n$ **(24)** with that of Me_2L **(20)**.

[Cu(MeL)Cl]$_n$ (24)

The crystal structure of compound **24** consists of neutral monomeric [Cu(MeL)Cl] units linked by single chloro bridges, building up a zig-zag polymeric chain. A view of the monomeric unit is shown in figure 72.

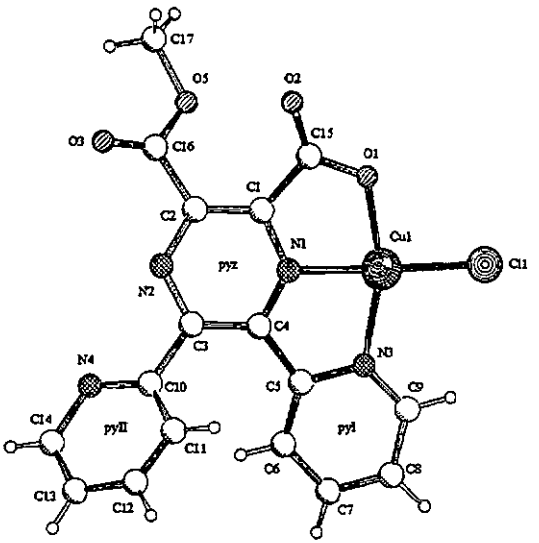

Figure 72. View of the crystallographically independent [Cu(MeL)Cl] monomeric unit.

The disposition of donor atoms around the copper(II) ion can be well described as a slightly distorted square-pyramide (τ= 0.09), the basal positions being occupied by two N-atoms and one O-atom of a partially hydrolysed ligand molecule and a chloride atom. The pyramid base is not exactly planar, the *trans* atoms O1 and N3 lying

0.091(4)Å and 0.092(4)Å above the best least-squares plane through the four ligating atoms while Cl1 and N1 lie –0.165(4)Å and –0.118(2)Å below it. As is commonly observed in tetragonal-pyramidal complexes, the metal atom lies 0.099(3)Å above the basal plane towards the axial ligand. The axial position is occupied by a chloride atom (the Cu1-Cl1^{i} axial distance of 2.9106(2)Å being considerably larger than the Cu1-Cl1 basal distance of 2.2068(1)Å), which is part of the base of the adjacent tetragonal pyramide. The chain is propagated along the crystallographic c-axis through the sharing of this chloride atom. The Cu1...Cu1^{i} (symmetry code i= 1-x, y, 0.5-z) distance of 3.8561(2)Å is considerably shorter than the Cu...Cu distances reported in the literature for mono-(μ-chloro)-bridged Cu(II) chain compounds[70,71,73,74]. The Cu1-Cl1-Cu1^{i} bridging angle of 96.829(5)° is narrower than that found in such chain complexes. The CuL moieties are located on alternate sides of the chain, presumably to minimise steric crowding. Thus, no interaction between aromatic rings of different units is observed (see figure 73).

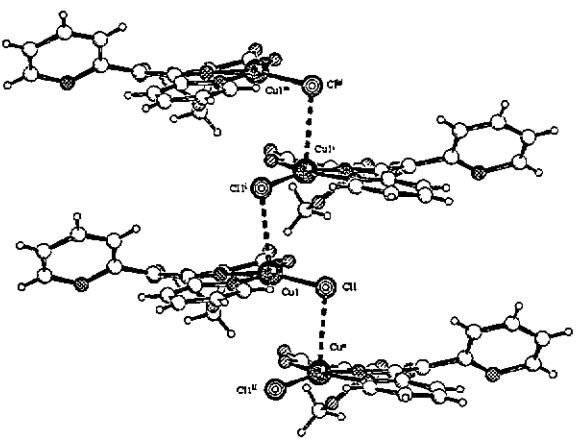

Figure 73. View of the zig-zag chain structure of compound **24** along the c-axis.

The magnetic bebaviour of complex **24** is shown in figure 74 in the form of both χ_M and μ_{eff} versus T plots. The value of μ_{eff} at room is 2.13 M.B., this value being higher than the spin-only value for a single copper atom (1.77 M.B.). The μ_{eff} decreases upon cooling and it vanishes at 0K. The occurrence of a maximum in the low temperature region is observed in the magnetic susceptibility curve (T_{max}= 2.2K, χ_M= $9.91 \cdot 10^{-2}$ $cm^3 \cdot mol^{-1}$). All these features are indicative of a weak intrachain antiferromagnetic coupling in complex **24**.

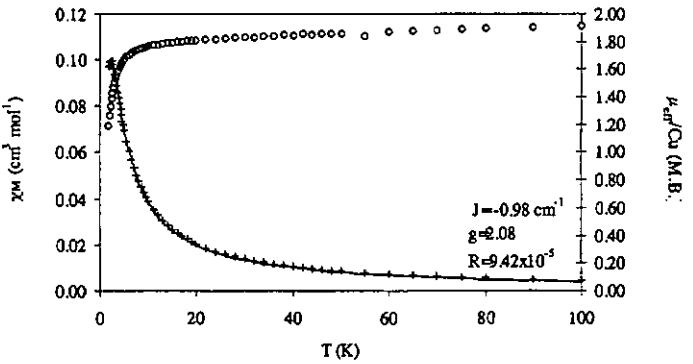

Figure 74. Magnetic properties of complex $[Cu(MeL)Cl(H_2O)_2]_n$ **(24).**

From a magnetic point of view, compound **24** can be treated as an uniformly-spaced chain of spin S=1/2. In order to analyse its magnetic behaviour, we have used the polynomial expression developed by Hall[69] which describes well the magnetic properties of chains of S=1/2 ions.

$$\chi = \frac{Ng^2\beta^2}{kT}\frac{0.250 + 0.14995x^{-1} + 0.30094x^{-2}}{1 + 1.9862x^{-1} + 0.68854x^{-2} + 6.0626x^{-3}} \text{ with } x = \frac{kT}{|J|}$$

The result of the best fit through the above equation leads to J= -0.98 cm^{-1}, g=2.08 and R= $9.42 \cdot 10^{-5}$, where R is the agreement factor defined as $R = \sum(\chi_{calc} - \chi_{obs})^2 / \sum \chi^2_{obs}$.

The value of J is small in agreement with the results reported for monochloro-bridged copper(II) compounds exhibiting an out-of-plane bridging framework[70]. Selected magneto-structural data of the known out-of-plane monochloro-bridged copper(II) compounds are grouped in Table 25[70].

Table 25. Structural and magnetic data of mono-μ-chloro bridged copper(II) chains[70].

Compound	J (cm^{-1})	Cu-Cl_{basal} (Å)	Cu-Cl_{axial} (Å)	Cu...Cu (Å)	Cu-Cl-Cu (°)
$Cu(dmso)Cl_2$	-6.1	2.290(2)	2.702(2)	4.757(2)	144.6(1)
$Cu(imH)Cl_2$	-2.1	2.365(4)	2.751(6)	4.37	117
$Cu(pepci)Cl^+$	-1.39	2.245(7)	2.797(8)	4.766(5)	138.3(3)-
		2.276(7)	2.868(7)		134.7(3)
$Cu(bipy)Cl_2$	-1.15	2.291(2)	2.674(3)	4.010(3)	107.5(1)
$Cu(MeL)Cl(H_2O)_2$ **(24)**	-0.98	2.067(2)	2.911(1)	3.856(1)	96.83(1)
$Cu(caf)Cl_2(H_2O)_2$	0.48	2.319(2)	2.788(2)	4.597(2)	128.1(?)
$Cu(maep)Cl_2$	1.58	2.300(2)	2.785(2)	4.263(2)	114.58(5)

It can be seen from Table 25 that there is no correlation between the value of J and the copper-copper separation. Consequently, a through-space mecbanism for excbange coupling can be ruled out, and another superexchange mechanism must be considered[71].

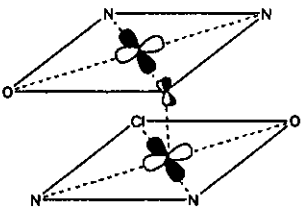

Figure 75. Superexchange mechanism in the out-of-plane monochloro-bridged Cu(II) compound $[Cu(MeL)Cl]_n$ **(24)** showing the poor overlap between magnetic orbitals.

The magnetic orbital in the observed geometry consists mainly of the $d_{x^2-y^2}$ orbital, which is situated, in the $CuClN_2O$ plane. For the different monomeric units the $d_{x^2-y^2}$ orbitals are parallel. Therefore, the direct overlap between these orbitals is zero. The exchange via the orbitals of the chloride bridge can be considered to be very small. Thus, the magnetic interaction between copper(II) ions is very weak.

In a paper of Estes et al.[70] the relationship between the value of the exchange coupling constant and the geometry has been established for a series of single chloride-bridged copper(II) chain compounds. The authors suggest that the angle at the chloro bridge is not the relevant parameter (as can be seen from Table 25), and they note that all these compounds exhibit geometries comprised between SP and TBP. The values of *trans*

L-Cu-L' angles have been used to follow this change in the copper geometry. These angles would be 180° for an ideal square pyramid. The smaller this angle, the greater the deviation from the SP geometry and the closer the TBP and, therefore, an increase of spin density on the bridge is expected. The values of the *trans* L-Cu-L' angles in the monochloro-bridged copper(II) chains are presented in Table 26.

Hay et al.[45] have performed molecular orbital calculations on a hypothetical monochloro-bridged copper(II) dimer and have shown an increase of the antiferromagnetic coupling as the distortion proceeds from the SP geometry toward the TBP.

Table 26. Geometry distortion about the copper atoms in monochloro-bridged copper(II) chains[70].

Compound	α (°)†	β(°)†	τ	J (cm^{-1})
$Cu(dmso)Cl_2$	146.1	173.0	0.45	-6.1
$Cu(imH)Cl_2$	166.9	174.3	0.12	-2.1
$Cu(pepci)Cl^+$	158.3-154.4	172.0-169.3	0.25-0.23	-1.39
$Cu(bipy)Cl_2$	158.5	171.5	0.21	-1.15
$Cu(MeL)Cl(H_2O)_2$	166.5	160.7	0.09	-0.98
$Cu(caf)Cl_2(H_2O)_2$	178.8	161.0	0.30	0.48
$Cu(maep)Cl_2$	176.0	165.7	0.17	1.58

† See page 69.

The distortion from the SP (measured by the index of trigonallity, τ, introduced by Addison et al.[68]) increases in the order $Cu(dmso)Cl_2$> $Cu(caf)Cl_2(H_2O)$> $Cu(dmso)Cl_2$> $Cu(bipy)Cl_2$> $Cu(maep)Cl_2$> $Cu(imH)Cl_2$> Cu(MeL)Cl, while the

angle at the chloro bridge increases in the order $Cu(dmso)Cl_2$>$Cu(pepci)Cl^+$> $Cu(caf)Cl(H_2O)$> $Cu(imH)Cl_2$> $Cu(maep)Cl_2$> $Cu(bipy)Cl_2$> Cu(MeL)Cl. In the light of these two trends, clearly the stronger antiferromagnetic coupling is predicted for $Cu(dmso)Cl_2$ and the weaker for Cu(MeL)Cl, as observed. In the other cases these two parameters play against one another.

5.3 Zinc(II) complex

The reaction of the ester ligand with $ZnCl_2$ led to a complex characterised as $[ZnCl_2(Me_2L)]$ **(25)**.

$$ZnCl_2 + Me_2L \xrightarrow[MeOH,\ rt]{} [ZnCl_2(Me_2L)] \quad \textbf{(25)}$$

The IR spectra of complex **25** show that both –COOMe groups have not been hydrolysed and remain uncoordinated.

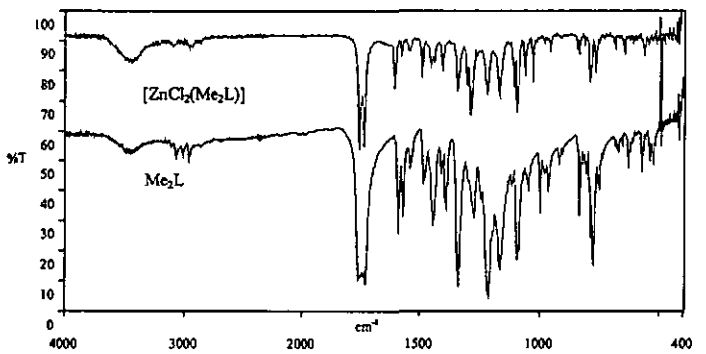

Figure 76. A comparison of the IR spectra of complex $[ZnCl_2(Me_2L)]$ **(25)** with that of Me_2L **(20)**.

[ZnCl$_2$(Me$_2$L)] (25)

Complex **25** consists of discrete mononuclear [ZnCl$_2$(Me$_2$L)] molecules, in which the zinc atom achieves a tetrahedral coordination by means of two nitrogen atoms of the ester ligand and two terminal chlorides.

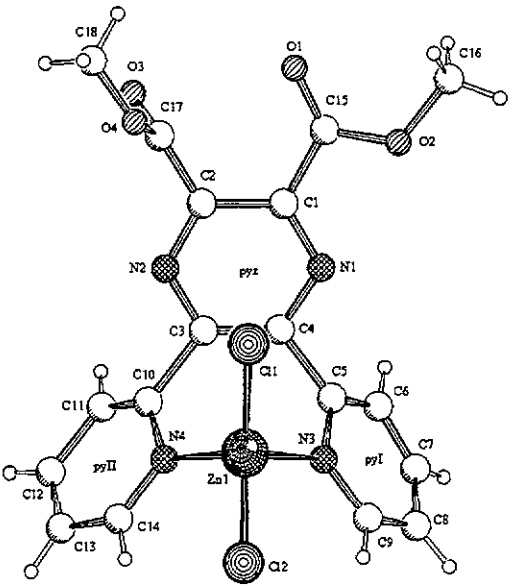

Figure 77. Molecular structure of complex [ZnCl$_2$(Me$_2$L)] **(25).**

The deviation from the regular geometry is very small, being mainly reflected in the N3-Zn1-N4 chelate angle of 87.98° which departs significantly from the ideal tetrahedral angle. The most relevant bond distances and angles are given in Table 27. The Zn-N and Zn-Cl distances are in good agreement with the standard values[76].

Table 27. Selected bond lengths (Å) and angles (°) for $[Zn(Me_2L)Cl_2]$ (25)

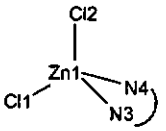

		Zn(1)-N(3)	2.04(3)
		Zn(1)-N(4)	2.05(3)
		Zn(1)-Cl(1)	2.18(1)
		Zn(1)-Cl(2)	2.20(1)
N(3)-Zn(1)-N(4)	88(1)	N(4)-Zn(1)-Cl(1)	112.4(5)
N(3)-Zn(1)-Cl(1)	114.3(7)	N(4)-Zn(1)-Cl(2)	109.3(7)
N(3)-Zn(1)-Cl(2)	107.2(7)	Cl(1)-Zn(1)-Cl(2)	120.8(4)

It is worth noting the unusual bidentate behaviour of the ester ligand in which coordination occurs via the N-atoms of both pyridine rings giving rise to a seven-membered chelate ring.

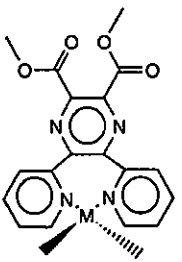

The pyridine rings are almost perpendicular to each other; the dihedral angle between them is 86(1)°. Moreover, the pyridine rings are rotated by 58(1)° (pyz^pyI) and 61(1)° (pyz^pyII) out of the plane of the pyrazine ring. The uncoordinated carboxylates are twisted by 43(1)° and 87(1)° with respect to the pyrazine system. A similar coordination mode has been reported previously for $[CuCl_2(TPPZ)]\cdot CH_3CN$[86].

5.4 Cadmium(II) complex

Reaction of $CdCl_2$ with Me_2L produces a polymeric complex, $[CdCl_2(Me_2L)]_n$ (26).

$$CdCl_2 \cdot 2H_2O + Me_2L \xrightarrow[MeOH,\ rt]{} [CdCl_2(Me_2L)]_n \quad (26)$$

The more significant feature observed in the IR spectrum of the present compound is the υ(C=O) absorption band at 1751 cm^{-1}, appearing close to the frequency observed in the free ligand (1743 cm^{-1}), which indicates that none of the ester groups have been hydrolysed. The υ(C=N) and υ(C=C) frequencies in complex **26** compared to those observed in the free ligand agree with the participation of the heterocyclic rings in the metal coordination.

Table 28. Comparison of the IR absorptions (cm^{-1}) of compound $[Cd(Me_2L)Cl_2]_n$ (26) with those of the free ligand Me_2L (20).

	Me_2L (20)	$[Cd(Me_2L)Cl_2]_n$ (26)
υ(C=O)/ $\upsilon_{as}(COO^-)$	1738 s, 1729 vs	1751 s
υ(C=N), υ(C=C)	1587 m, 1572 m, 1540 w, 1479 m, 1450 m, 1437 m, 1401 m	1593 vs, 1568 w, 1549 w, 1479 m, 1450 m, 1403 m
$\upsilon_s(COO^-)$	1330 s	1339 s

vs very strong, s strong, m medium, w weak

$[CdCl_2(Me_2L)]_n$ (26)

The crystal structure of complex 26 can be described as a linear $[CdCl_2(Me_2L)]_n$ chain in which the Cd(II) ions are bridged by a bis-bidentate Me_2L molecule with a Cd…Cd distance of 7.892(1)Å.

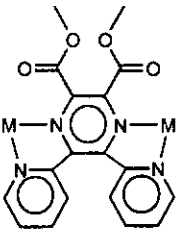

The asymmetric unit contains half of the $[CdCl_2(Me_2L)]$ repeating unit, which possesses a crystallographic two-fold axis.

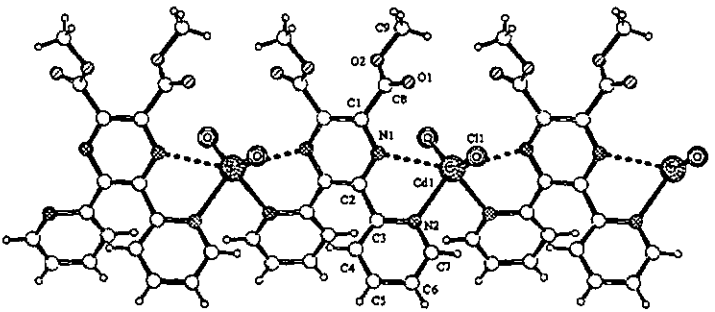

Figure 78. Polymeric structure of complex $[Cd(Me_2L)Cl_2]_n$ **(26)**.

The approximately octahedral coordination around the cadmium atom is completed by two terminal chloride ions. The distortion from the regular octahedral geometry in 26 is significant. This distortion is mainly due to the small bite angle of the bis-chelate ligand. Moreover, the long M-N_{pyz} distance could be considered as a secondary interaction. Then, the geometric parameters around the cadmium atom should correspond better to a tetrahedral coordination. However, this description does not agree with the bond angles found in 26, which depart considerably from the ideal tetrahedral angle. Selected bond lengths and angles are given in Table 29.

Table 29. Selected bond lengths (Å) and angles (°) for $[Cd(Me_2L)Cl_2]_n$ (26)

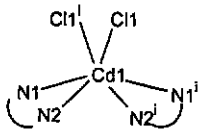

		N(2)-Cd(1)-N(2)^i	85.01(9)
		N(2)-Cd(1)-Cl(1)^i	110.88(5)
		N(2)^i-Cd(1)-Cl(1)^i	96.81(4)
		N(2)-Cd(1)-Cl(1)	96.81(4)
Cd(1)-N(2)	2.386(2)	N(2)^i-Cd(1)-Cl(1)	110.88(5)
Cd(1)-N(2)i	2.386(2)	Cl(1)^i-Cd(1)-Cl(1)	142.41(4)
Cd(1)-Cl(1)^i	2.4137(6)	N(2)-Cd(1)-N(1)	64.19(6)
Cd(1)-Cl(1)	2.4137(6)	N(2)^i-Cd(1)-N(1)	140.69(6)
Cd(1)-N(1)	2.776(2)	Cl(1)^i-Cd(1)-N(1)	74.16(4)
Cd(1)-N(1)^i	2.776(2)	Cl(1)-Cd(1)-N(1)	97.18(4)

Symmetry operator: i= -x+3/2, y, -z+3/2.

It is remarkable that within the $[CdCl_2(Me_2L)]$ units the chelating parts of the ligand deviate from planarity, with the coordinated pyridine rings twisted by 40.6(1)° out of the plane of the pyrazine ring. The pyridine rings are inclined to each other by

67.3(1)°. Moreover, the dihedral angle between the uncoordinated carboxylate groups is 61.5(3)° which could be attributed to the steric hindrance caused by the presence of the methyl groups.

5.5 Mercury(II) complex

The addition of Me_2L to a methanolic solution of $HgCl_2 \cdot 2H_2O$ leads to a complex of formula $[HgCl_2(Me_2L)]_n$.

$$HgCl_2 \cdot 2H_2O + Me_2L \xrightarrow[MeOH,\ rt]{} [HgCl_2(Me_2L)]_n \quad (27)$$

The IR spectra of compound **27** shows a similar pattern to that observed for complex **26**. Thus, complex **27** was expected to exhibit a similar structure.

Table 30. Comparison of the IR absorptions (cm^{-1}) of compound $[Cd(Me_2L)Cl_2]_n$ **(26)** with those of compound $[Hg(Me_2L)Cl_2]_n$ **(27)**.

	$[Cd(Me_2L)Cl_2]_n$ **(26)**	$[Hg(Me_2L)Cl_2]_n$ **(27)**
υ(C=O)/ $\upsilon_{as}(COO^-)$	1751 s	1747 vs
υ(C=N), υ(C=C)	1593 vs, 1568 w, 1549 w, 1479 m, 1450 m, 1403 m	1590 m, 1568 m, 1546 w, 1477 m, 1447 m, 1402 m
$\upsilon_s(COO^-)$	1339 s	1338 s

vs very strong, s strong, m medium, w weak

[HgCl$_2$(Me$_2$L)]$_n$ (27)

The structural characterisation of compound **27** has shown that it is isomorphus with the cadmium complex **26** described above.

The structure of complex **27** consists of [HgCl$_2$(Me$_2$L)] monomeric units which repeat by translation to give a linear chain that propagates along the crystallographic a-axis. The intrachain Hg...Hg distance is 8.104(1)Å.

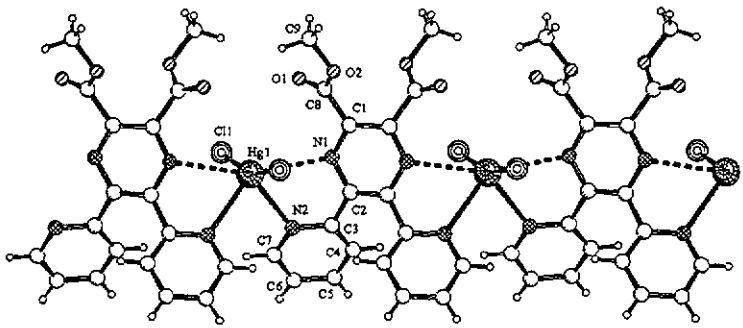

Figure 79. Polymeric structure of complex [Hg(Me$_2$L)Cl$_2$]$_n$ **(27).**

Each mercury atom is coordinated to two bis-bidentate Me$_2$L molecules belonging to consecutive monomeric units. The coordination around the mercury atoms is completed by two terminal chlorides. The mercury atom is in a considerably distorted octahedral environment where the angles about Hg range between 158.9(1)° and 60.9(1)°. The most relevant bond lengths and angles in complex **27** are given in Table 31.

Table 31. Selected bond lengths (Å) and angles (°) for $[Hg(Me_2L)Cl_2]_n$ (**27**)

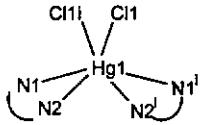

		N(2)-Hg(1)-N(2)^i	83.2(2)
		N(2)-Cd(1)-Cl(1)^i	93.0(1)
		N(2)^i-Hg(1)-Cl(1)^i	102.9(1)
		N(2)-Hg(1)-Cl(1)	102.9(1)
Hg(1)-N(2)	2.591(5)	N(2)^i-Hg(1)-Cl(1)	93.0(1)
Hg(1)-N(2)^i	2.591(5)	Cl(1)-Hg(1)-Cl(1)^i	158.9(1)
Hg(1)-Cl(1)^i	2.346(2)	N(2)-Hg(1)-N(1)	61.0(1)
Hg(1)-Cl(1)	2.346(2)	N(2)^i-Hg(1)-N(1)	137.7(1)
Hg(1)-N(1)	2.877(5)	Cl(1)^i-Hg(1)-N(1)	100.7(1)
Hg(1)-N(1)^i	2.877(5)	Cl(1)-Hg(1)-N(1)	75.7(1)

Symmetry operator: i= -x+1/2, y, -z+3/2.

The ligand itself is not planar in complex **27**. The pyridine rings are twisted by 42.1(1)° with respect to the central pyrazine ring and by 67.2(2)° to each other. On the other hand, the uncoordinated carboxylate groups are rotated 41.2(4)° out of the pyrazine plane, being inclined by 62.1(8)° to each other.

Comparison of structures 25-27

The addition reaction of Me_2L to zinc-group chlorides has always led to 1:1 adducts, $[MCl_2(Me_2L)]$ (M= Zn(II), Cd(II) and Hg(II)) even though several metal to ligand molar ratios up to 4:1 have been employed. The structural characterisation of these complexes indicated that zinc chloride behaves differently to Cd(II) and Hg(II) chlorides. While reaction of $ZnCl_2$ with the ester ligand produces a monomeric

compound $[ZnCl_2(Me_2L)]$ where the ester molecule coordinates in a mono-bidentate manner by means of both pyridine nitrogen atoms, reactions based on Cd(II) and Hg(II) chlorides have been shown to produce $[MCl_2(Me_2L)]_n$ (M= Cd(II) and Hg(II)) polymeric species with the Me_2L molecule acting as a bis-bidenate ligand through the pyrazine and pyridine nitrogen atoms.

To sum up, two new coordination modes of the ester ligand led to two different structure types. The coordination mode adopted for the ligand seems to be dictated by the size and geometry preferences of the metal ion. It is interesting to note that in none of these coordination modes are the ester groups involved in the coordination to the metal ion, remaining non-hydrolysed.

DISCUSSION-CONCLUSION

1. DISCUSSION-CONCLUSION

1.1 The ligand 5,6-bis(2-pyridyl)pyrazine-2,3-dicarboxylic acid and its derivatives

The ligand 5,6-bis(2-pyridyl)pyrazine-2,3-dicarboxylic acid was chosen for the formation of coordination polymers and has been prepared according to the procedure described in the literature[28].

An outstanding characteristic of this ligand is its amphoteric character. We believe the acid-base equilibrium present in aqueous solution may be one of the factors responsible for the coordination diversity of this ligand.

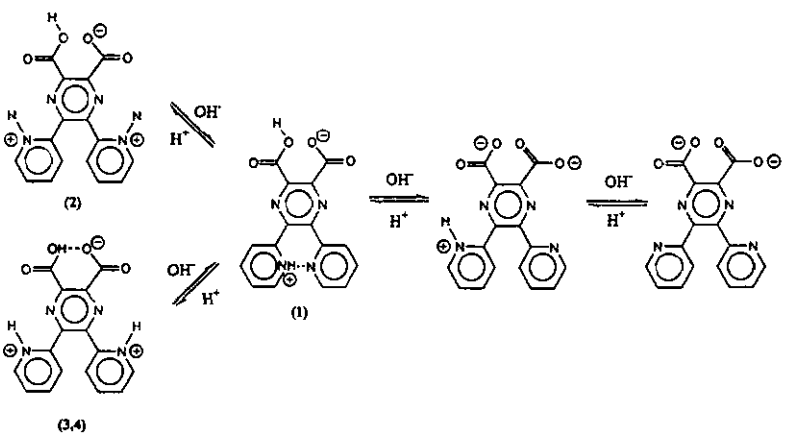

A study of the crystal structures of the ligand has shown that the ligand can exist in various forms depending on the pH. Two different protonated forms of the ligand have been obtained upon recrystallization of H_2L from HCl 1M (**2**), $HClO_4$ 1M (**3**) and $AgPF_6$ (**4**) aqueous solution (the protonated forms **3** and **4** are isomorphous). The diverse conformations of the ligand results from the different protonation of the substituents on the pyrazine ring. Protonation of both pyridine rings in **2-4** hinders the planar conformation observed in the zwitterionic form H_2L (**1**); in order to minimize the steric repulsion between the protons attached to the N-atoms the pyridine rings are rotated out of the plane of the pyrazine ring. Apart from the rotation of the pyridine rings with respect to the pyrazine ring, the triprotonated forms $[H_3L]Cl{\cdot}2.25H_2O$ (**2**) and $[H_3L]X{\cdot}3H_2O$ $X=ClO_4^-$(**3**), PF_6^-(**4**) differ in the orientation of adjacent carboxylate groups. While in $[H_3L]Cl{\cdot}2.25H_2O$ (**2**) the adjacent carboxylate groups are almost perpendicular to each other, $[H_3L]X{\cdot}3H_2O$ $X=ClO_4^-$(**3**), PF_6^-(**4**) exhibits a strong and symmetric intramolecular bydrogen-bond between adjacent carboxylate groups which forces them to be simultaneously coplanar to the pyrazine system.

The ester derivatives of the ligand have been prepared and the behaviour of Me_2L towards transition metal ions bas been investigated. We can distinguish three types of behaviour: (a) the reaction of Me_2L with M^{2+} in aqueous conditions gives rise to the total bydrolysis of the ester groups; however, when the reaction is carried out in methanol either (b) partial hydrolysis or (c) non-hydrolysis of the ester groups was observed, even though hydrated metal salts were used.

Total Hydrolysis

$Co(NO_3)_2 \cdot 6H_2O + Me_2L \xrightarrow[H_2O,\ rt]{} [CoL(H_2O)_3] \cdot 3H_2O$ **(8)**

Partial Hydrolysis

$MnCl_2 \cdot 4H_2O + Me_2L \xrightarrow[MeOH,\ rt]{} [Mn(MeL)Cl(H_2O)_2]$ **(23)**

$CuCl_2 \cdot 2H_2O + Me_2L \xrightarrow[MeOH,\ rt]{} [Cu(MeL)Cl]_n$ **(24)**

No hydrolysis

$ZnCl_2 + Me_2L \xrightarrow[MeOH,\ rt]{} [ZnCl_2(Me_2L)]$ **(25)**

$CdCl_2 \cdot 2H_2O + Me_2L \xrightarrow[MeOH,\ rt]{} [CdCl_2(Me_2L)]_n$ **(26)**

$HgCl_2 \cdot 2H_2O + Me_2L \xrightarrow[MeOH,\ rt]{} [HgCl_2(Me_2L)]_n$ **(27)**

1.2 The diversity of the ligand coordination behaviour

The coordination behaviour of H_2L towards transition metal ions has been explored. The results of these studies have shown the flexibility of the ligand, which is able to coordinate up to four metal ions. H_2L can act either as a terminal ligand, when bonded via one side, or as a bridging spacer giving rise to oligo- or polymeric compounds. A range of coordination possibilities exists depending on the metal ion involved, the solvent, the pH of the media, etc. The rich conformational diversity of this ligand gives rise to a variety of structures, which illustrates the difficulty of attempting to predict the 3-D structure of the resulting complexes.

Mononuclear complexes

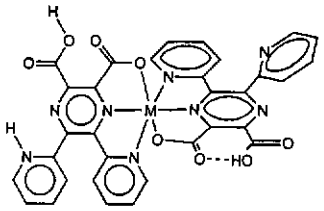

$[Co(HL)(H_2L)]ClO_4 \cdot H_2O$ **(7)**

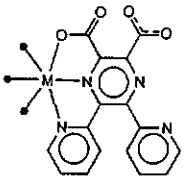

$[CoL(H_2O)_3] \cdot 3H_2O$ **(8)**

$[NiL(H_2O)_3] \cdot 3H_2O$ **(10)**

$[ZnL(H_2O)_3] \cdot 3H_2O$ **(15)**

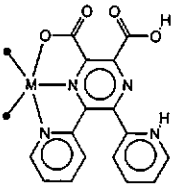

$[ZnCl_2(H_2L)]$ **(16)**

$[HgCl_2(H_2L)]$ **(19)**

Binuclear complexes

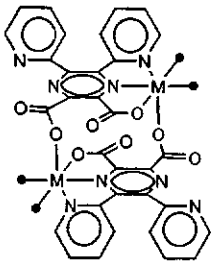

$[Mn_2L_2(H_2O)_4] \cdot 4H_2O$ **(5)**

$[Fe_2L_2(H_2O)_4] \cdot 4H_2O$ **(6)**

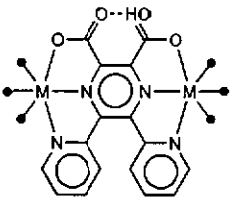

$[Co_2(HL)Cl_2(H_2O)_4] \cdot 4H_2O$ **(9)**

Trinuclear complex

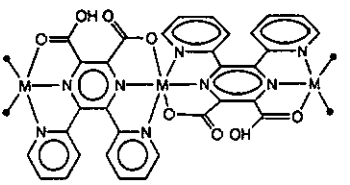

$[Cd_3(HL)_2I_4]$ **(18)**

One-dimensional polymers

a) Uniform helical chain

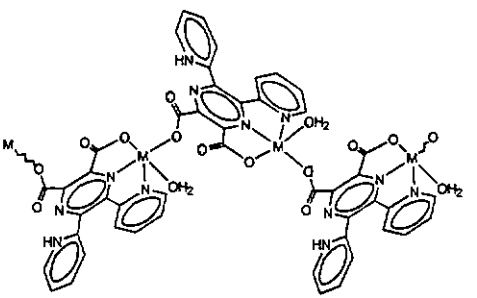

$\{[Cu(HL)(H_2O)]ClO_4 \cdot 3H_2O\}_n$ **(11)**

b) Alternating zig-zag chains

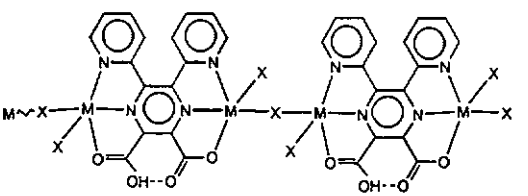

$\{[Cu_2(HL)Cl_3] \cdot H_2O\}_n$ **(12)**

$\{[Cu_2(HL)Br_3] \cdot H_2O\}_n$ **(13)**

Two-dimensional polymers

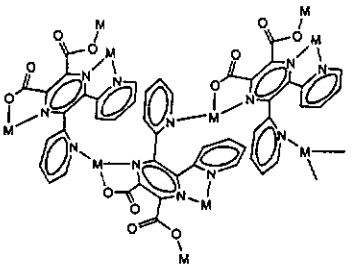

$\{[Ag_4L_2(NH_3)_2] \cdot H_2O\}_n$ (14)

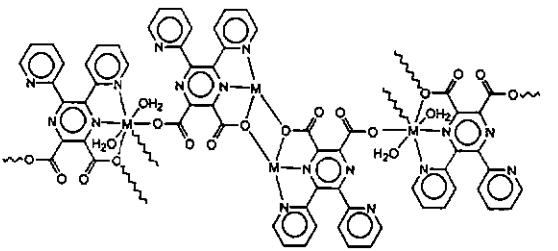

$[CdL(H_2O)_2]n$ (17)

The main structural parameters of compounds **5-27**, described in the present work, are summarized in Table 32. A search in the CSD for related compounds[8-10,12,21-23,26,27,29,31,37-39,57,60,61,75,83,84] has been carried out, and the average bond distance found for such complexes is given in Table 32 as standard value.

Table 32. A comparison of metal bond distances (Å), chelate and dihedral angles (°) in complexes containing the ligand H_2L and Me_2L.

Compound	*Bond distances (Å)*					*Bond angles (°)*		*Chelate angles (°)*	
	$M\text{-}N_{pyz}$	$M\text{-}N_{py}$	$M\text{-}O_{chelate}$	$M\text{-}O_{mono.}$	M-L-M	$N_{pyz}\text{-}M\text{-}N_{py}$	$N_{pyz}\text{-}M\text{-}O$	Pyz^py	Pyz^Carboxyl.
M= Mn (5)	2.242(2)	2.311(3)	2.227(2)	2.139(2)	6.581(1)	70.06(1)	71.8(1)	19.6(2), 64.4(1)	7.8(5), 80.6(2)
(23)	2.295(7)	2.37(1)	2.28(1)	2.76(1)	4.329(6)	67.7(3)	70.8(3)	19.1(5), 42.6(3)	7(1), 64.8(5)
Standard Value	2.316	2.267	2.198	2.176					
M= Fe (6)	2.126(2)	2.205(3)	2.132(2)	2.105(2)	6.501(1)	72.9(1)	74.9(1)	14.7(2), 64.6(1)	7.3(5), 79.3(1)
Standard Value	2.169	2.18	2.092						
M= Co (7)	2.048(5)	2.097(5)	2.086(5)	-	-	75.1(2)-	76.5(2)-	9.3(3), 74.2(2),	3.5(8), 3(1),
	2.049(5)	2.139(5)	2.136(5)			76.3(2)	77.4(2)	16.9(2), 48.6(2)	7.9(8), 16(1)
(8)	2.08(1)	2.157(9)	2.135(9)	-	-	74.1(3)	76.4(4)	12.2(6), 44.4(3)	15(1), 63.2(6)
(9)	2.101(3)	2.121(4)	2.117(4)	-	6.879(1)	74.7(1)-	74.7(1)-	24.4(2), 24.0(2)	7.5(8), 5.5(5)
	2.117(4)	2.140(4)	2.154(3)			75.0(1)	75.4(1)		
Standard Value	2.138	2.131	2.068						
M= Ni (10)	1.980(6)	2.126(8)	2.129(7)	-	-	79.6(3)	77.0(3)	14.1(5), 43.2(2)	10(1), 65.0(4)
Standard Value	2.065	2.081	2.035						
M= Cu (11)	1.917(5)	2.051(5)	1.987(5)	1.942(5)	7.747(1)	79.5(2)	81.5(2)	17.9(2), 42.9(2)	8.4(1), 80.5(9)
(12)	1.960(1)	1.930(2)	2.076(2)		6.563(4)				
(13)	1.962(1)	2.011(1)	1.969(1)		6.528(1)				
(24)	1.954(7)	2.036(7)	1.954(6)	-	3.856(1)	79.1(3)	81.8(3)	12.5(3), 40.4(2)	18.2(8), 37.9(7)
Standard Value	2.012	2.006	1.946	1.986					

Compound	*Bond distances (Å)*					*Bond angles (°)*		*Chelate angles (°)*	
	$M\text{-}N_{pyz}$	$M\text{-}N_{py}$	$M\text{-}O_{chelate}$	$M\text{-}O_{mono.}$	M-L-M	$N_{pyz}\text{-}M\text{-}N_{py}$	$N_{pyz}\text{-}M\text{-}O$	Pyz^py	Pyz^Carboxyl.
M= Ag (14)	2.341(1)	2.216(1)	2.211(1)	2.577(1)	6.168(1)				
	2.339(1)	2.254(1)	2.268(1)		7.399(2)				
Standard Value	2.352	2.299	2.363	2.313					
M= Zn (15)	2.087(4)	2.172(5)	2.150(5)	-	-	74.0(1)	76.7(2)	14.1(3), 43.8(1)	13.7(9), 64.1(3)
(16)	2.144(2)	2.165(2)	2.165(2)	-	-	73.69(8)	73.54(8)	14.6(1), 47.4(1)	10.4(3), 13.4(4)
(25)	-	2.04(3)	-	-	-	-	-	57(1), 61(1)	87(1), 43(2)
		2.05(3)							
Standard Value	2.114	2.147	2.132	2.122					
M= Cd (17)	2.417(4)	2.430(4)	2.372(4)-	-	3.876(1),	65.4(1)	68.0(1)	16.9(3), 60.2(2)	1.9(6), 87.0(4)
			2.426(4)		8.674(1)				
(18)	2.207(1)-	2.219(1)-	2.364(1)-	-	7.235(1)	68.8(5),	67.3(5),	24.0(9), 32(1)	9(4), 13(2)
	2.373(1)	2.377(1)	2.366(1)			74.9(7)	69.2(7)		
(26)	2.776(2)	2.386(2)	-	-	7.892(1)	64.2(1)	-	40.56(5)	42.6(1)
Standard Value	2.393	2.419	2.331	2.266					
M= Hg (19)	2.494(6)	2.374(7)	2.495(7)	-	-	66.6(2)	64.3(2)	20.0(4), 46.5(3)	11(2), 11(1)
(27)	2.877(5)	2.591	-	-	8.104(1)	60.96(1)	-	43.2(9)	41.2(4)
Standard Value	2.480-	2.335-							
	2.613	2.656							

Except in compounds $[HgCl_2(H_2L)]$ (19) and $[MCl_2(Me_2L)]_n$ with M= Cd (26) and Hg (27), the metal-nitrogen (pyrazine) distances have been found to be shorter than the metal-nitrogen (pyridine) bond distances. A similar trend was also observed in TPPZ[78] and 3,6-bis(2-pyridyl)pyrazine-2,5-dicarboxylic acid[28] complexes.

It is worth to note that compounds 8, 10 and 15 are isostructural, the primary difference in their structures being those expected as a result of the different size of the metal ions (see Table 33).

Table 33. A comparison of selected bond distances (Å) and angles (°) in the isostructural complexes $[ML(H_2O)_3]\cdot 3H_2O$.

Compound	M-N_{pyz}	M-N_{py}	M-O	M-O_w	N_{pyz}-M-N_{py}	N_{pyz}-M-O	N_{py}-M-O
M= Co (8)	2.08(1)	2.157(9)	2.135(9)	1.979(8)-	74.1(3)	76.4(4),	149.7(3)
	2.09(1)	2.167(9)	2.133(9)	2.146(9)	74.7(4)	76.2(4)	150.2(4)
M= Ni (10)	1.980(6)	2.126(8)	2.129(7)	2.028(6)-	77.0(3)	79.6(3)	156.5(3)
				2.081(7)			
M= Zn (15)	2.087(4)	2.172(5)	2.150(5)	2.003(4)-	74.0(2)	76.7(2)	150.7(2)
				2.133(5)			

H_2L is a sterically hindered ligand and in all crystallographically investigated complexes the ligand molecule is substantially distorted from planarity. This distortion is characterized by a twist of the pyrazine ring and by the dihedral angle between adjacent pyridine rings and adjacent carboxylic groups. The twist of the pyrazine ring varies from 1.4(5)° to 9(1)° and the dihedral angles pyz^py and pyz^COO from 9.3(3)° to 74.2(2)° and from 1.9(6)° to 87.0(4)°, respectively. This distortion is pressumably a consequence of a close contact between adjacent pyridine rings and the adjacent carboxylic groups. The steric repulsion between adjacent

substituents is reduced by rotation out of the plane of the pyrazine system and a twist in the pyrazine ring itself.

The strong H-bonding character of the ligand molecule, with N- and O-donor/acceptor atoms, makes the design of 3D supramolecular structures via H-bonding linkages possible.

1.3 Magnetic exchange through the ligand

One of the aims of the present work was to study the magnetic interaction through the ligand 5,6-bis(2-pyridyl)pyrazine-2,3-dicarboxylic acid. The magnetic susceptibility measurements indicate no significant spin interactions between metal ions through this ligand. The fact that the magnetic exchange is negligible can be explained from the observed crystal structures. The exchange coupling only occurs if there is a significant overlap between the orbitals of the interacting paramagnetic centers and the bridging ligand. The small values of the coupling constant, J, determined experimentally for H_2L complexes can be attributed to the fact that the ligand coordinates in the asymmetric bridging mode which combines a tridentate domain and a monodentate carboxylate group almost perpendicular to the pyrazine ring. Such a situation leads to a poor overlap between the magnetic orbitals of the metal ions and the orbitals of the bridging ligand and, therefore no significant magnetic exchange occurs.

In Table 34 the magnetic properties of compounds containing the ligand H_2L are summarized and compared with those found for related compounds. The strongest magnetic exchange is found in the copper complex of TPPZ $[Cu_2(TPPZ)(H_2O)_4](ClO_4)_4 \cdot 2H_2O$[39]. It is well-known that the shorter the M...M distance the stronger the spin coupling. Since in pyrazine complexes the M...M separation depends on the Cu-Npyz distance, the strongest spin coupling is expected to occur in the compound exhibiting the shortest M-Npyz distance, as observed form Table 34. It is worth noting that even if in compound 11 the M-Npyz distance is short, there is no effective orbital overlap which is necessary to transmit the magnetic exchange.

Table 34. Magnetic properties in some-pyrazine bridged complexes

Compound	Magnetic properties		*Distances* (Å)		
	J (cm^{-1})	g	M-pyz-M	M-pyz-COO-M	M-N_{pyz}
$[Mn_2L_2(H_2O)_4]\cdot 4H_2O$ **(5)**	-0.14	2.00		6.581(1)	2.242(2)
$\{(H_3O)_2[Mn(pyzdc)_2]\}_n$[23]	-0.02	2.00			2.308(1)
$\{[Mn(pyzdc)(H_2O)_2]\cdot 2H_2O\}_n$[23]	-0.27	2.00			2.294(2)
$[Mn_2(SCN)_4(bppz)_3]\cdot 2CH_3OH$[24]	<1		7.426(2)		2.349(3)
$\{[Mn(H_2pyztc)(H_2O)_2]\cdot 2H_2O\}_n$[27]		1.90	7.644(1)		2.463(1)
$\{K_2[Mn(pyztc)(H_2O)]\cdot 2.25H_2O\}_n$[27]		1.90		7.762(2)	2.198(4)
$[Fe_2L_2(H_2O)_4]\cdot 4H_2O$ **(6)**	-0.30	2.11		6.501(1)	2.126(2)
$\{[Fe(H_2pyztc)_2(H_2O)_2]\cdot 2H_2O\}_n$[60]	<1	2.11	7.170		2.219(8)
$[Fe_2(SO_4)_2(bppz)(H_2O)_6]\cdot 2H_2O$[24]	<1		7.091(5)		2.18(1)
$\{[Cu(HL)(H_2O)]\ 3H_2O\}_n$ **(11)**	-0.24	2.24		7.747(1)	1.917(5)
$\{[Cu(Hpyzdc)]Cl\}_n$[21]	+1.9	2.26	6.678		2.01
$[Cu_2(TPPZ)(H_2O)_4](ClO_4)_4\cdot 2H_2O$[39]	-30.5	2.13	6.497(1)		1.975(4)
$[Cu_2(TPPZ)Cl_4]\cdot 5H_2O$[39]	-17.0	2.05	6.565(1)		1.962(3)
$[Cu_2(dapz)(dien)_2](ClO_4)_4$[46]	-1.7	2.11	6.850		2.052(5)

H_4pyztc= pyrazine-2,3,5,6-tetracarboxylic acid H_2pyzdc= pyrazine-2,3-dicarboxylic acid, bppz= 2,5-bis(2-pyridyl)pyrazine, TPPZ= 2,3,5,6-tetra(2-pyridyl)pyrazine, dapz= 2,5-di(aminomethyl)pyrazine

1.4 Suggestions for further investigations

The research described here has revealed several possibilities for further investigations.

1. It would be interesting to design a strategy to obtain beteronuclear compounds. This may be possible by reacting the ligand-complexes where not all the potential donor-atoms are involved in coordination with metal-ions of higher acceptor capacity.

2. Amides are generally less reactive than the corresponding carboxylic acid esters. They can be hydrolyzed with either acidic or basic catalysis at high temperatures. In general, bydrolysis of amides requires more drastic conditions than the hydrolysis of esters. Some Cu(II) complexes of the ligands pyrazine-2-carboxamide[87] and pyrazine-2,3-dicarboxamide[88-90] bave been reported in the chemical literature. It is interesting to note that an amide can coordinate either through the N- or the O-atom:

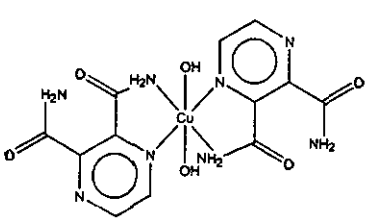

Therefore, an attractive idea would be to prepare the amide derivatives of the ligand H_2L, and study the coordinating properties of these new ligands.

3. Reduction of the ethyl ester Et_2L to the corresponding alcohol would also provide a new ligand, the 5,6-bis(2-pyridyl)pyrazine-2,3-bis(methylhydroxy)pyrazine. Complexation of such a ligand may involve much stronger complexation with first row transition metals, perhaps leading to a stronger magnetic coupling.

1.5 Open questions

This section describes several novel complexes that could not be readily prepared. Further work is needed to obtain such compounds with a reasonable synthetic effort.

1. Heteronuclear complexes

Part of the research on heteronuclear compounds is focused on obtaining systems with new magnetic properties, e.g. ferromagnets. The synthesis of heteronuclear complexes becomes possible using asymmetric ligands. Modification of the ligand H_2L to provide different coordination sites for the metal ions allows a good strategy towards obtaining heteronuclear compounds.

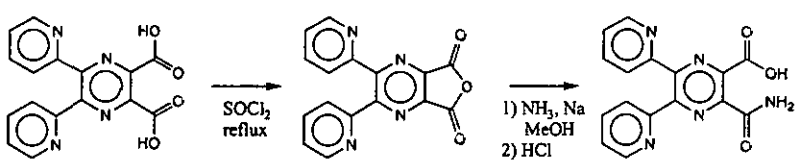

Despite the nature of the ligand carboxylate groups, which can be easily modified, we were unable to isolate the asymmetric amide as a pure compound.

2. Mixed-ligand complexes

One-dimensional alternating chains can be achieved by alternating the bridging ligands between the metal ions in a ...-L-M-L'-M-L-... sequence. When CuX_2 (X= Cl, Br) is reacted with H_2L the alternating polymeric chains $[Cu_2(HL)X_3]\cdot 2H_2O\}_n$ (12, 13) are obtained. However, combination of H_2L and $RCOO^-$ bridges has not been successful to date.

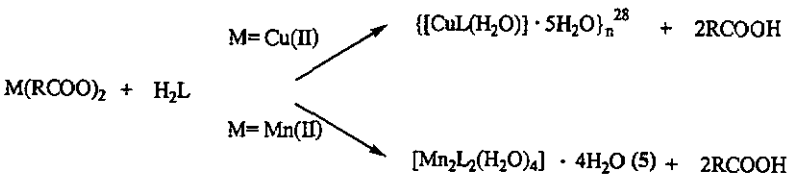

The higher acidity of H_2L and the capacity of this ligand to coordinate in a stable tridentate manner dominates. The tendency of L^{2-} to bridge metal ions appears to be significantly higher than that of $RCOO^-$ (R= CH_3-, Ph-, MePh- and ClPh-).

3. M(III) complexes

In the course of our studies on the coordination behavior of H_2L we have been involved in the synthesis of M(III) (M= Cr, Mn, Fe, Co) compounds. We were unable to isolate crystalline products with a well-defined stoichiometry. Possibly, prolongated efforts would afford single crystals of M(III) complexes with H_2L that may allow their structural characterization.

4. Ln(III) complexes

The ligand H_2L has been used in attempts to form trivalent lanthanide (Ln(III)) complexes in aqueous medium. Slow evaporation of the resulting aqueous solutions resulted in the formation of gels. A possible explanation can be attributed to the water coordinating ability of the oxophilic lanthanide ions together with its hydrogen-bonding capability. On the other hand, a low affinity of H_2L for Ln(III) ions is expected due to the small size of the coordination cavity.

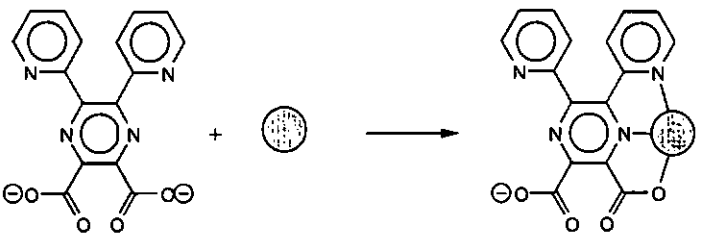

Ⓛ = Ln(III)

SUMMARY

In the last decade, a series of new substituted pyrazine ligands have been synthesized and a systematic study of their coordination chemistry has been undertaken[24,28,78,91-93]. Our primary interest in these systems is related to the possibility of obtaining coordination polymers. As an extension of this work the coordination chemistry of the ligand 5,6-bis(2-pyridyl)pyrazine-2,3-dicarboxylic acid (H_2L) has been investigated. A number of H_2L coordination compounds have been prepared and characterized by X-ray diffraction. They show a remarkable variety of 3-D structures ranging from monomeric complexes such as $[ML(H_2O)_3]\cdot 3H_2O$ M= Co **(8)**, Ni **(10)**, Zn **(15)** to two-dimensional polymers. The different structures of the H_2L complexes appear to be dictated by the different coordination number and the geometrical preferences of the metal ion, the solvent and the pH conditions in which the reaction is carried out. Hydrogen-bonding also appears to be an important factor in influencing the overall structure. In addition, the ligand itself shows a variety of coordination modes.

The present study has shown that by combining suitable transition metal ions and H_2L it is possible to build up coordination polymers with different structural features, including: uniform-helical-chains $\{[Cu(HL)(H_2O)]\cdot 3H_2O\}_n$ **(11)**, alternating-zig-zag-chains $\{[Cu_2(HL)X_3]\cdot 2H_2O\}_n$ X= Cl **(12)**, Br **(13)**, and two-dimensional uniform polymers $\{[Ag_4L_2(NH_3)_2]\cdot H_2O\}_n$ **(14)** and $[CdL(H_2O)_2]_n$ **(17)**.

Another objective of this work has been the study of the metal-catalyzed hydrolysis of the ester derivatives. In this context the methyl- (Me_2L), ethyl- (Et_2L) and isopropyl (i-Pr_2L) esters of the ligand have been prepared. The metal can act as a Lewis acid and the catalytic hydrolysis of the ester groups has been studied. It has been shown that in aqueous conditions the metal assisted hydrolysis is complete and always occurs. When the reaction is carried out in methanol a partial hydrolysis is observed for M= Cu(II) and Mn(II), and the non-coordinated carboxylic group remains non-hydrolyzed. However, for Zn(II), Cd(II) and Hg(II) no hydrolysis of the ester groups is observed, hence they are not involved in coordination.

Finally, a study of the magnetic properties of the complexes with paramagnetic metal ions has also been carried out. The magnetic susceptibility measurements have shown that H_2L and its derivatives are rather ineffective in transmitting spin interactions between paramagnetic metal ions. That is, no significant magnetic exchange through this ligand has been found, as expected from the structural data. Although in H_2L complexes where the M-Npyz distance is short, the ligand conformation does not favour an effective overlap between the orbitals of the interacting metal ions and the bridging ligand leading to a weak spin coupling.

EXPERIMENTAL

1 GENERALITIES

1.1. Starting Materials

All chemicals employed were commercially available reagent grade materials (Fluka and Aldrich Chemicals), used as supplied, without further purification.

Caution! Perchlorate salts with organic ligands are potentially explosive and should be handled with the necessary precautions.

2 PHYSICAL MEASUREMENTS

2.1 Elemental analyses

C, H and N microanalyses were performed by the 'Forschungszentrum' of Ciba-Geigy AG, Marly and the 'Mikroelementaranalytische Laboratorium' of the ETH-Zentrum, Zürich.

2.2 Infrared Spectroscopy

IR spectra were recorded on a PERKIN-ELMER FT-IR 1720X spectrometer using KBr pellets. The absorption bands were determined in wave numbers (cm^{-1}). The abbreviation for the described intensities are: vs= very strong, s= strong, m= medium, w= weak, sh= shoulder, br= broad.

2.3 Nuclear Magnetic Resonance spectroscopy

The ^{1}H- and ^{13}C-NMR spectra of all compounds were recorded on a VARIAN GEMINI 200 (200 MHz) or a BRUKER AMX-400 (400MHz) spectrometers. The chemical shift (δ), with respect to TMS as internal standard or DDS while D_2O was used as solvent, is given in ppm. The abbreviation for the multiplicities are: s= singlet, d= doublet, t= triplet, m= multiplet, b= broad.

2.4 Ultraviolet-Visible spectroscopy

UV-Vis spectra were recorded on a UVIKON 930 spectrophotometer. Quartz dust-plates (1 cm) were used for all measurements in solution.

2.5 Mass spectroscopy

The mass spectra were obtained on a DELSI-NERMAG R30-10 MS-MS system, at 70eV for EI and DCI.

2.6 EPR spectroscopy

The EPR spectra were recorded on polycrystalline samples at X-band frequencies with a BRUKER ESP-300E spectrometer in the temperature range 4-298K. The measurements were carried out by the 'Departament de Química Inorgànica, Universitat de Barcelona, Barcelona (Spain)'.

2.7 Magnetic measurements

Variable-temperature magnetic measurements were carried out on polycrystalline samples using a Faraday type magnetometer MANICS DSM8 equipped with an helium continuous-flow cryostat, working in the 4-300K temperature range and a DURSCH EAF 16UE electromagnet or a Quantum Design SQUID susceptometer. The magnetic field was approximately 1.5 and 1 Tesla, respectively. The diamagnetic corrections were estimated from the Pascal's tables. The measurements were performed by the 'Departament de Química Inorgànica, Universitat de Barcelona, Barcelona (Spain)' and the 'Departement of Chemistry and Biochemistry, Universität Bern'.

2.8 X-ray structure analysis

The intensity data were collected on either a STOE AED2 four circle diffractometer or a STOE IPDS imaging plate diffractometer both using graphite monochromated Mo Kα radiation (λ= 0.71073). The structures were solved by direct methods or Patterson heavy-atom technique using the program SHELXS-97[94]. The program SHELXL-97[95] was used for refinement. The data collection was carried out at 223 ± 2K for some complexes due to the loss of solvent. Crystal data, details of data collection and refinement, atomic coordinates, isotropic thermal parameters (Ueq), interatomic distances, bond angles and hydrogen-bonding geometry are given in the crystallographic part.

The figures were drawn using the programs SCHAKAL-97[96] and PLUTON/PLATON-97[97].

3 SYNTHESIS OF THE LIGAND 5,6-BIS(2-PYRIDYL)PYRAZINE-2,3-DICARBOXYLIC ACID AND COMPLEXES CONTAINING THIS LIGAND

5,6-bis(2-pyridyl)pyrazine-2,3-dicarboxylic acid (1)

a) 2,3-bis(2-pyridyl)-quinoxaline

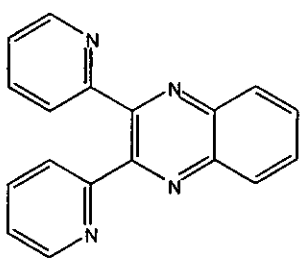

This compound was prepared according to the procedure described by Goodwin and Lions[35]. 2,2'-pyridyl (16g, 0.075mol) was dissolved in refluxing ethanol (200ml), an ethanolic solution (125ml) of o-phenylenediamine (8.11g, 0.075 mol) was slowly added with magnetic stirring. The reaction mixture was refluxed for 1h30min. The resulting brown solution was filtered hot in order to get rid of black impurities. Orange crystals were obtained on cooling (17.56g, 81.9%). Recrystallization from refluxing ethanol with a slurry of charcoal afforded 2,3-bis(2-pyridyl)-quinoxaline as pale yellow crystals.

Yield: 10.30g, 48 %

M. p: 180.7-181.5°C.

Selected IR bands (KBr pellet): ν= 3057(m), 3006(m), 1588(s), 1567(m), 1557(m), 1480(s), 1471(m), 1455(w), 1441(w), 1432(m), 1394(w), 1351(s), 1328(m), 1282(m), 1261(w), 1141(m), 1130(m), 1091(m), 1076(s), 1051(m), 997(s), 985(m), 897(w), 823(w), 808(w), 791(s), 757(s), 745(s), 719(w), 707(m) cm^{-1}.

^1H NMR ($CDCl_3$, 400 MHz): δ= 7.23 (m, 2H, pyH), 7.80 (m, 4H, pyH), 7.98 (m, 2H, pyH), 8.22 (m, 2H, pyH), 8.38 (m, 2H, pyH) ppm.

^{13}C NMR ($CDCl_3$, 50 MHz): δ= 123.0, 124.3, 129.4, 130.5, 136.7, 141.2, 148.6, 152.5, 157.5 ppm.

EI-MS m/z: 284(M^+, 35), 283(base), 256(9), 179(6), 153(1), 142(4), 129(2), 102(1), 78(6).

b) 5,6-bis(2-pyridyl)-pyrazine-2,3-dicarboxylic acid (H_2L) (1)

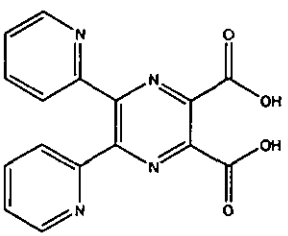

5,6-bis(2-pyridyl)-pyrazioe-2,3-dicarboxylic acid was prepared by the method of Jones and McLaughlin[98]. 5.70g (20mmol) of 2,3-bis(2-pyridyl)-quinoxaline was dissolved in 450ml deionized water. The resulting suspension was heated to 95-97°C with mechanical stirring and 25g (0.16mol) of $KMnO_4$ was added in 2-3g portions over a period of 2h, each subsequent additioo of $KMnO_4$ being made after the violet colour of the solutioo disappeared. The reactioo mixture was stirred for an additional hour and then the temperature decreased to 70°C. 10ml of ethanol was added to remove any exces of $KMnO_4$. The MnO_2 was filtered off and washed with hot water (3x25ml). The combined filtrate and washings were concentrated under reduced pressure to 50 ml and carefully acidified with 6N HCl to a pH= 2.0-2.5. A pale yellow solid precipitated on cooling in an ice bath containing NaCl. The product was filtered off, washed with ethanol and dried under vacuum to afford 5,6-bis(2-pyridyl)pyrazine-2,3-dicarboxylic acid (H_2L).

Yield: 3.9g, 60.5%

M.p: 203.7-204.4°C.

Selected IR bands (KBr pellet): v= 3424(br. m), 3099(w), 3084(w), 3029(w), 2568(br. w), 1709(m), 1659(s), 1602(vs), 1488(s), 1435(m), 1340(m), 1297(m), 1270(s),

1149(s), 1115(s), 1084(s), 1046(m), 997(w), 944(m), 877(m), 820(m), 810(m), 792(vs), 743(m), 622(w), 563(m), 546(m) cm^{-1}.

^1H NMR (D_2O, 400 MHz): δ= 8.63(d, 2H, J= 5.2Hz, pyH), 8.24(td, 2H, J= 7.9Hz, J'= 1.2, pyH), 7.91(d, 2H, J= 7.9Hz, pyH), 7.10(dd, 2H, J= 5.2Hz, J'= 1.2, pyH) ppm.

^{13}C NMR (D_2O, 100 MHz): δ= 171.37, 152.05, 149.29, 148.85, 148.25, 145.58, 129.75, 129.60 ppm.

DCI-MS m/z: 323(MH^+, 4), 322(M^+,2).

$C_{16}H_{10}N_4O_4$(322.28)	calcd.	C: 59.63	H: 3.13	N: 17.39 %
	found	C: 59.51	H: 3.02	N: 17.30 %

$[H_3L]Cl·2.25H_2O$ (2)

Compound 2 was obtained by dissolving compound 1 (32mg, 0.1mmol) in a 1M HCl aqueous solution (20ml). Slow evaporation yielded colourless rod-like crystals.

Selected IR bands (KBr pellet): ν= 3543(w), 3289(br. s), 3083(w), 3051(w), 2839(br. s), 2200(w), 2044(w), 1981(w), 1891(br. w), 1727(vs), 1619(m), 1602(s), 1548(m), 1527(m), 1468(m), 1440(m), 1379(m), 1364(m), 1332(m), 1298(s), 1261(m), 1249(s), 1221(s), 1171(vs), 1113(w), 1091(s), 1026(w), 1000(m), 965(m), 865(m), 801(m), 790(m), 775(m), 729(m), 650(w), 620(w), 603(w), 549(m) cm^{-1}.

$[H_3L]ClO_4·3H_2O$ (3)

Compound 3 was obtained by dissolving compound 1 (32mg, 0.1mmol) in a 1M $HClO_4$ aqueous solution (20ml). Slow evaporation yielded pale yellow block-like crystals.

Selected IR bands (KBr pellet): ν= 3417(br. s), 3349(br. s), 3100(w), 3044(w), 2872(br. m), 2585(br. w), 2012(br. w), 1733(vs), 1633(m), 1620(m), 1607(s), 1529(m), 1460(m), 1436(w), 1375(m), 1355(m), 1321(w), 1288(m), 1240(s), 1210(m), 1168(s), 1158(s), 1141(s), 1115(vs), 1089(vs), 1010(w), 874(w), 794(s), 765(s), 725(s), 627(vs), 549(m) cm^{-1}.

$[H_3L]PF_6 \cdot 3H_2O$ (4)

Compound 4 was obtained by dissolving compound 1 (32mg, 0.1mmol) in an aqueous solution (20ml) containing an equimolar amount of $AgPF_6$. Slow evaporation yielded pale yellow block-like crystals.

Selected IR bands (KBr pellet): ν=3387(br. s), 3111(w), 2590(br. m), 2107(br. w), 1652(s), 1617(s), 1600(s), 1539(m), 1456(m), 1378(vs), 1299(m), 1269(w), 1178(s), 1112(w), 1091(m), 1065(w), 1002(w), 843(vs), 778(m), 772(m), 749(w), 666(m), 556(s) cm^{-1}.

3.1 Complex of Mn(II)

$[Mn_2L_2(H_2O)_4] \cdot 4H_2O$ (5)

H_2L (64mg, 0.20mmol) was added in solid form to an aqueous solution (15ml) of $MnCl_2 \cdot 4H_2O$ (45mg, 0.20mmol). The yellow solution immediately obtained was stirred for 10 min at room temperature, filtered to avoid any impurity and allowed to slowly evaporate. After two weeks orange square rod-like crystals were obtained, separated by filtration and dried in air.

Yield: 54mg, 54.5 %.

Selected IR bands (KBr pellet): ν= 3226(br. s), 3080(w), 1636(s), 1598(vs), 1545(w), 1475(m), 1440(m), 1410(w), 1366(s), 1348(s), 1301(w), 1275(w), 1170(m), 1126(m), 1007(w), 954(w), 850(w), 790(m), 562(m) cm^{-1}.

$C_{32}H_{24}N_8Mn_2O_{12}$ (822.47):	calcd.	C: 46.73	H: 2.94	N: 13.62 %.
	found:	C: 46.62	H: 3.48	N: 13.54 %.

3.2 Complex of Fe(II)

$[Fe_2L_2(H_2O)_4]\cdot 4H_2O$ (6)

A degassed aqueous solution (20ml) of H_2L (32mg, 0.10mmol) was treated with $FeCl_2\cdot 4H_2O$ (20mg, 0.10mmol). The violet solution immediately obtained was stirred under N_2 at 70°C for 1h, filtered to avoid any impurity and allowed to slowly evaporate. After two months deep violet block-like crystals were obtained, separated by filtration and air dried. Precipitation of small amounts of iron(III) hydroxide accompanies the formation of crystals of **6**.

Yield: 20mg, 44.6 %.

Selected IR bands (KBr pellet): ν= 3477(br. s), 3291(br. s), 3078(w), 1640(s), 1593(vs), 1545(w), 1475(m), 1440(m), 1405(w), 1359(m), 1300(w), 1286(w), 1269(w), 1172(m), 1124(m), 1008(w), 954(w), 847(w), 789(m), 772(w), 677(w), 565(m), 549(w), 494(m) cm^{-1}.

$C_{32}H_{32}N_8Fe_2O_{16}$ (896.36)	calcd.	C: 42.88	H: 3.60	N: 12.50 %.
	found	C: 42.96	H: 3.61	N: 12.50 %.

3.3 Complexes of Co(II)

$\{Co(HL)(H_2L)\}ClO_4 \cdot 2H_2O$ (7)

To a stirred aqueous solution (15ml) of $Co(ClO_4) \cdot 6H_2O$ (37mg, 0.1mmol), H_2L (32mg, 0.1mmol) was added in solid form. The orange solution immediately obtained was stirred at room temperature for 20min, filtered to avoid any impurity and the filtrate layered with MeOH (10ml). Orange plate-like crystals were formed within a month. After selectiog suitable crystals for X-ray analysis, the rest of the product was collected by filtration, washed with water and dried in air.

Yield: 20mg, 24%.

Selected IR bands (KBr pellet): v= 3474(br. m), 3102(w), 3061(w), 2997(w), 2769(br. m), 2371(br. w), 1740(m), 1725(s), 1657(vs), 1632(s) 1602(vs), 1541(m), 1525(m), 1506(m), 1473(m), 1447(m), 1402(w), 1354(s), 1295(m), 1265(w), 1245(w), 1223(m), 1191(m), 1122(vs), 1094(s), 1055(m). 1103(s), 1073(m), 1007(w), 997(w), 855(w), 832(m), 806(m), 784(m), 774(m), 764(m), 624(m), 562 (m) cm^{-1}.

$C_{32}H_{23}N_8ClCoO_{14}$ (837.96)	calcd.	C: 45.87	H: 2.77	N: 13.37 %.
	found	C: 45.67	H: 2.79	N: 13.27 %.

$[CoL(H_2O)_3] \cdot 3H_2O$ (8)

$Co(NO_3)_2 \cdot 6H_2O$ (87mg, 0.3mmol) was dissolved in water (15ml), H_2L (32mg, 0.1mmol) was added in solid form. The orange solution immediately obtained was stirred at room temperature for 1hour, filtered to avoid any impurity and left

undisturbed. Very thin orange needle-like crystals were obtained by slow evaporation, filtered off and air dried.

Yield: 41mg, 83%.

Selected IR bands (KBr pellet): ν= 3166(br. m), 3073(w), 1640(sh. s), 1619(br. s), 1598(br. vs), 1540(sh. m), 1470(m), 1450(m), 1426(w), 1403(m), 1366(s), 1340(s), 1280(m), 1231(m), 1193(m), 1166(w), 1118(m), 1089(w), 1049(w), 997(m), 840(m), 811(m), 796(m), 780(m), 749(m), 696(m), 677(w), 631(w), 568(m) cm^{-1}.

$C_{16}H_{20}N_4CoO_{10}$ (487.33)	calcd.	C: 39.43	H: 4.14	N: 11.50 %.
	found	C: 39.31	H: 3.91	N: 11.12 %.

$[Co_2(HL)Cl_2(H_2O)_4]Cl{\cdot}4H_2O$ (9)

To a methanolic solution (20ml) of $CoCl_2{\cdot}6H_2O$ (283mg, 1mmol), H_2L (32mg, 0.10mmol) was added in solid form. The colour of the reaction mixture changed immediately to orange. After stirring at room temperature for 1h30 min, the reaction mixture was filtered in order to avoid any impurity and left undisturbed. Upon slow evaporation, orange plate like crystals of the complex were deposited along with red crystals identified as the $CoCl_2{\cdot}6H_2O$ used in excess.

Yield: 7mg, 22%.

Selected IR bands (KBr pellet): ν= 1701(m), 1628(s), 1600(vs), 1544(m), 1472(m), 1454(m), 1372(vs), 1303(w), 1269(w), 1242(m), 1215(m), 1131(m), 1014(w), 793(m), 637(m), 566 (m) cm^{-1}.

3.4 Complex of Ni(II)

$[NiL(H_2O)_3]\cdot 3H_2O$ (10)

$NiSO_4\cdot 7H_2O$ (56mg, 0.2mmol) dissolved in water (25ml) was reacted with $[H_3L]Cl$ (35mg, 0.1mmol). The pale green solution immediately obtained was stirred at room temperature for 2h, filtered to avoid any impurity and the filtrate left undisturbed. After two weeks very thin needle-like crystals were obtained.

Yield: 29mg, 68%.

Selected IR bands (KBr pellet): ν= 3166(br. s), 3073(w), 1610(s), 1599(vs), 1540(m), 1469(m), 1452(m), 1428(w), 1401(m), 1368(s), 1336(s), 1308(m), 1282(m), 1226(m), 1195(m), 1167(w), 1121(m), 1088(w), 1049(w). 1013(w), 845(m), 811(m), 793(m), 748(m), 632(m), 569 (m).

$C_{16}H_{20}N_4NiO_{10}$ (426.06)	calcd.	C: 39.46	H: 4.14	N: 11.50 %.
	found	C: 39.49	H: 4.25	N: 11.66 %.

3.5 Complexes of Cu(II)

$\{[Cu(HL)(H_2O)]ClO_4\cdot 3H_2O\}_o$ (11)

To a solution of squaric acid (58mg, 0.5mmol) in 20ml of a H_2O/MeOH (1:1) mixture, $Cu(ClO_4)_2\cdot 6H_2O$ (227mg, 0.6mmol) was added. The resulting yellow solution was treated with H_2L (20mg, 0.06mmol). The colour of the reaction mixture changed immediately to deep green. After stirring at 50°C for 30min, the solution was filtered in order to avoid any impurity and allowed to stand for 2 months. Deep green prism-like crystals were obtained, collected by filtration and dried in air.

Yield: 20mg, 61%

Selected IR bands (KBr pellet): ν= 3392(br. m), 3140(w), 3080(w), 1682(vs), 1620(s), 1605(s), 1570(m), 1541(m), 1477(m), 1453(m), 1374(s), 1318(m), 1294(m), 1185(m), 1165(w), 1121(vs), 1099(vs), 977(m), 854(m), 781(m), 628(m), 565(m) cm^{-1}.

$\{[Cu_2(HL)Cl_3]\cdot 2H_2O\}_n$ (12)

In the reaction of an aqueous solution of $CuCl_2\cdot 2H_2O$ with H_2L in a 10:1 molar ratio the immediate precipitation of a pale green solid was always observed, whicb was shown to be the polymeric compound $\{[Cu(L)(H_2O)]\cdot 5H_2O\}_n$[28]. However, on leaving the above solution to slowly evaporate a small amount of deep green prism-like crystals of **12** were also obtained, separated by filtration and dried in air.

Yield: 15mg, 26%

Selected IR bands (KBr pellet): ν= 3313(br. m), 3108(m), 3087(m), 3066(m), 1694(vs), 1665(s), 1599(m), 1570(w), 1547(m), 1469(m), 1451(w), 1422(m), 1374(m), 1313(m), 1289(m), 1268(m), 1245(m), 1231(w), 1207(m), 1167(m), 1126(m), 1101(w), 1019(m), 853(m), 804(m), 791(m), 774(m), 573(m) cm^{-1}.

$\{[Cu_2(HL)Br_3]\cdot 2H_2O\}_n$ (13)

Deep green prism-like crystals of **13** were obtained as described above for compound **12**.

Selected IR bands (KBr pellet): ν= 3465(br. m), 3104(m), 3064(w), 1691(vs), 1663(m), 1598(s), 1570(m), 1552(m), 1470(s), 1422(m), 1368(s), 1311(w), 1301(w), 1289(m), 1245(m), 1228(m), 1204(w), 1166(m), 1135(w), 1122(m), 1017(m), 849(m), 788(m), 768(m), 571(m) cm^{-1}.

3.6 Complex of Ag(I)

$\{[Ag_4L_2(NH_3)_2]\cdot H_2O\}_n$ (14)

Compound 14 was prepared by interacting 4:1 stoichiometric amounts of $AgNO_3$ (68mg, 0.4mmol) and H_2L (32mg, 0.1mmol) in a total volume of 20ml of 10% aqueous ammonia solution. The resulting colourless solution was allowed to slowly evaporate at room temperature in the dark. Yellow square-rod crystals together with a red microcrystalline powder began to precipitate after standing for 3 days. The yellow crystals were separated carefully and used for X-ray analysis.

Yield: 60mg, 54%.

Selected IR bands (KBr pellet): ν= 3436(br. s), 1610(sh.s), 1599(br. vs), 1570(sh. m), 1535(w), 1475(m), 1437(m), 1425(m), 1369(s), 1353(m), 1293(w), 1262(m), 1163(m), 1117(m), 1050(m), 994(w), 951(w), 847(m), 815(w), 787(m), 749(w) cm^{-1}.

$C_{16}H_{11}N_5Ag_2O_4$ (553.03)	calcd.	C: 34.74	H: 2.00	N: 12.66 %.
	found	C: 34.68	H: 1.97	N: 12.54 %.

3.7 Complexes of Zn(II)

$[ZnL(H_2O)_3]\cdot 3H_2O$ (15)

An aqueous solution (20ml) of H_2L (64mg, 0.20mmol) was added to a solution of $ZnSO_4\cdot 7H_2O$ (57mg, 0.20 mmol) in water (20ml). The resulting colourless solution was stirred at 50°C for 1h30 min, filtered to avoid any impurity and left undisturbed. After one week colourless plate like crystals were obtained, filtered off and dried in the air.

Yield 60mg, 61 %.

Selected IR bands (KBr pellet): ν= 1651(s), 1618(s), 1600(vs), 1474(m), 1449(m), 1404(m), 1370(s), 1341(m), 1308(w), 1283(m), 1194(m), 1118(m), 1088(w), 1049(w), 1012(w), 847(m), 811(m), 794(m), 748(m), 630(m), 566(m) cm^{-1}.

$C_{16}H_{20}N_4O_{10}Zn$ (493.75)	calcd.	C: 38.92	H: 4.08	N: 11.35 %.
	found:	C: 38.94	H: 4.05	N: 11.13 %.

$[ZnCl_2(H_2L)]$ (16)

To an aqueous solution (20ml) of $ZnCl_2$ (28mg, 0.2mmol), $[H_3L]Cl$ (36mg, 0.1mmol) was slowly added in solid form. After stirring for 2h at room temperature, the reaction mixture was filtered to avoid any impurity and allowed to slowly evaporate. After two months pale yellow rod-like crystals were formed.

Yield: 35mg, 76%.

Selected IR bands (KBr pellet): ν= 3503(br. m), 3160(m), 3101(m), 3068(m), 3041(m), 3003(m), 2921(br. w), 2771(br. w), 1715(m), 1632(s), 1615(vs), 1598(s), 1582(m), 1534(m), 1465(s), 1370(vs), 1297(m), 1203(m), 1179(w), 1157(m),

1098(w), 1050(m), 938(m), 860(m), 816(m), 788(m), 775(m), 748(m), 725(w), 654(m), 635(m), 624(m), 560(m) cm^{-1}.

3.8 Complexes of Cd(II)

$[Cd(L)(H_2O)_2]_n$ (17)

H_2L (32mg, 0.10mmol) was added in solid form to an aqueous solution (25ml) of $CdCl_2 \cdot 2H_2O$ (22mg, 0.10mmol). The colourless solution immediately obtained was stirred 1h at room temperature, filtered to avoid any impurity and allowed to slowly evaporate. After two weeks small colourless plate like crystals were obtained, separated by filtration and dried in air.

Yield 40mg, 42.5 %.

Selected IR bands (KBr pellet): v= 1630(m), 1598(vs), 1533(m), 1469(m), 1442(m), 1414(m), 1362(s), 1301(m), 1273(m), 1176(m), 1165(m), 1119(m), 1043(w), 992(w), 829(m), 789(m), 759(m), 675(m), 562(m), 513(m) cm^{-1}.

$C_{16}H_{12}N_4O_6Cd$ (468.71):	calcd.	C: 41.00	H: 2.58	N: 11.95 %.
	found	C: 40.70	H: 2.43	N: 11.80 %.

$[Cd_3I_4(HL)_2]$ (18)

CdI_2 (37mg, 0.1mmol) was dissolved in 20ml deionized water, an equimolar amount of H_2L (36mg, 0.1mmol) was slowly added in solid form. After stirring at room temperature for 1h, the resulting colourless solutioo was filtered and left undisturbed until yellow plate-like crystals separated.

Yield: 48mg, 32%.

Selected IR bands (KBr pellet): ν= 3444(br. m), 3061(w), 3038(w), 2955(m), 2923(m), 2853(m), 1726(m), 1705(m), 1633(m), 1596(s), 1547(w), 1520(m), 1448(m), 1433(m), 1370(vs), 1297(m), 1275(m), 1236(m), 1202(m), 1156(m), 1142(m), 1122(m), 1097(m), 1050(m), 1011(m), 924(w), 867(w), 810(w), 789(w), 771(m), 760(w), 724(w), 556 (w), 492(s) cm^{-1}.

$C_{32}H_{18}N_8Cd_3I_4O_8$ (1487.38):	calcd.	C: 25.84	H: 1.22	N: 7.53 %.
	found	C: 26.43	H: 1.22	N: 7.92 %.

3.9 Complex of Hg(II)

[$HgCl_2(H_2L)$] (19)

H_2L (32mg, 0.1mmol) was added in solid form to an aqueous solution (20ml) of $HgCl_2 \cdot 2H_2O$ (30mg, 0.1mmol) with any colour change. After stirring at room temperature for 10min, the reaction mixture was filtered and the colourless filtrate allowed to stand at room temperature for several days until well-shaped colourless block-like crystals were obtained.

4 SYNTHESIS OF THE ESTER DERIVATIVES OF THE LIGAND 5,6-BIS(2-PYRIDYL)PYRAZINE-2,3-DICARBOXYLIC ACID AND COMPLEXES CONTAINING THESE LIGANDS

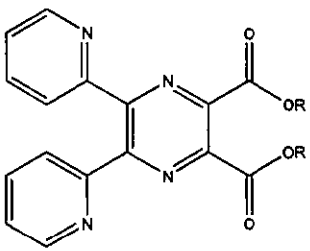

The esters dimethyl-, diethyl- or diisopropyl-5,6-bis(2-pyridyl)pyrazine-2,3-dicarboxylate were obtained by the usual esterification procedure in acidic medium from 5,6-bis(2-pyridyl)-pyrazine-2,3-dicarboxylic acid and an excess of the corresponding alcobol[81].

Dimethyl-5,6-bis(2-pyridyl)pyrazine-2,3-dicarboxylate (Me_2L) (20)

5,6-bis(2-pyridyl)-pyrazine-2,3-dicarboxylic acid (1.00g, 3.11mmol) was heated under reflux in freshly destilled MeOH (40ml) containing H_2SO_4 conc. (98%, 1ml) during 16h. After stopping the reaction the temperature of the solutioo was allowed to cool to room temperature and then poured into an aqueous solution of NaOAc (6g in 150ml deionized water). The resulting solution was stirred in an ice bath containing NaCl to afford a white solid whicb was removed by filtraton, washed with cold water and dried under vacuum. Single crystals suitable for X-ray analysis were obtained by the slow diffusion technique from CH_2Cl_2 and MeOH.

Yield: 0.77g, 65%.

M.p: 137.2-138.7°C.

Selected IR bands (KBr pellet): ν= 3056(w), 3016(w), 2955(w), 1743(s), 1729(vs), 1587(m), 1572(m), 1540(w), 1479(m), 1450(m), 1437(m), 1401(m), 1339(s), 1302(s),

1283(vs), 1260(m), 1217(m), 1189(w), 1164(s), 1089(vs), 1049(m), 996(m), 954(w), 844(w), 829(w), 803(m), 791(m), 773(m), 747(m), 504(w) cm^{-1}.

^1H NMR ($CDCl_3$, 400 MHz): δ= 8.34(dt, 2H, J= 4.1Hz, J'= 1.0Hz, pyH), 7.99(dt, 2H, J= 7.7Hz, J'= 1.0Hz, pyH), 7.82(td, 2H, J= 7.7Hz, J'= 1.0Hz, pyH), 7.26(td, 2H, J= 7.7Hz, J'= 1.0Hz, pyH), 4.04(s, 6H, CH_3) ppm.

^{13}C NMR ($CDCl_3$, 50 MHz): δ= 165.53, 155.98, 153.35, 149.26, 142.92, 137.64, 125.41, 124.49, 54.11 ppm.

DCI-MS m/z: 351(MH^+), 318, 279, 255, 208.

$C_{18}H_{14}N_4O_4$ (350.36)	calcd.	C: 61.70	H: 4.04	N: 15.99 %.
	found	C: 61.46	H: 3.91	N: 15.65 %.

Diethyl-5,6-bis(2-pyridyl)pyrazine-2,3-dicarboxylate (Et_2L) (21)

This compound was prepared by the same method as for 20. 5,6-bis(2-pyridyl)-pyrazine-2,3-dicarboxylic acid in freshly destilled EtOH containing catalytic amounts of H_2SO_4 conc. gave compound 21 as a white solid in 62% yield. Slow evaporation of an ethanolic solution afforded colourless crystals suitable for X-ray analysis.

Yield: 0.70g, 62%

M.p: 117.5-118.3°C.

Selected IR bands (KBr pellet): ν= 3055(w), 2991(w), 2965(w), 2944(w), 2904(w), 1737(s), 1723(vs), 1587(m), 1571(m), 1539(w), 1479(m), 1467(m), 1438(m), 1408(m), 1387(w), 1368(s), 1333(m), 1301(s), 1276(vs), 1257(m), 1210(s), 1178(m), 1161(s), 1086(vs), 1049(m), 1010(m), 995(m), 862(m), 802(m), 768(m), 747(m), 628(w), 606(w), 561(w) cm^{-1}.

^{1}H NMR ($CDCl_3$, 400 MHz): δ= 8.33(d, 2H, J= 4Hz, pyH), 8.01(d, 2H, J= 7.7Hz, pyH), 7.81(t, 2H, J= 7.7Hz, pyH), 7.24(t, 2H, J= 4.4Hz, pyH), 4.52(m, 4H, J= 7Hz, CH_2), 1.45(t, 6H, J= 7.4Hz, CH_3) ppm.

EI-MS m/z: 378(34), 349(9), 232(95), 206(66), 179(25), 152(11), 129(9), 78(base), 46(38).

$C_{20}H_{18}N_4O_4$ (378.39)	calcd.	C: 63.49	H: 4.79	N: 14.81 %.
	found	C: 63.49	H: 4.61	N: 14.77 %.

Di-isopropyl-5,6-bis(2-pyridyl)pyrazine-2,3-dicarboxylate (i-Pr_2L) (22)

This compound was prepared by the same method as above. 5,6-bis(2-pyridyl)-pyrazine-2,3-dicarboxylic acid in dry isopropanol containing catalytic amounts of H_2SO_4 conc. gave compound 22 as a white solid.

Yield: 0.5g, 40%

M.p: 98.2-100°C

Selected IR bands (KBr pellet): ν= 3095(w), 2983(w), 2938(w), 1740(vs), 1720(vs), 1589(m), 1570(m), 1538(m), 1468(m), 1414(w), 1388(w), 1375(m), 1360(s), 1325(m), 1278(s), 1240(s), 1225(vs), 1182(m), 1147(w),1102(s), 1084(vs), 1023(w), 995(w), 954(m), 863(m), 822(w), 785(m), 749(w), 677(m), 621(m), 560(m) cm^{-1}.

^{1}H NMR ($CDCl_3$, 400 MHz): δ= 8.32(d, 2H, J= 4.4Hz, pyH), 8.05(d, 2H, J= 8Hz, pyH), 7.84(t, 2H, J= 7.6Hz, pyH), 7.25(t, 2H, J= 4.1Hz, pyH), 5.38(m, 2H, J= 6.2Hz, CH), 1.45(d, 12H, J= 6.2Hz, CH_3) ppm

$C_{22}H_{22}N_4O_4$ (406.44)	calcd.	C: 65.01	H: 5.45	N: 13.78 %.
	found	C: 64.89	H: 5.31	N: 13.77 %.

4.1 Complex of Mn(II)

[Mn(MeL)Cl(H_2O)$_2$] (23)

Me_2L (76mg, 0.2mmol) was slowly added to a solution of $MnCl_2 \cdot 4H_2O$ (90mg, 0.4mmol) in dry MeOH (20ml). The pale yellow solution immediately obtained was stirred at room temperature for 10min, filtered to avoid any impurity and allowed to slowly evaporate. After two weeks pale-yellow needle-like crystals of the complex deposited along with colourless single crystals of the ester ligand.

Selected IR bands (KBr pellet): ν= 3408(br. m), 3053(w), 1738(s), 1682(br. vs), 1600(s), 1569(m), 1531(m), 1488(m), 1463(m) 1442(m), 1412(m), 1401(m), 1380(m), 1359(m), 1335(w), 1294(m), 1249(m), 1217(m), 1175(m), 1164(m), 1087(m), 1044(m), 1014(m), 946(m), 864(m), 819(m), 799(m), 769(m), 740(m), 650(m), cm^{-1}.

4.2 Complex of Cu(II)

[Cu(MeL)Cl] (24)

Me_2L (35mg, 0.1mmol) was added in solid form to a solution of $CuCl_2 \cdot 2H_2O$ (17mg, 0.1mmol) in dry MeOH (20ml). A pale green solution was immediately obtained, stirred at room temperature for 30min, filtered to avoid any impurity and allowed to stand over several days until deep green needle-like crystals of the complex deposited. Yield: 39mg, 90%.

Selected IR bands (KBr pellet): ν= 3127(w), 3059(w), 1738(s), 1682(br. vs), 1640(sh. s), 1600(m), 1569(m), 1488(m), 1471(m), 1442(m), 1401(m), 1331(m), 1294(m), 1176(m), 1155(m), 1111(s), 1006(m), 993(m), 974(m), 923(w), 839(m), 817(m), 793(m), 756(m), 565(m) cm^{-1}.

4.3 Complex of Zn(II)

$[ZnCl_2(Me_2L)]$ (25)

Me_2L (35mg, 0.1mmol) in 10ml dry MeOH was carefully layered on top of a solution of $ZnCl_2$ (14mg, 0.1mmol) in 10ml dry MeOH. Very thin plate-like crystals deposited within a month.

Selected IR bands (KBr pellet): ν= 3083(w), 3002(w), 2952(w), 1752(vs), 1732(vs), 1604(s), 1574(w), 1542(w), 1490(m), 1451(m), 1403(m), 1340(s), 1302(m), 1286(s), 1217(m), 1167(m), 1106(m), 1093(s), 1059(m), 1026(m), 954(w), 842(w), 832(w), 786(m), 766(m), 645(w), 562(m) cm^{-1}.

4.4 Complex of Cd(II)

$[CdCl_2(Me_2L)]_n$ (26)

$CdCl_2 \cdot 2H_2O$ (22mg, 0.1mmol) in 25ml dry MeOH was slowly added to a solution of Me_2L in 10ml dry MeOH. The colourless solution was stirred at room temperature for 1h, filtered to avoid any impurity and allowed to stand over several days until colourless square rod-like crystals were obtained.

Yield: 40mg, 75%.

Selected IR bands (KBr pellet): ν= 3066(w), 2997(w), 1751(vs), 1593(m), 1568(w), 1549(w), 1479(m), 1450(m), 1403(m), 1339(s), 1297(m), 1273(m), 1261(m), 1228(s), 1193(m), 1177(m), 1162(m), 1120(m), 1109(w), 1088(s), 1009(m), 974(m), 918(w), 827(m), 803(m), 789(m), 770(w), 758(m), 554(m) cm^{-1}.

$C_{18}H_{14}N_4CdCl_2O_4$ (533.63)	calcd.	C: 40.51	H: 2.64	N: 10.50 %.
	found	C: 40.49	H: 2.53	N: 10.59 %.

4.5 Complex of Hg(II)

$[HgCl_2(Me_2L)]_n$ (27)

Me_2L (35mg, 0.1mmol) was added in solid form to a solution of $HgCl_2 \cdot 2H_2O$ (30mg, 0.1mmol) in dry MeOH. The colourless solution immediately obtained was stirred at room temperature for 2h, filtered to avoid any impurity and allowed to slowly evaporate. After two days colourless needle-like crystals were obtained.

Yield: 47mg, 76%.

Selected IR bands (KBr pellet): v= 3065(w), 2997(w), 2951(w), 2882(w), 1747(vs), 1590(m), 1568(m), 1546(w), 1477(m), 1447(m), 1402(m), 1338(s), 1279(m), 1223(s), 1195(m), 1176(s), 1105(w), 1086(s), 1003(m), 973(w), 827(w), 802(m), 788(m), 769(m), 755(m), 553(m) cm^{-1}.

$C_{18}H_{14}N_4Cl_2HgO_4$ (621.82)	calcd.	C: 34.77	H: 2.27	N: 9.01 %.
	found	C: 34.79	H: 2.44	N: 9.03 %.

REFERENCES

1. Inoue, M.; Kubo, M. *Coord. Chem. Rev.* **21**, 1 (1976)
2. Steel, J. *Coord. Chem. Rev.* **106**, 227 (1990)
3. Wolff, L. *Ber. Dtsch. Chem. Ges.*, 26, 721 (1893)
4. Otieno, T.; Rettig, S.J.; Thompson, R.C.; Trotter, J. *Can. J. Chem.* 67, 1964 (1989)
5. Real, J.A.; De Munno, G.; Muñoz,.M.C.; Julve, M. *Inorg. Chem.* 30, 2701 (1991)
6. Kitawaga, S.; Munakata, M.; Tanimura T. *Inorg. Chem.* 31, 1714 (1992)
7. MacGillivray, L.R.; Subramanian, S.; Zaworotko, M.J. *J. Chem. Soc., Chem. Comm.* 1325 (1994)
8. Carlucci, L.; Ciani, G.; Proserpio, D.M.; Sironi, A. *Angew. Chem., Int. Ed. Engl.* **34**, 1895 (1995)
9. Carlucci, L.; Ciani, G.; Proserpio, D.M.; Sironi, A. *J. Am. Chem. Soc.* **117**, 4562 (1995)
10. Venkataraman, D.; Lee, S.; Moore, J.S.; Zhang. P.; Hirsch, K.A.; Gardner, G.B.; Covey, A.C.; Prentice, C.L. *Chemistry of Materials*, 8, 2030 (1996)
11. Halasyamani, P. Heier, K.R.; Willis, M.J.; Stern, C.L.; Poeppelmeier, K.R. *Z. anorg. Allg. Chem.* **622**, 479 (1996)
12. Carlucci, L.; Ciani, G.; Proserpio, D.M.; Sironi, A. *J.Chem.Soc., Chem. Comm.* 1393 (1996)
13. Otieno, T.; Rettig, S.J.; Thompson, R.C.; Trotter, J. *Inorg. Chem.* 32, 1607, (1993)
14. Kitawaga, S.; Kawata, S.; Kondo, M.; Nozaka, Y.; Munakata, M. *Bull. Chem. Soc. Japan* 66, 3387 (1993)
15. Jaber, F.; Charbonnier, F.; Faure, R. *J. Chem. Cryst.* 24, 681 (1994)
16. Shaima, R.P.; Bhasin, K.K.; Tiekink, E.R.T. *Acta. Cryst., Sect. C*, 52, 2140 (1996)
17. Goher, M.A.S.; Al-Salem, N.A.; Mautner, F.A. *Polyhedron*, 15, 3575 (1996)
18. Goher, M.A.S.; Al-Salem, N.A.; Mautner, F.A.; Klepp, K.O. *Polyhedron*, 16, 825 (1997)
19. Goher, M.A.S.; Abu-Youseff, M.A.M.; Mautner, F.A. *Polyhedron*, 17, 3305 (1998)
20. Morgan, L.W.; Goodwin, K.V.; Pennigton, W.T.; Petersen, J.D. *Inorg. Chem.* 31, 1103 (1992)

21. O'Connor, C.J.; Klein, C.L.; Majeste, R.J.; Trefonas, L.M.. *Inorg. Chem.* **21**, 64 (1982)
22. Richard, P.; Qui, D.T.; Bertaut, E.F. *Acta Cryst., Sect. B*, **29**, 1111 (1973)
23. Mao, L.; Rettig, S.J.; Thompson, R.C.; Trotter, J.; Xia, S. *Can. J. Chem.* **74**, 2413 (1996)
24. Neels, A. Ph. D. Thesis, Université de Neuchâtel, 1995
25. Constable, E.C.; Edwards, A.J.; Phillips, D.; Raithby, P.R. *Supramolecular Chemistry*, 5, 93 (1995)
26. Graf, M.; Stoeckli-Evans, H.; Whitaker, C.; Marioni, P.A.; Marty, W. *Chimia*, **42**, 202 (1993)
27. Marioni, P.A: Marty, W.; Stoeckli-Evans, H. Whitaker, C. *Inorg. Chim. Acta*, **219**, 161 (1994)
28. Wang, Y. Ph. D. Thesis, Université de Neuchâtel, 1996
29. Ferigo, M.; Bonhôte, P.; Marty, W.; Stoeckli-Evans, H. *J. Chem. Soc., Dalton Trans.*, 1549 (1994)
30. Lu, J.; Paliwala, T.; Lim, S.C.; Yu, C.; Niu, T.; Jacobson, A.J. *Inorg. Chem.* 36, 923 (1997)
31. Okubo, T.; Kondo, M.; Kawata, S.; Kitagawa, S.; Miyazaki; A., Enoki, T. *Mol. Cryst. Liq. Cryst.*, **286**, 115 (1996)
32. Bailey, R.D.; Pennington, W.T. *Polyhedron*, **16**, 417 (1997)
33. Turnbull, M.M.; Pon, G.; Willet, R.D. *Polyhedron*, **10**, 1835 (1991)
34. Hoskins, B.F.; Robson, R. *J. Am. Chem. Soc.* **112**, 1546 (1990)
35. Goodwin, H.A.; Lions, F. *J. Am. Chem. Soc.*, **81**, 6415 (1959)
36. Goodwin, H.A.; Sylva, R.N.; Vagg, R.S.; Watton, E.C. *Aust. J. Chem.* **22**, 1605 (1969)
37. Graf, M.; Greaves, B.; Stoeckli-Evans, H. *Inorg. Chim. Acta*, **204**, 239 (1993)
38. Graf, M.; Stoeckli-Evans, H. *Acta. Cryst., Sect. C*, **50**, 1461 (1994)
39. Graf, M.; Stoeckli-Evans, H.; Escuer, A.; Vicente, R. *Inorg. Chim.Acta*, **257**, 89 (1997)
40. Bonner, J.C.; Fisher, M.E. *Phys. Rev.*, **135A**, 640 (1964)
41. Eckberg, R.P.; Hatfield, W.E. *J. Chem. Soc., Dalton Trans.* 616 (1975)
42. Richardson, H.W.; Hatfield, W.E. *J. Am. Chem. Soc.* 98, 835 (1976)
43. Richardson, H.W.; Wasson, J.R.; Hatfield, W.E. *Inorg. Chem.* **16**, 484 (1977)
44. Blake, A.B.; Hatfield, W.E. *J. Chem. Soc., Dalton Trans.* 868 (1978)

45. Hay, P.J.; Thibeault, J.C.; Hoffmann, R. *J. Am. Chem. Soc.* **97**, 4884 (1975)

46. Oshio, H.; Nagasshima, U. *Inorg. Chem.*, **29**, 3321 (1990)

47. Munakata, M.; Wu, L.P.; Yamamoto, M.; Kuroda-Sowa, T.; Maekawa, M. *J. Am. Chem. Soc.*, **118**, 3117 (1996)

48. Barlin, G.B. *The Chemistry of Heterocyclic Compounds*; v. **41**, John Wiley Sons, Inc. (1982)

49. Nakamoto, K. *Infrared and Raman Spectra of Inorganic and Coordination Compounds*; John Wiley and Sons, Inc., New York (1986) p.233

50. Woznial, K.; Krygowski, T.M.; Grech, E.; Kolodziejski, W.; Klinowski, J. *J. Phys. Chem.* **97**, 1862 (1993)

51. Lynch, D.E.; Smith, G.; Byriel, K.A.; Kennard, C.H.L.; Whitaker, A.K. *Aust. J. Chem.* **47**, 309 (1994)

52. Smith, G.; Lynch, D.E.; Byriel, K.A.; Kennard, C.H.L. *Acta Cryst., Sect. C*, **51**, 2629 (1995)

53. Bock, H.; Vaupel, T.; Näther, C.; Ruppert, K.; Havlas, Z. *Angew. Chem. Int. Ed. Engl.* **31**, 299 (1992)

54. Greaves, B.; Stoeckli-Evans, H. *Acta Cryst., Sect. C*, **48**, 2269 (1992)

55. Graf, M.; Stoeckli-Evans, H. *Acta Cryst., Sect. C*, **52**, 3073 (1996)

56. Mehrotra, R.C.; Bohra, R. *Metal Carboxylates*, Academic Press, London (1983)

57. Neels, A.; Stoeckli-Evans, H. *Chimia*, **47**, 198 (1993)

58. Kahn, O. *Molecular Magnetism*, VCH, Weinheim (1993)

59. Klein, C.L.; O'Connor, C.J.; Majeste, R.J.; Trefonas, L.M.; *J. Chem. Soc. Dalton Trans.* 2419 (1982)

60. Marioni, P.A.; Stoeckli-Evans, H.; Marty, W.; Güdel, H.U.; Williams, A.F. *Helvetica Chimica Acta*, 69, 1004 (1986)

61. Lainé, P.; Gourdon, A.; Launay, J.P.; *Inorg. Chem.*, **34**, 5156 (1995)

62. Garge, P.; Chikate, R.; Padhye, S.; Savariault, J.M.; De Loth, P.; Tuchagues, J.P. *Inorg. Chem.*, **29**, 3315 (1990)

63. *International Tables far X-Ray Crystallography*, Volume C, Ed. Wilson, Kluwer Academic Publishers, Dordrecht (1995)

64. Banci, L.; Bencini, A.; Benelli, C.; Gatteschi, D.; Zanchini, C. *Structure and Bonding*, **52**, 38-85 (1982)

65. Carlin, R. L. *Magnetochemistry*, Springer, Berlin, Heidelberg (1986)

66. O'Connor, C.J.; Sinn, E. *Inorg. Chem.*, **20**, 545 (1981)

67. Bourdeaux, E.A.; Mulay, L.N. *Theory ond Applications of Moleculor Paromognetism*, John Wiley & Sons (1976)

68. Addison, A.W.; Rao, T.N.; Reedijk, J.; van Rijn, J.; Verschor, g.C.; *J. Chem. Soc., Dolton Trons.*, 1349 (1984)

69. Hall, J.W.; Ph. D. Dissertation, University of North Carolina (1977)

70. Estes, W.E.; Hatfield, W.E.; van Ooijen, J.A.C.; Reedijk, J. *J. Chem. Soc., Dalton Trons.* 2121 (1980)

71. Hernández-Molina, M.; González-Platas, J.; Ruiz-Pérez, C.; Lloret, F.; Julve, M. *Inorg. Chim. Acta*, 284, 258-265 (1999)

72. Landee, C.P.; Djili, A.; Mudgett, D.F.; Newhall, M.; Place, H.; Scott, B.; Willet, R.D. *Inorg. Chem.* 27, 620-627 (1988)

73. Rojo, T.; Cortés, R.; Ruiz de Larramendi, J.I.; Madariaga, G. *J. Chem. Soc., Dolton Trons.*, 2125 (1992)

74. Cortés, R.; Lezama, L.; Ruiz de Larramendi, J.I.; Madariaga, G.; Mesa, J.L.; Zuñiga, F.J.; Rojo, T. *Inorg. Chem.*, **34**, 778-786 (1995)

75. Smith, G.; Reddy, A.N.; Byriel, K.A.; Kennard, C.H.L. *J. Chem. Soc., Dalton Trans.* 3565 (1995)

76. Prince, R.H.; Wilkinson, G.; Gillard, R.D.; McCleverty, J.A. (eds). Comprehensive Coordination Chemistry, Vol. 5, Pergamon, Oxford (1987)

77. Hypodentate Zn: Constable, E.C. *Prog. Inorg. Chem.* 42, 67 (1994)

78. Graf, M. Ph. D. Thesis, Université de Neuchâtel, 1995

79. Garoufis, A.; Perlepes, S.P.; Screiber, A.; Bau, R.; Hadjiliadis, N. *Polyhedron*, **15**, 177 (1996)

80. Canty, A.J.; Tobias, R.S. *Inorg. Chem.* 18, 413 (1979)

81. Vogel, A.I. *Textbook of Practical Organic Chemistry*, Longman, London, 4th edn. (1978)

82. Dugas, H. *Bioorganic Chemistry: A Chemical Approach to Enzyme Action*, 2nd ed. Berlin: Springer-Verlag (1989)

83. Neels, A.; Stoeckli-Evans, H.; Wang, Y.; Clearfield, A.; Poojary, D.M. *Inorg. Chem.* 36, 5406 (1997)

84. Wang, Y.; Stoeckli-Evans, H. *Acta Cryst., Sect C*, 54, 306 (1998)

85. Hay, R.W.; Clark, C.R. *J. Chem. Soc., Dalton Trans.*, 1866 (1977)

86. Bock, H.; Schodel, H.; Vaupel, T. *Z. Naturforsch., Teil B*, 52, 515 (1997)

87. Sekizaki, M. *Acta Cryst., Sect B*, 29, 327 (1973)

88. Klein, C.L.; Stevens, E.D.; O'Connor, C.J.; Majeste, R.J.; Trefonas, L.M. *Inorg. Chim. Acta*, 70, 151 (1983)

89. Mondal, M.; Ray, S. *Acta Cryst., Sect B*, 33, 2297 (1977)

90. Sekizaki, M. *Bull. Chem. Soc. Jpn.* 54, 146 (1981)

91. Marioni, P.A. Ph. D. Thesis, Université de Neuchâtel, 1986

92. Ferigo, M. Ph. D. Thesis, Université de Neuchâtel, 1988

93. Posel, M. Ph. D. Thesis, Université de Neuchâtel, 1998

94. Sheldrick, G.M. (1997). *SHELXS97. Progrom for the Solution of Crystal Structures*. University of Göttingen, Germany.

95. Sheldrick, G.M. (1997). *SHELXL97. Program for the Refinement of Crystal Structures*. University of Göttingen, Germany.

96. Keller, E. (1997). *SCHAKAL, Program for the Graphic Representation of Molecular and Crystollogrophic Models*, University of Freiburg, Germany.

97. Spek, A.L. (1990). *Acta Crystollogr.* A46, C-34.

98. Jones, R.G.; McLaughlin, K.C. Org. Synth., 30, 86 (1950)